Development of a 35 GHz Network Analyzer Based Polarimetric Scatterometer

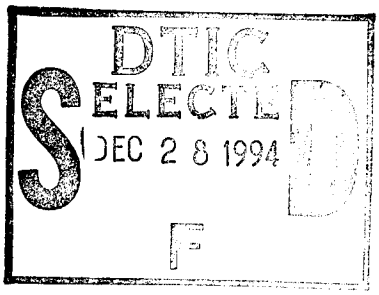

A Thesis Presented

by

José G. Colom

Submitted to the Graduate School of the
University of Massachusetts in partial fulfillment
of the requirements for the degree of

Master of Science in Electrical and Computer Engineering

September 1991

Department of Electrical and Computer Engineering

Development of a 35 GHz Network Analyzer based Polarimetric Scatterometer

A Thesis Presented

by

José G. Colom

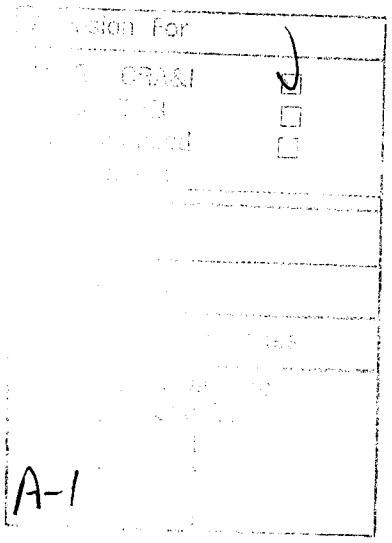

Submitted to the Graduate School of the
University of Massachusetts in partial fulfillment
of the requirements for the degree of

Master of Science in Electrical and Computer Engineering

September 1991

Department of Electrical and Computer Engineering

Development of a 35 GHz Network Analyzer based Polarimetric Scatterometer

A Thesis Presented

by

José G. Colom

Approved as to style and content by:

Calvin T. Swift, Chair, E.C.E.

Robert E. McIntosh, Member, E.C.E.

Neal G. Anderson, Member, E.C.E.

Keith R. Carver, Department Head
Electrical and Computer Engineering

To my wife, my daughter and my parents

ACKNOWLEDGEMENT

I would like to thank Professors Calvin T. Swift and Robert E. McIntosh for their invaluable help during this project, and for the unique opportunity they provided of utilizing all the state-of-the-art equipment in MIRSL. This work would not have been completed without the help of my fellow students; Steve Sekelsky and Kaz Grzeslak. I also owe thanks to all the people who help in the collection of data; Jim Menashi, Paul Ferraro, Phil Langlois, Steve Frasier and Steve Lohmeier, and also to Ivan Popstefanija and Dave Parker for their valuable help in computer software; and to my wife for typing this thesis in LaTeX

And most of all I would like to thank my wife and my daughter Natalí for all their love.

ABSTRACT

DEVELOPMENT OF A 35 GHZ NETWORK ANALYZER

BASED POLARIMETRIC SCATTEROMETER

SEPTEMBER 1991

JOSÉ G. COLOM, B.S.E.E., UNIVERSITY OF PUERTO RICO

M.S.E.C.E., UNIVERSITY OF MASSACHUSETTS

Directed by: Professor Calvin T. Swift

The Microwave Remote Sensing Laboratory (MIRSL) at the University of Massachusetts has developed a 35 GHz stepped FM-CW network analyzer based polarimetric scatterometer for the remote sensing of natural targets. Operation of the system at this frequency is achieved with upconversion and harmonic downconversion. The network analyzer facilitates real time data reduction employing different internal processing techniques. The primary function is to collect polarimetric data of stationary targets such as snow, saline ice and simulated sea ice to characterize the power returned from the target at different states (i.e. rough, smooth, dry, wet, etc.). An indoor facility at the Cold Regions Research Engineering Laboratory (CRREL) in Hanover, New Hampshire allows temperature control, so that data are collected at different growth phases.

The system operates over a 2 GHz bandwidth and therefore achieves a range resolution of 7.5 cm. Using the radar range equation, the normalized radar cross section of the ice and snow was computed as a function of incidence angle at different antenna polarizations.

During the past year the system was automated and now the angle of incidence, polarization and system temperature are controlled from a remote computer.

This winter (1990-1991) snow data at different states were collected at CRREL, and additional saline ice experiments were performed. This time a polarimetric calibration was developed along with a polarization synthesis software implementation to determine polarimetric signatures of the ice.

TABLE OF CONTENTS

List of Figures

CHAPTER 1

INTRODUCTION

A scatterometer is a radar that measures the scattering properties of a distributed target. The scatterometer may be designed to make measurements at a particular frequency, incidence angle and polarization. Typically a frequency of interest is selected, and measurements are made with different configurations of receiving and transmitting antenna polarizations at various incidence angles. Usually, the system is capable of transmitting and receiving a set of orthogonal polarizations (i.e. horizontal and vertical), then the scattered signal is measured at four different combinations of linear antenna polarizations: HH, HV, VH, and VV, where the first letter refers to the receiver polarization and the second refers to the transmit polarization. The measurements are later processed and the backscattering coefficient, σ^o, of the distributed target is calculated for each polarization and incidence angle using the radar range equation. The scatterometer measures only the magnitude of the received signal and no–phase information is recorded. Hence, an absolute calibration at the range of interest will be sufficient to achieve precise σ^o measurements.

With the introduction of the vector network analyzer, the design of a scatterometer has been greatly simplified. The network analyzer measures the magnitude and phase characteristics of a device under test (DUT) with respect to a reference signal. With the use of harmonic mixers and upconverters, an HP 8510B network analyzer is configured to operate in the millimeter–wave range. If the polarization of the antennas is changed the scatterometer operates as a polarimetric radar that measures the magnitude and phase of the scattered signal at different combinations of antenna polarization (HH, HV, VH and VV in this case).

There are many advantages to using a network analyzer in a scatterometer configuration. Detection, processing, time-gating and different error-correction techniques are readily available features. Using the polarization synthesis technique [Ulaby and Elachi, 1990], σ^o of the target for any receiving and transmitting polarization configuration angle is computed at a specific incidence angle. A calibration procedure is used to correct for polarimetric errors in the measurement system. This is achieved by illuminating targets of known scattering properties (NRCS and polarization). These values are stored in matrix form and a correction matrix is constructed for the receiver and transmitter polarization distortions.

During the last two years, the Microwave Remote Sensing Laboratory (MIRSL) at the University of Massachusetts developed a 35 GHz polarimetric scatterometer based around the HP 8510B network analyzer. This instrument operates in a step-frequency mode transmitting up to 801 frequencies over a 2 GHz bandwidth (34-36 GHz). With the use of a polarizer switch and a rotary joint before the transmit and receive antenna, respectively, the system is able to measure the scattered signal of a target at the four different linear polarizations.

This system has been used to measure scattering properties of stationary distributed targets, such as urea ice (simulated sea ice), saline ice and snow in different states (i.e. rough, smooth, dry, wet, etc). The purpose of these measurements is to characterize σ^o as a function of incidence angle, and to plot the polarimetric response of the target. This thesis is divided into five main parts. Chapter II is a review on polarimetry and radar theory. Chapter III explains the development of the system which includes operation of a network analyzer, scatterometer configuration, millimeter-wave configuration, and the polarimetric scatterometer. Chapter IV is a discussion on the calibration of the system, it includes polarimetric, external and internal calibration techniques. Finally chapter V presents results from the data collected, conclusions and some future recommendations for the system.

CHAPTER 2

BACKGROUND

2.1 Introduction to Radar Theory

A scatterometer is a radar that measures the scattering properties of a distributed target. A general block diagram of a scatterometer is shown in figure 2.1. A wave travels, interacts with the target, and some energy is reflected and coupled by the receive antenna to be later processed and detected into the receiver to extract different characteristics of the target.

There are different types of scatterometers configurations. The most commonly used are:

1. The Continuous–Wave (CW) Radar

This radar is the most basic system used to make radar backscatter and transmission measurements. The transmitter consists of a radio frequency (RF) signal source or oscillator which produces a continuos, single frequency signal and an antenna which directs the power toward the target (see figure 2.2). The receiver is comprised of a similar antenna connected to a detector which produces a DC voltage proportional to the power in the received RF signal. There are two problems with this system. Without modulation on the CW signal, range cannot be determined. In addition the noise power generated in the system components varies with the reciprocal of the frequency. Since the detected signal is at DC, we get a low signal to noise ratio. The noise problem is reduced by mixing down to an intermediate frequency (IF) and then amplifying and detecting. With knowledge of the range to the target and the received and transmitted power, the data is processed to obtain scattering characteristics of the target.

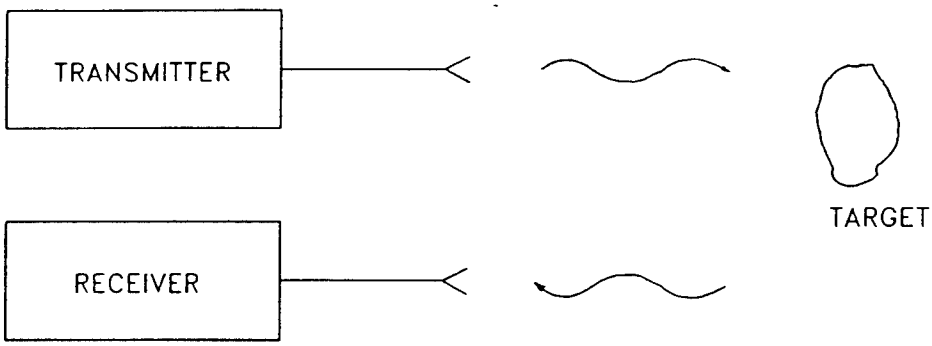

Figure 2.1. General block diagram of a scatterometer.

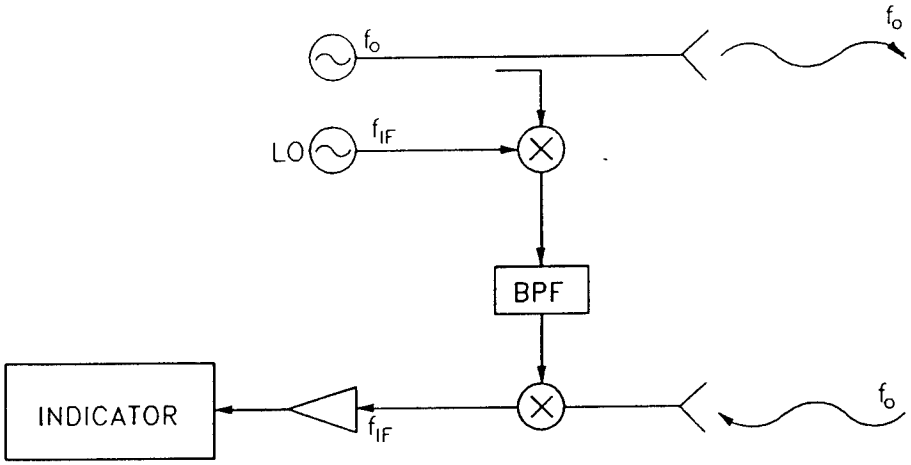

Figure 2.2. Block diagram of a CW radar.

2. Frequency Modulated–Continous Wave (FM–CW) Radar

To overcome the limitations of range-measurements with a CW system (see figure 2.3), the signal is modulated so that a timing mark is applied to the carrier. The FM–CW radar system measures target range by varying the transmit frequency in time and measuring the frequency of the received signal. The transmitted and received signals of an FM–CW system illuminating a point target are shown on figure 2.4 for a linear frequency modulation. Since a stationary target is assumed in figure 2.4, no Doppler shift is detected on the scattered signal. The range is given by $R = ct/2$ where t is the time it takes the signal leaving the transmitter to arrive back at the receiver. The IF frequency is given by [Skolnik, 1980]:

$$f_{IF} = \frac{2R}{c} 2 f_m B \tag{2.1}$$

where,

f_{IF} = IF frequency at mixer output

R = Range to point target

c = Speed of light

f_m = Modulation rate

B = Modulation Bandwidth

The minimum range resolution is calculated from the modulation bandwidth B and is given by:

$$\Delta R = \frac{c}{2B} \tag{2.2}$$

3. Pulse Radar

Figure 2.5 shows a block diagram of a pulse radar system. The pulse modulator shown in the diagram generates high power pulses of a particular shape and duration. The pulse modulates an RF oscillator and the signal is directed to the transmit antenna. The signal returns from the target, it is mixed down to an IF, and is

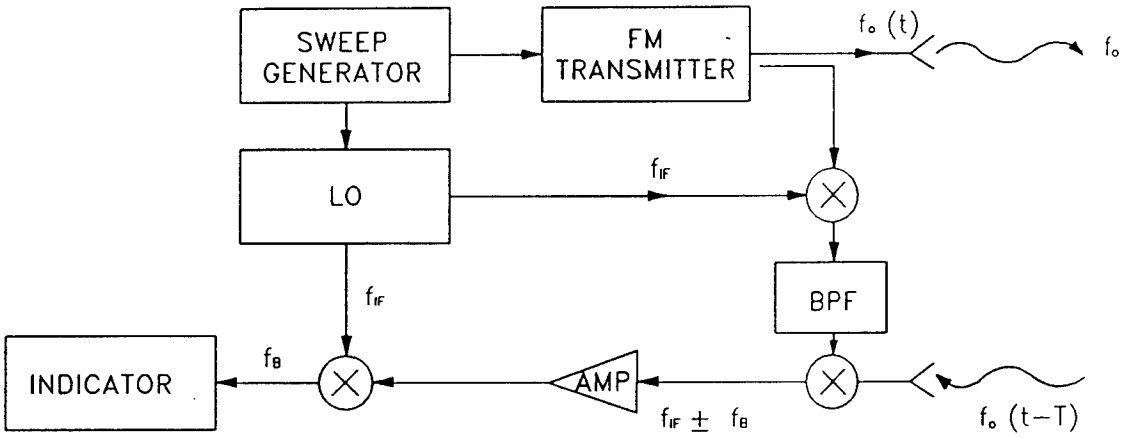

Figure 2.3. Block diagram of an FM–CW radar.

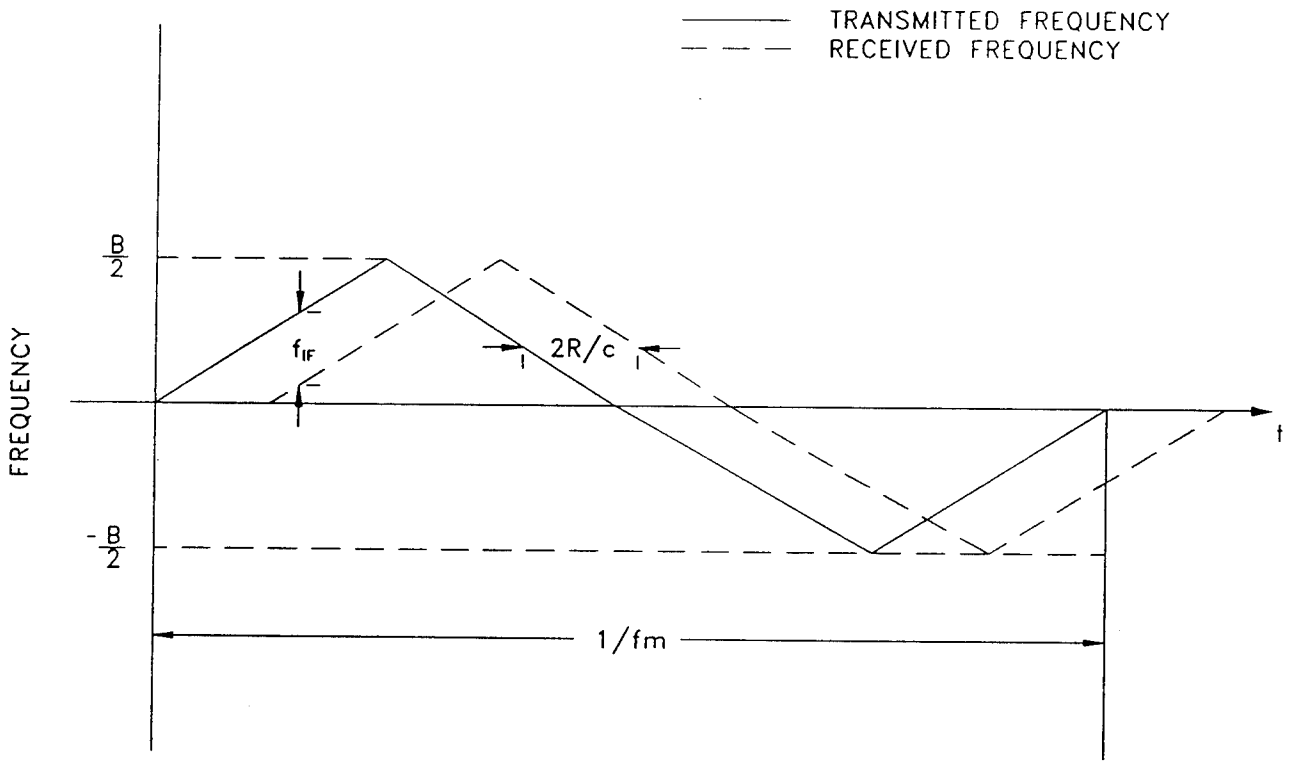

Figure 2.4. Transmitted and received signal from a point target with an FM–CW radar.

amplified. Then, it is detected and displayed to determine range information by measuring the time delay, T, between the leading edge of the transmitted pulse and the leading edge of the received pulse.

For a point target, the time delay is given by $T = 2R/c$, where R is the range to the target and c is the speed of light. The minimum range resolution is determined by the pulse length, τ, and is given by [Eaves and Reedy, 1987]:

$$\Delta R = c\tau/2 \tag{2.3}$$

The bandwidth, B, of the system is usually chosen to be $1/\tau$ to match the radar receiver. Hence, for both FM–CW and pulse radars the minimum range resolution is obtained from $\Delta R = c/2B$. From this we can see that at higher frequencies it is easier to obtain a better range resolution by increasing the modulated bandwidth of an FM–CW radar than by decreasing the length of the transmitted pulse in a pulse radar system. With the use of a network analyzer based scatterometer, the bandwidth of the system can be increased to the order of a few Gigahertz. This implies that to achieve the same range resolution with a pulse system, the length of the pulse has to be less than 1 nanosecond. Pulse compression techniques can be used to simultaneously take advantage of the high energy in the radiated long pulse, while still obtaining the high range resolution of a short pulse.

4. Stepped Frequency Radar

The block diagram of the FM–CW radar shown in figure 2.3 is modified to provide frequency stepped transmission by replacing the sweep generator with a frequency synthesizer. The output frequency is selectable in N discrete steps of Δf size each. The total bandwidth required for the transmitter is now $N \times \Delta f$. High range resolution can be achieved by using a wideband frequency stepped waveform and processing the received signal using FFT techniques. The Fourier transform capabilities of a network analyzer based scatterometer are used by displaying the

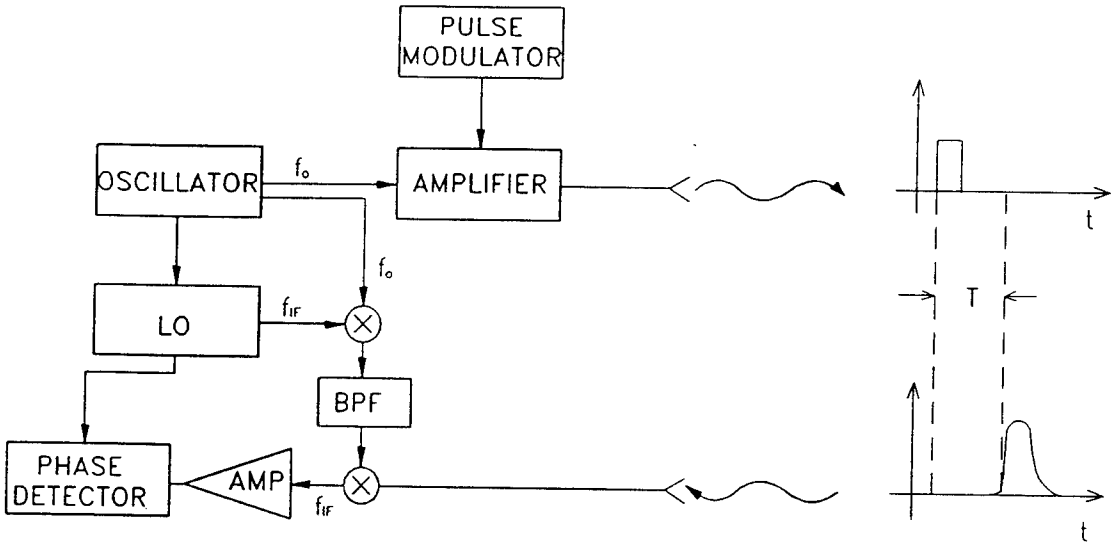

Figure 2.5. General block diagram of a pulse radar system.

returned signal in the time domain. This technique allows us to create a picture of the returned power versus range for the whole scene illuminated by the antennas.

As mentioned before, a CW system does not measure range, but it is possible to obtain a range measurement by measuring the phase of the received wave relative to the phase of the transmitted signal [Skolnik, 1980]. For instance, if a CW-system transmits a single frequency sine wave of the form $sin(2\pi f_o t)$ (assuming amplitude equals unity), the signal received is given by $sin[2\pi f_o(t-T)]$, where T is the ellapsed time between transmission and reception. If the transmitted and received signal are compared in a phase detector the result is the phase difference between the two. The phase difference is given by:

$$\Delta\phi = 2\pi f_o T \tag{2.4}$$

but recall that,

$$T = 2R/c \tag{2.5}$$

then,

$$\Delta\phi = \frac{4\pi f_o R}{c} \tag{2.6}$$

hence $\Delta\phi$ can be used to measure range as;

$$R = \frac{c\Delta\phi}{4\pi f_o} = \frac{\lambda}{4\pi}\Delta\phi \tag{2.7}$$

Unfortunately, the phase difference is ambiguous if $\Delta\phi$ exceeds 2π radians. Substituting $\Delta\phi = 2\pi$ in the above equation;

$$R_{unamb} = \frac{\lambda}{2} \tag{2.8}$$

At microwave frequencies this unambiguous range is too small for remote sensing applications. The region of unambiguous range can be extended significantly by

transmitting two or more CW signals. The phase difference for the case where two CW electromagnetic waves (f_1, f_2) are transmitted, is given by:

$$\Delta\phi = \frac{4\pi(f_1 - f_2)R}{c} = \frac{4\pi\Delta f R}{c} \tag{2.9}$$

then,

$$R_o = \frac{c\Delta\phi}{4\pi\Delta f} \tag{2.10}$$

for $\Delta\phi = 2\pi$,

$$R_{unamb} = \frac{c}{2\Delta f} \tag{2.11}$$

where Δf is the spacing between the frequencies. Note that R_{unamb} is large for small differences in the two frequencies, Δf.

The range resolution of the system is given by [Currie and Brown, 1987]:

$$\Delta R = \frac{c}{2B_T} \tag{2.12}$$

where $B_T = N \times \Delta f$, and N is the number of transmitted frequencies.

Consider for example a 2 GHz bandwidth stepped frequency system transmitting 51 frequency points. The spacing between frequencies would be,

$$\Delta f = \frac{2 \times 10^9}{51} = 39 \times 10^6 \text{ Hz} \tag{2.13}$$

which would yield a range resolution of,

$$\Delta R = \frac{c}{2(2 \times 10^9)} = 0.075 \text{ m} \tag{2.14}$$

and an unambiguous range of

$$R_{unamb} = \frac{c}{2(39 \times 10^6)} = 3.8 \text{ m} \tag{2.15}$$

Now, keeping the same bandwidth of 2 GHz and transmitting 401 frequencies, would yield a spacing between frequencies of,

$$\Delta f = \frac{2 \times 10^9}{401} = 5 \times 10^6 \text{ Hz} \tag{2.16}$$

which would yield a range resolution of,

$$\Delta R = \frac{c}{2(2 \times 10^9)} = 0.075 \text{ m} \tag{2.17}$$

and an unambiguous range of,

$$R_{unamb} = \frac{c}{2(5 \times 10^6)} = 30 \text{ m} \tag{2.18}$$

Note that the range resolution is not affected by the number of frequencies that are transmitted.

The disadvantage of using the frequency stepped technique lies in the complexity of the synthesizer and the stability of the components over a wide bandwidth. In addition the synthesizer speed may be very slow, confining the system to measure stationary targets only.

All the systems discussed so far are coherent. In such a system the phase of the transmitted signal is stored to be later compared with the received signal maintaining phase coherence of the system. In addition, the above systems are based on the superheterodyne principle, which means that the received wave at RF is downconverted to an Intermediate Frequency (IF) by mixing it with a local oscillator (LO) signal. Subsequent amplification and detection are performed on the IF signal.

The backscattering characteristics of a particular target are contained on the radar cross section (RCS) of the target σ. The radar cross section is a ficticious area (m^2) which gathers all power incident on it and reradiates it isotropically yielding the same echo as the true target. The power received at the terminal of the antenna is given by [Eaves and Reedy, 1987]:

$$P_R = \frac{P_t \lambda^2 G_T G_R \sigma}{64\pi^3 R^4} \tag{2.19}$$

where,

P_t = Transmitted power

λ = wavelength

G_T = Gain of the transmitter antenna

G_R = Gain of the receiver antenna

σ = Radar cross section of the target

R = Range from the antenna to the target

The radar cross section of the target can be calculated from the received measured power by solving for σ in the above equation. The RCS is not necessarily related to the physical area of the target except that the larger the size, the larger the cross section is likely to be.

For distributed targets, the above equation can be expressed in terms of the normalized radar cross section (NRCS) σ^o ($\sigma^o = \sigma/A_{ill}$, where A_{ill} is the area illuminated by the antenna). Now, the equation is used to compute the scattering coefficient of a surface area. Similarly, an equation to calculate the scattering coefficient for a volume can be developed.

A polarimatric radar measures the radar cross section of a target for any desired combination of transmit and receive antenna polarizations. In this work the collection of data was performed with a network analyzer based polarimetric scatterometer used in a stepped frequency mode.

The system was used for short range measurements (1-3 m) which makes it sensitive to leakage signals close to the target range. This signals are removed with the network analyzer correction routines. Also a dual antenna radar configuration was used to achieve higher isolation between the transmitter and receiver channels.

2.2 Introduction to Polarimetric Theory

An electromagnetic radiation is represented as a vector quantity with a given polarization state. The polarimetric response of a target can be generated either by hardware or software implementation. The hardware implementation adds complex-

ity to the radar design and therefore increases its cost. For this reason the software or polarization synthesis technique is preferred.

For a plane wave propagating along the $+z$ direction, a horizontal and a vertical component are usually utilized to characterize an electric field vector, E as;

$$\mathbf{E} = (E_v \mathbf{v} + E_h \mathbf{h}) e^{ik_z z} \tag{2.20}$$

where E_v and E_h are the vertical and horizontal components of the wave, and $\mathbf{v}$ and $\mathbf{h}$ are the corresponding unit vectors in those directions. The wave number is denoted as k_z and is equal to $2\pi/\lambda$. This electric field can also be expressed in matrix notation or the Jones vector as:

$$\mathbf{E} = \begin{bmatrix} E_v \\ E_h \end{bmatrix} = \begin{bmatrix} |V| e^{j\delta_v} \\ |H| e^{j\delta_h} \end{bmatrix} \tag{2.21}$$

where, $|V|$ and $|H|$ refer to the magnitudes and δ_v and δ_h to the phases of the vertical and horizontal fields, respectively. The polarization state of a TEM wave traveling in the $+z$ direction is described in terms of an ellipse traced by the tip of the E–field as a function of time at a specific point in space, $z = z_o$ (see figure 2.6). The polarization state of the wave is completely specified in terms of electric field quantities by the ellipse parameters, ϕ and τ [Born and Wolf, 1965] as:

$$\tau = \frac{1}{2} \sin^{-1}\left(\frac{2|V||H| \sin\delta}{|H|^2 + |V|^2}\right) \tag{2.22}$$

$$\phi = \frac{1}{2} \tan^{-1}\left(\frac{2|V||H| \cos\delta}{|V|^2 - |H|^2}\right) \tag{2.23}$$

where ϕ and τ are the orientation and ellipticity angles, as defined in figure 2.6, and δ is the phase difference between the vertical and horizontal field components $(\delta_v - \delta_h)$. There are certain values of τ and ϕ in which the ellipse degenarates to a straight line ($\tau = 0°$) or a circle ($\tau = 45°$), for these cases the polarization is called linear and circular, respectively. Also the sense of rotation of the E–field in the plane of polarization is determined with the ellipse polarization angles (τ, ϕ).

For instance, right hand waves are represented by $\tau > 0$. For example, $\tau = 0^o$ and $\phi = 90^o$ describe the state of a horizontal polarized wave. To describe a vertical polarization τ and ϕ, both are 0^o.

The scattering characteristics of a single target are contained in the complex scattering matrix [S]. The transmitted and received Jones vectors are related by the scattering matrix as [Jones, 1941]:

$$\mathbf{E}^s = \frac{e^{jkr}}{r}[\mathbf{S}]\mathbf{E}^t \tag{2.24}$$

where r is the distance between the scatterer and the receiving antenna. Assuming that a linear basis is used (say, horizontal and vertical) $\mathbf{E}^t$ represents the field incident on the target given by,

$$\mathbf{E}^t = E_v^t\mathbf{v} + E_h^t\mathbf{h} \tag{2.25}$$

and $\mathbf{E}^s$ represents the scattered field given by,

$$\mathbf{E}^s = E_v^s\mathbf{v} + E_h^s\mathbf{h} \tag{2.26}$$

The complex scattering matrix [S] is given by,

$$[\mathbf{S}] = \begin{pmatrix} S_{vv} & S_{vh} \\ S_{hv} & S_{hh} \end{pmatrix} \tag{2.27}$$

Reciprocity requires that $S_{hv} = S_{vh}$ for monostatic measurements (transmitter and receiver co-located) so that the number of quantities needed to characterize [S] is five, as long as three phases are known with respect to a fourth.

With [S] known, RCS of a point target for any of the principal linear polarizations combinations can be obtained from [Ulaby *et al.*, 1990]:

$$\sigma_{ij} = 4\pi|S_{ij}|^2; \quad i,j = \text{v or h} \tag{2.28}$$

For any other state of polarization for the transmit and receive antenna defined by the polarization angles (ϕ_t, τ_t) and (ϕ_r, τ_r) the radar cross section for a point target can be computed applying the polarization synthesis equation [Kennaugh, 1951]:

$$\sigma(\phi_r, \tau_r; \phi_t, \tau_t) = 4\pi|\mathbf{p}^r \cdot [\mathbf{S}]\mathbf{p}^t|^2 \tag{2.29}$$

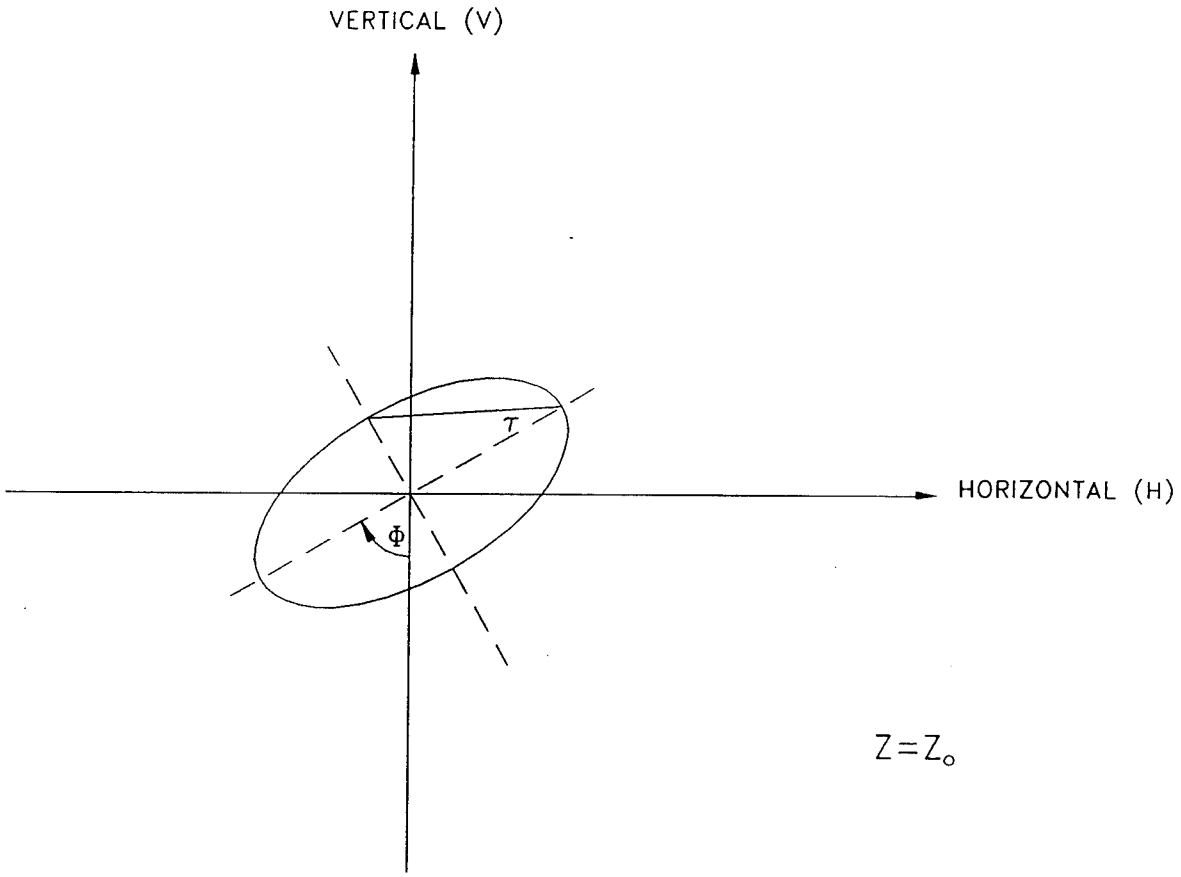

Figure 2.6. Elliptically polarized wave.

where $\mathbf{p}^r$ and $\mathbf{p}^t$ are the normalized polarization vectors of the receive and transmit antennas, and are given by:

$$\mathbf{p}^m = \frac{\mathbf{E}^m}{|\mathbf{E}^m|} \tag{2.30}$$

Figure 2.7 depicts the polarization signatures for a trihedral corner reflector. A polarization signature is a representation of the response of a target for every possible combination of transmitter and receiver antenna polarizations. It plots the normalized σ as a function of the polarization parameters (ϕ_r,τ_r;ϕ_t,τ_t). Figure 2.7a shows the co-polarized response, in which case $\phi_r = \phi_t$ and $\tau_r = \tau_t$. The cross-polarized response is shown in figure 2.7b. In this case the transmitter and receiver are orthogonal to each other and $\phi_r = \phi_t + \pi/2$ and $\tau_r = -\tau_t$.

For distributed targets the polarization synthesis technique is identical to the technique used with point targets and σ^o is given by:

$$\sigma^o(\phi_r, \tau_r; \phi_t, \tau_t) = \frac{4\pi}{A_{ill}\, N} \sum_{i=1}^{N} |\mathbf{p}^r \cdot [\mathbf{S}]_i \mathbf{p}^t|^2 \tag{2.31}$$

where N is the number of samples measured, A_{ill} is the area illuminated by the antennas, and $[\mathbf{S}]_i$ is the scattering matrix of the i^{th} sample.

To represent a target polarization state, N scattering matrices are measured and the magnitude squared is averaged. A single scattering matrix will not completely characterize the target due to target random motion, radar platform motions and changes in the radar waveform.

Instead of repeating the process N times to obtain σ^o, a more efficient approach based on the Stokes scattering operator [M] can be used [Ulaby *et al.*, 1990].

To understand this technique we start describing the polarization state of a wave with the Stokes vector $\mathbf{F}$ in terms of the ellipse parameters τ and ϕ:

$$\mathbf{F}(\phi,\tau) = \begin{bmatrix} I_o \\ Q \\ U \\ V \end{bmatrix} = \begin{bmatrix} |V|^2 + |H|^2 \\ |V|^2 - |H|^2 \\ 2|V|\,|H|\cos\delta \\ 2|V|\,|H|\sin\delta \end{bmatrix} = \begin{bmatrix} I_o \\ I_o \cos 2\phi \cos 2\tau \\ I_o \sin 2\phi \cos 2\tau \\ I_o \sin 2\tau \end{bmatrix} \tag{2.32}$$

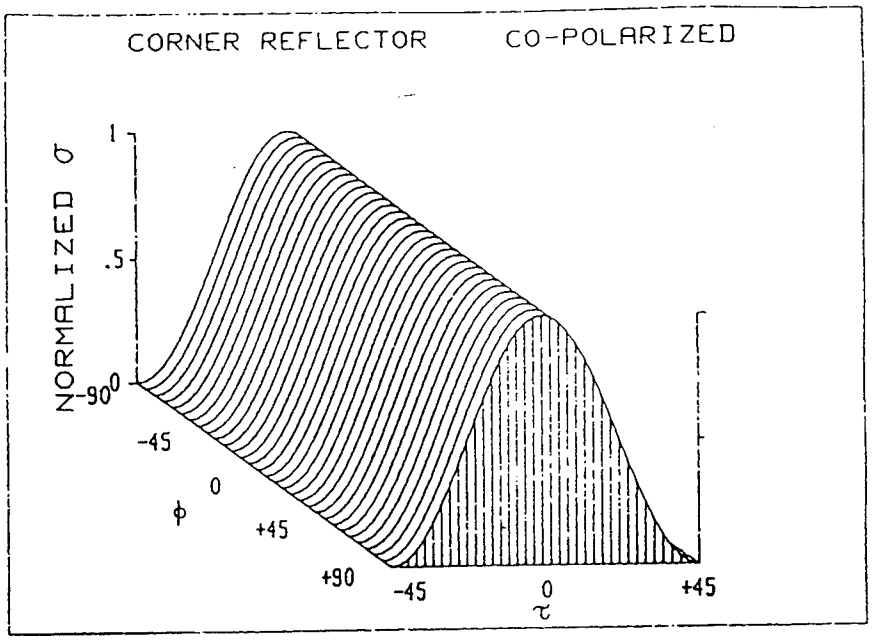

(a)

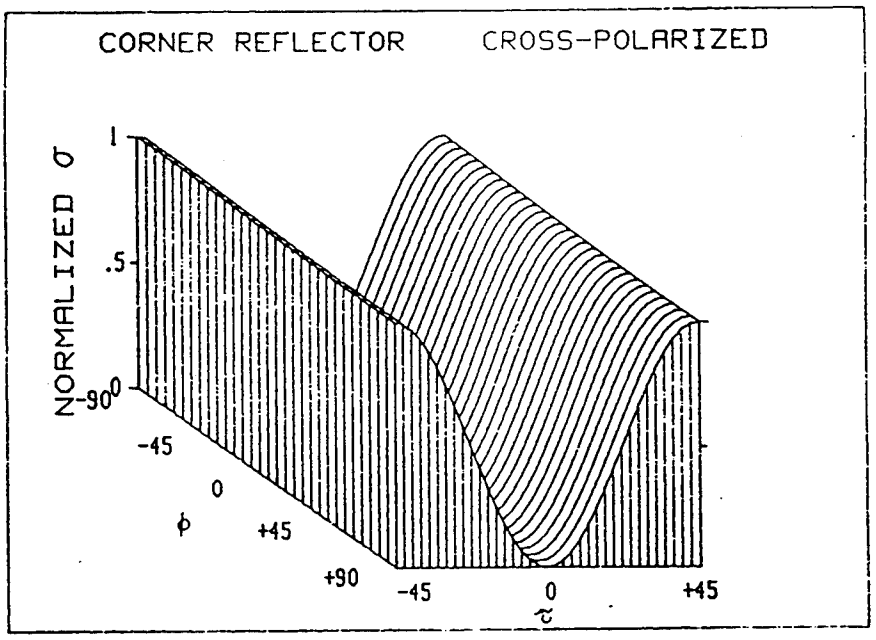

(b)

Figure 2.7. Co-polarized (a), and cross-polarized (b) polarimetric signatures for a trihedral corner reflector.

where $I_o = |H|^2 + |V|^2$.

A normalized Stokes vector describing a wave vertically polarized is given by,

$$\mathbf{F}(90^\circ, 0^\circ) = \begin{bmatrix} 1 \\ -1 \\ 0 \\ 0 \end{bmatrix}$$

And for horizontal polarization,

$$\mathbf{F}(0^\circ, 0^\circ) = \begin{bmatrix} 1 \\ 1 \\ 0 \\ 0 \end{bmatrix}$$

In the same manner that a scattered and transmitted wave described by the Jones vector are related by the scattering matrix [S], the scattered and transmitted wave described by the Stokes vector are related by the Mueller matrix [L] by the following relation:

$$\mathbf{F}^s = \frac{1}{r^2}[\mathbf{L}]\mathbf{F}^t \tag{2.33}$$

where [L] is a 4x4 real matrix given in terms of the elements of the scattering matrix [S].

A polarization synthesis equation for a point target is related to the transmitted and scattered Stokes vectors and the Stokes scattering operator [M] by:

$$\sigma(\phi_r, \tau_r; \phi_t, \tau_t) = 4\pi \mathbf{A}^r \cdot [\mathbf{M}]\mathbf{A}^t \tag{2.34}$$

where $\mathbf{A}^r$ and $\mathbf{A}^t$ are the normalized Stokes vectors for the receive and transmit antennas respectively ($\mathbf{A}^m = \mathbf{F}^m/I_o$) and [M] is known as the Stokes scattering

operator given as real quantities and is directly related to the Mueller matrix [L] by:

$$[\mathrm{M}] = [\mathrm{Q}][\mathrm{L}] \tag{2.35}$$

where [Q] is a constant, and after matrix multiplication the Stokes scattering operator is reduced to [Ulaby and Elachi, 1990]:

$$[\mathrm{M}] = \begin{bmatrix} \frac{1}{2}\langle |a|^2 + |b|^2 + |c|^2 + |d|^2 \rangle & \frac{1}{2}\langle |a|^2 - |b|^2 + |c|^2 - |d|^2 \rangle & Re\langle ab^* + cd^* \rangle & Im\langle ab^* + cd^* \rangle \\ \frac{1}{2}\langle |a|^2 + |b|^2 - |c|^2 - |d|^2 \rangle & \frac{1}{2}\langle |a|^2 - |b|^2 - |c|^2 + |d|^2 \rangle & Re\langle ab^* - cd^* \rangle & Im\langle ab^* - cd^* \rangle \\ Re\langle ac^* + bd^* \rangle & Re\langle ac^* - bd^* \rangle & Re\langle ad^* + bc^* \rangle & Im\langle ad^* - bc^* \rangle \\ Im\langle ac^* + bd^* \rangle & Im\langle ac^* - bd^* \rangle & Im\langle ad^* + bc^* \rangle & -Re\langle ad^* - bc^* \rangle \end{bmatrix} \tag{2.36}$$

where, for ease of notation, we used the following definitions; $a = S_{vv}$, $b = S_{vh}$, $c = S_{hv}$, and $d = S_{hh}$. For a distributed target, N scattering matrices are obtained from which N matrices [M] can be computed. The backscattering coefficient is synthesized for any transmit and receive antenna polarization from:

$$\sigma^o(\phi_r, \tau_r; \phi_t, \tau_t) = \frac{4\pi}{A_{ill}} \mathbf{A}^r \cdot \langle [\mathrm{M}] \rangle \mathbf{A}^t \tag{2.37}$$

where $\langle [\mathrm{M}] \rangle$ is the averaged Stokes scattering operator defined as,

$$\langle [\mathrm{M}] \rangle = \frac{1}{N} \sum_{\ell=1}^{n} ([\mathrm{M}])_\ell \tag{2.38}$$

This approach is computationally superior to the direct synthesis approach in which the scattering matrix is averaged. In the later case, the averaged is performed prior to applying the synthesis equation.

In summary, with the knowledge of the scattering matrix of a target, the Stokes scattering operator is computed, and the polarization synthesis equation is applied for either point or distributed targets to determine the polarization response of the target.

CHAPTER 3

DEVELOPMENT OF A 35 GHZ NETWORK ANALYZER BASED POLARIMETRIC SCATTEROMETER

As previously mentioned, a scatterometer is a radar that measures scattering properties from a point or distributed target. Originally, it was confined to measure the absolute value of σ^o as a function of incidence angle. In order to measure the complex scattering matrix of a target, the magnitude and phase have to be stored for four different combinations of receiving and transmitting antenna polarizations. With knowledge of the magnitude and the phase for each element of the scattering matrix, the polarization synthesis technique can be used to compute σ^o of the target for any combination of transmitting–receiving antenna polarization.

In recent years network analyzers have been available from different companies. These instruments can be easily configured as polarimetric scatterometers to measure both phase and magnitude. This chapter discuss the development of a network analyzer based polarimetric radar, from the basic principles of a network analyzer to millimeter–wave configuration, and finally the scatterometer configuration.

The discussion will be confined to an HP 8510B Network Analyzer, since this system was used in developing the polarimetric scatterometer.

3.1 Operation of a Network Analyzer

When a device is stimulated with a microwave signal, some of the incident energy will be reflected due to the impedance difference at the input, some will be dissipated in the device and the rest will be transmitted through the device. The reflection

coefficient is defined as the ratio of the reflected energy to the incident energy. The transmission coefficient is defined as the voltage ratio of the transmitted energy to the incident energy (see figure 3.1).

The HP 8510B uses a sinusoidal wave as the stimulus signal generated by some RF source. A sample of the incident signal is used as a reference and is compared to the reflected or transmitted signal from the device. The ratio of the signals is measured by the network analyzer in complex quantities consisting of linear magnitude and a phase angle relative to the incident signal [Hewlett–Packard, 1987]. Figure 3.2 shows a simple block diagram to measure a two port device with a network analyzer. Note that the network analyzer has three inputs, a_1, which is used to direct the reference signal to the analyzer and, b_1 and b_2 that are used for the reflected and transmitted signals respectively.

The responses of two ratios can be displayed on the screen of the network analyzer:

$$S_{11} = \frac{b_1}{a_1} \quad \text{and} \quad S_{21} = \frac{b_2}{a_1} \tag{3.1}$$

these ratios are complex quantities known as the scattering parameters (S-parameters). The S-parameters of a test device are a precise and complete means of describing how a device will respond to an arbitrary input. They are conceptually simple and they give an exact definition of the signal flow through the device.

Figure 3.3 shows a flowgraph representation of a two port device. There are four S-parameters and two of them (S_{11} and S_{22}) describe the complex reflection coefficient at each port and the other two describe the forward and reverse transmission coefficients (S_{21} and S_{12}). In the case of figure 3.2 the device has to be physically reversed to measure the four S-parameters. There are alternatives to measuring the S-parameters of a two port device that do not require reversing it.

The S-parameter test set is an HP system (HP 8515) that can be used in conjunction with the swept source and the HP 8510B providing automatic selection

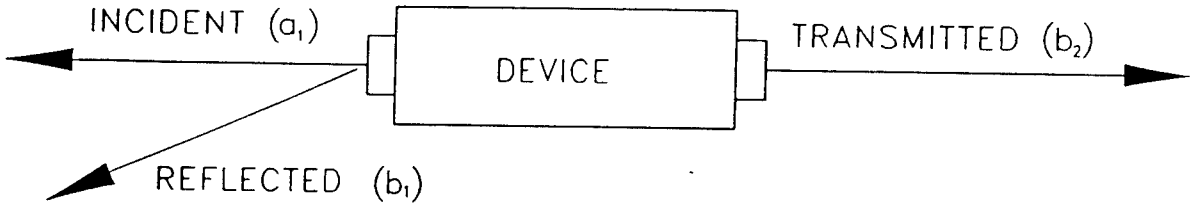

- Reflection coefficient $= \frac{b_1}{a_1} = S_{11}$
- Transmission coefficient $= \frac{b_2}{a_1} = S_{21}$

Figure 3.1. Wave incident on a device under test (DUT).

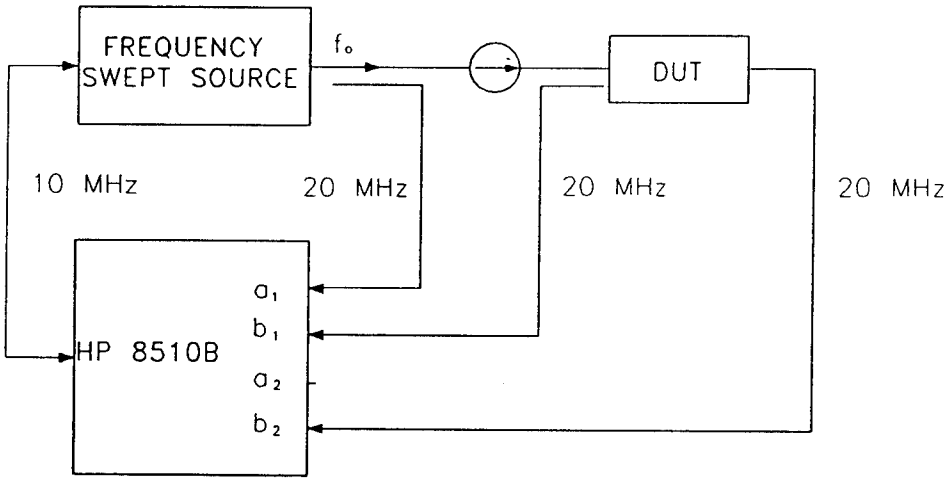

Figure 3.2. Measurement of a two port device with a network analyzer.

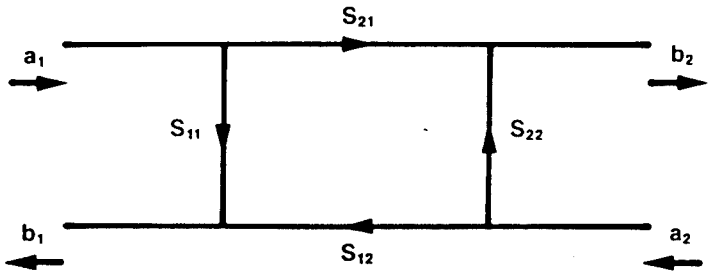

a_1 = Forward Reference
b_2 = Forward Transmitted
b_1 = Reflected at Port 1
a_2 = Reverse Reference

Figure 3.3. Flowgraph for a two port device.

of any of the parameters. The source input is automatically switched for forward or reverse measurement via a switch/splitter. The test device is usually connected between two test port extension cables, making symmetrical signal paths between test set port 1 and port 2 (see figure 3.4 for details).

In addition, there are two inputs for reference signals (a_1 and a_2) which are used for the incident signals from port 1 and port 2, respectively.

The RF signal from the HP source is controlled with the HP 8510B front panel, this signal can sweep within a maximum frequency range of 45 MHz to 26.5 GHz. The signal is incident to the device through port 1 or port 2 (depending on the S-parameter of interest) and internally downconverted by harmonic mixing to a suitable IF (20 MHz). The IF signals (a_1, b_1, a_2, b_2) are directed to the detector section of the HP 8510B and downconverted a second time to a 100 KHz signal. Because the frequency conversion is phase coherent and the IF signals paths are carefully matched, magnitude and phase relationships between the input signals are maintained throughout the frequency conversion and detection steps.

The network analyzer has substantial signal processing and data transfer capabilities. Features such as time-domain are available in real time. Also, available in the time and frequency domain are gating, averaging, complex-math functions, internal correction routines and memory. Data are easily transferred via the HP-Interface Bus (HP-IB) in different formats (ASCCI, binary, corrected, raw, etc.). The network analyzer also contains different error-correction routines. Calibrations for reflection and transmission measurements are also available. These calibrations correct for unwanted non-varying signals through the use of calibrated standards such as short circuits, matched loads, and open circuits. These corrections can significantly improve the system noise performance.

There are other S-parameters test sets available to make measurements up to 50 GHz. Also with the help of external harmonic mixers and frequency upconverters

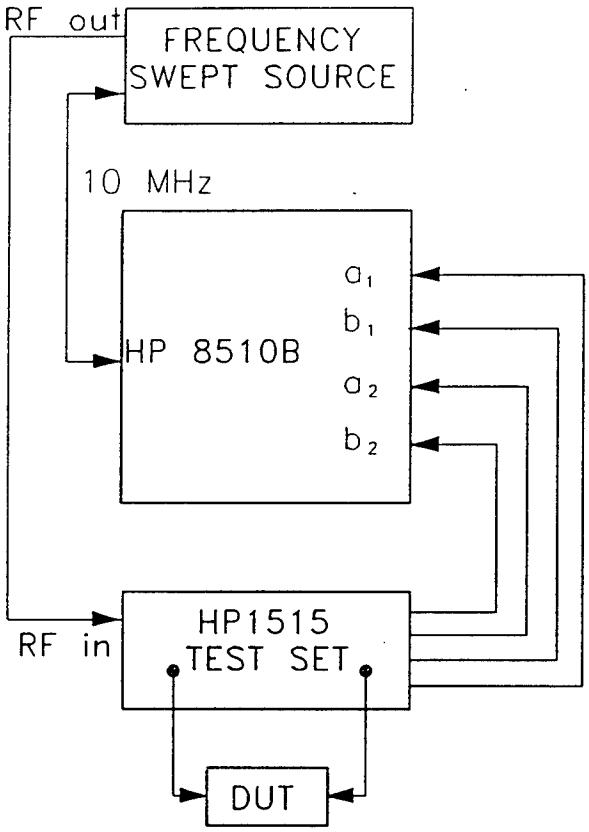

Figure 3.4. Network Analyzer with an S-parameter test set.

the frequency range is expanded up to 110 GHz. In the next section the use of a network analyzer in the millimeter–wave region will be discussed.

3.2 Millimeter–Wave Configuration

The HP 8510B can be configured to operate in the millimeter–wave region (up to 110 GHz) with the addition of frequency multipliers and harmonic downconverters. A block diagram of the system is shown in figure 3.5 The S-parameter test set is not used in this configuration since the 20 MHz signals (a_1, b_1, a_2, b_2) are obtained from the external harmonic mixers and directed straight to the HP 8510B for the second downconversion. An extra synthesizer source locked to the test signal source is used as an LO signal to the harmonic mixers. Note also that the device under test is stimulated from one direction (forward) and it has to be reversed to measure the four S-parameters.

Let us consider a specific example to understand the operation in the millimeter-wave region. If the S-parameters of a DUT that operates in the R-band (26.5 - 40 GHz) are to be measured over a 3 GHz bandwidth centered at a frequency of 34.5 GHz, a test signal from 11 to 12 GHz is generated using the step frequency mode. The signal is amplified and upconverted ($\times 3$) with the HP 83554A frequency multiplier which generates an output stepping from 33 to 36 GHz. Next, a sample of the reference, transmitted and reflected signals are downconverted to 20 MHz when mixed with the LO signal. The LO signal is phase–locked to the test signal and is stepping in frequency from 6.604 GHz to 7.204 GHz. Since the mixer uses its fifth harmonic for the downconversion, harmonics sweeping from 33.02 to 36.02 GHz are generated to obtain the 20 MHz IF at the output of the mixer. The signals are amplified once more and directed to the HP 8510B for the second downconversion and detection. For a more detailed block diagram of the millimeter-wave configuration, the reader is referred to HP 8510B reference manual.

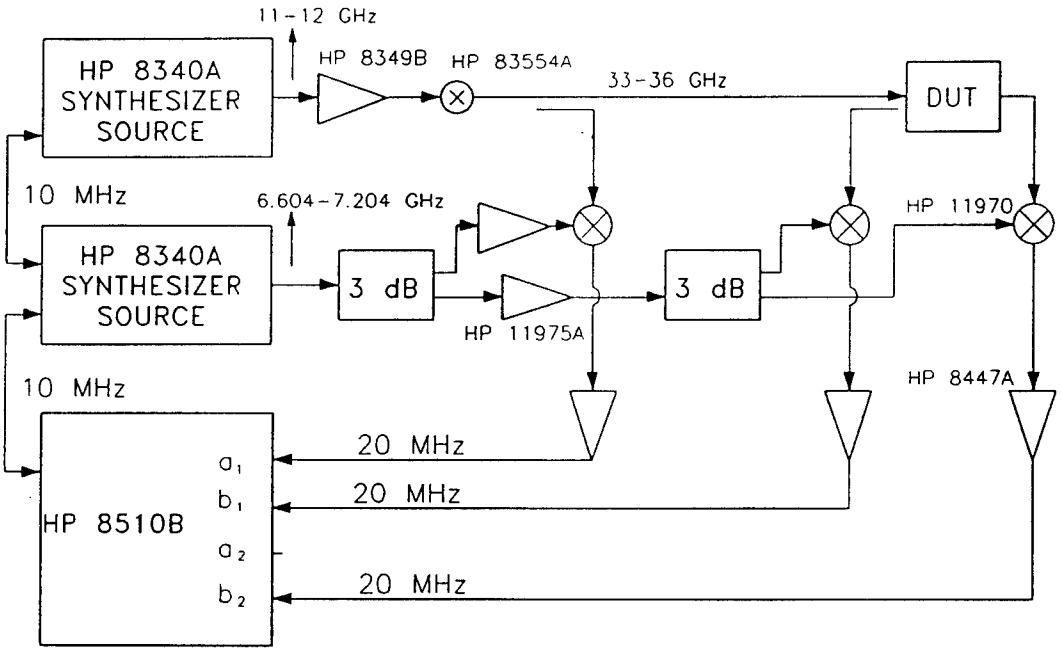

Figure 3.5. Millimeter-wave configuration.

The same set-up is used for other frequency bands (R, Q, U, V, W). The only difference being the size of the waveguide employed. All the features discussed from the network analyzer are still available at millimeter-wave in both, the time and frequency domains. The same principle to measure the S-parameters of a DUT is used to measure the radar cross section of a device which is now the target. Operation of the network analyzer as a scatterometer will be discussed in the next section for both microwaves and millimeter–wave.

3.3 Scatterometer Configuration

To operate the network analyzer as a scatterometer, an RF signal is transmitted using an antenna. The antenna couples the signal to free space (transmission line) and travels to the target (device under test). The signal that is reflected from the target is then received with another antenna and is compared with a sample of the transmitted RF signal.

Figure 3.6 shows a block diagram of the scatterometer configuration. Note that only two channels are used (a_1, b_1) so that S_{11} gives the ratio of the received signal and the reference signal $(S_{11} = \frac{V_{Rec}}{V_{Ref}})$. The extra channel (b_2) can also be utilized when signals with different polarization are measured at the same time. For millimeter-wave, a similar procedure is used, converting the system from figure 3.5 in the scatterometer of figure 3.7.

In the millimeter-wave region, the size of the antenna is not a limiting factor. For this reason two antennas are often used to avoid noise problems due to a single antenna system and improve the dynamic range. The Fourier transform techniques of the HP 8510B allows the returned signal to be displayed as a function of time or range. The complex–math operations are also very useful for measuring point targets in an anechoic chamber. Responses of the chamber and mounting alone are

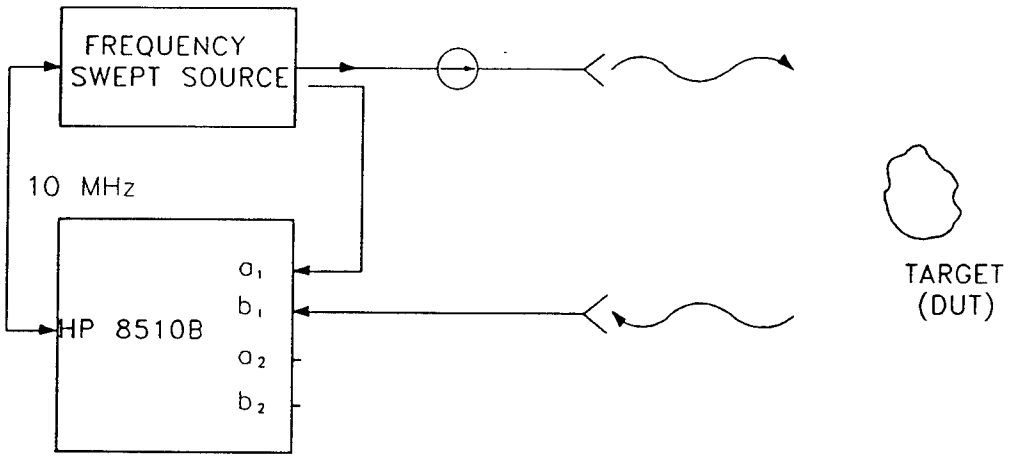

Figure 3.6. Scatterometer configuration.

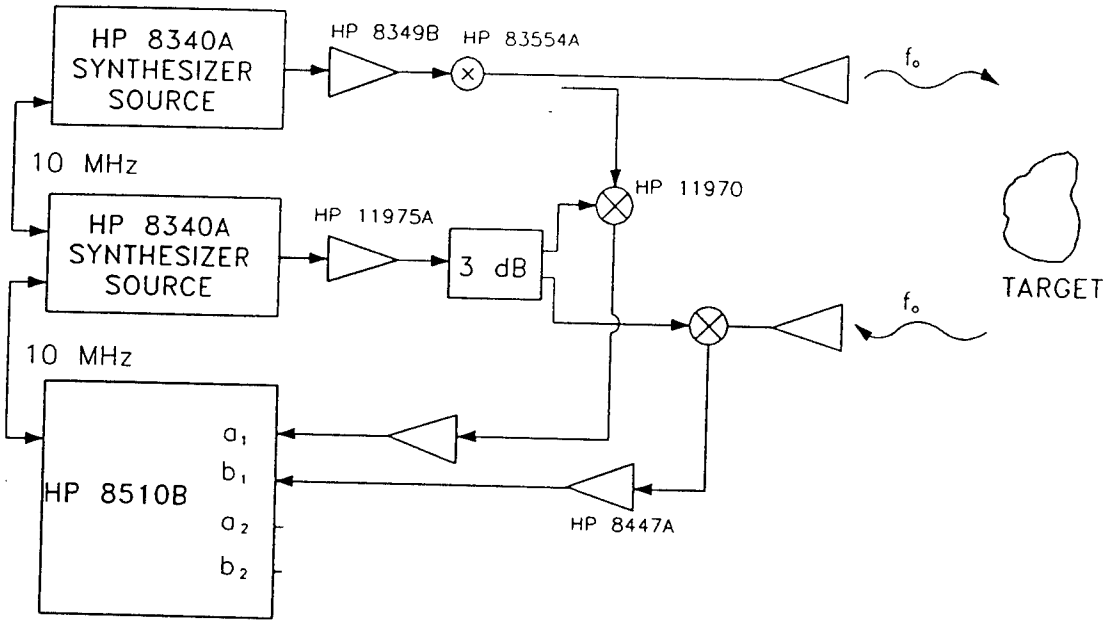

Figure 3.7. Millimeter–wave scatterometer configuration.

stored in memory and later subtracted from the response with the target in place. The remaining trace is due to the target alone [Hewlett–Packard, 1985].

The network analyzer based scatterometer is used for short range operation, typically 1 to 3 meters. Hence, unwanted signals due to multiple reflections might appear at the target range. These unwanted signals are removed using a time-gating option in the time domain operation mode. The signal is transformed back to the frequency domain to obtain the frequency response with the unwanted signal removed. See figure 3.16 for details.

When the system operates as a scatterometer there is a time delay between the transmitted and received signal. During this delay time the reference signal has changed frequency by an amount Δf, which introduces a phase error in degrees given by:

$$\Delta\phi = 360\Delta f\tau \tag{3.2}$$

where $\tau = 2r/c$ is the delay time.

In order to keep a phase coherent system, this error cannot exceed a few degrees over the delay time τ. One alternative to overcome this problem is to use a frequency synthesizer source. In this case, the transmitted signal is stepped in frequency instead of continuously swept to keep the reference signal at the same frequency as the received signal. This is only true for short range measurements where the delay time τ is short [Ulaby and Elachi, 1990].

For a scatterometer with a continuously swept (CW) frequency, the phase error is related to τ and the sweep rate, f_s, by the relation $\Delta\phi = 360 f_s \tau^2$. For a phase error of less than one degree and $f_s = 20$ MHz/ms [Hewlett–Packard, 1987], $\tau \leq 373$ ns (or ≤ 56 m). Therefore, a scatterometer operating in the range of 1 to 3 meters has a negligible phase error. In conclusion, network analyzers can operate effectively by using stepped frequency or swept frequency mode.

So far the discussion of the scatterometer configuration has been confined to a single polarization. In order to measure the full scattering matrix of a target, four different combinations of antenna polarization have to be obtained with an orthogonal basis. In the next section the development of a network analyzer based polarimetric scatterometer will be discussed in more detail.

3.4 Polarimetric Scatterometer

To obtain the full complex scattering matrix of a target, measurements with four different combinations of linear antenna polarization are performed. Using a network analyzer based scatterometer the detection, processing and data transfer are supplied by the unit, and the design is confined to RF hardware only. With this in mind, the designer has different options to build a polarimetric scatterometer in a short amount of time. Figure 3.8 shows three alternative ways to build a polarimetric scatterometer. All of them are dual antenna systems to avoid the noise associated with a single antenna at high frequencies.

A block diagram of the polarimetric scatterometer developed in the Microwave Remote Sensing Laboratory is shown in figure 3.9. The system operates in the same way as the one in figure 3.7, the only exception being the introduction of a polarizer switch and a rotary joint before the transmitter and receiver antenna respectively, to obtain the antenna polarization desired.

All the waveguide components, such as couplers, mixers and multipliers are contained in a separate aluminum box which may be mounted in different configurations. The input to the box are the test and local oscillator signals after the amplification. The output are the reference and received signals (a_1 and b_1) before the IF amplification takes place. The box is also connected to the computer via a General Purpose Input Output (GPIO) card which drives different digital boards inside to change angle of incidence, receiver and transmitter polarization

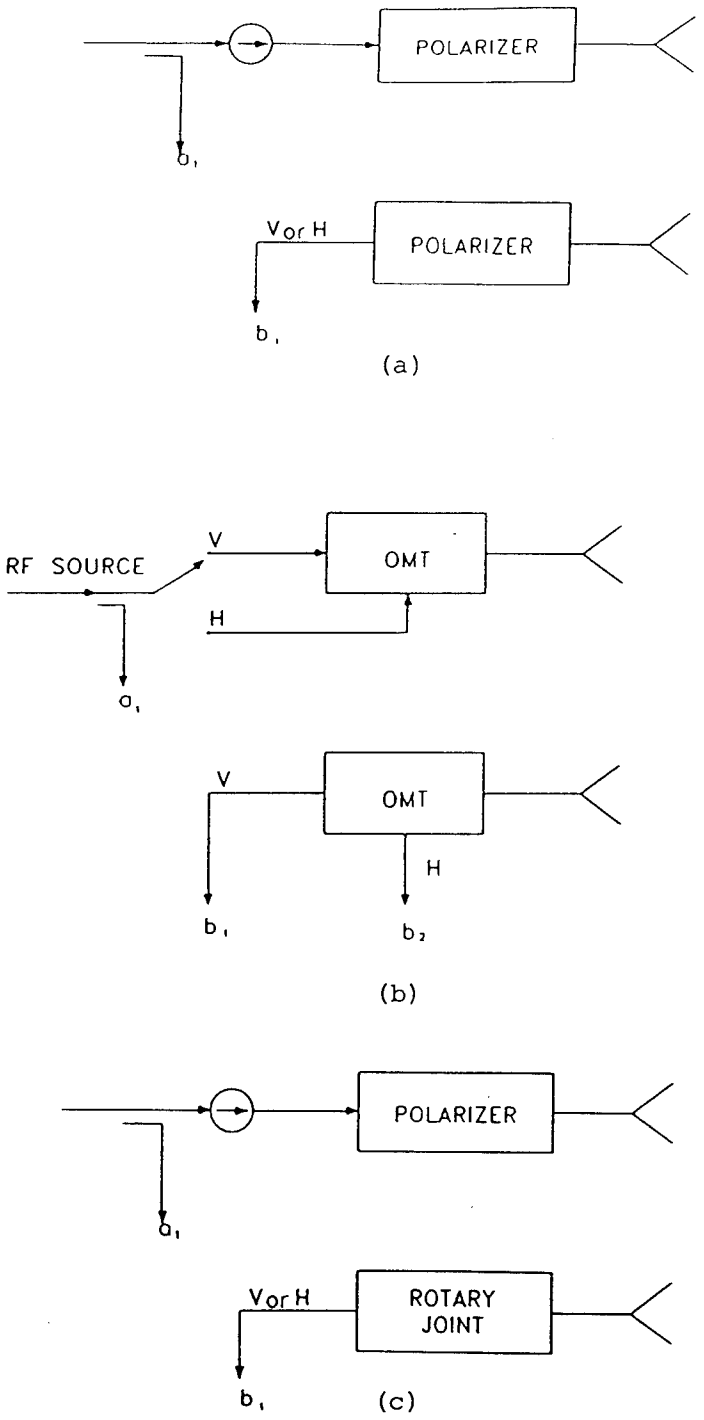

Figure 3.8. Two antenna system using polarizers (a), orthomode transducers (b), polarizer and rotary joint (c)

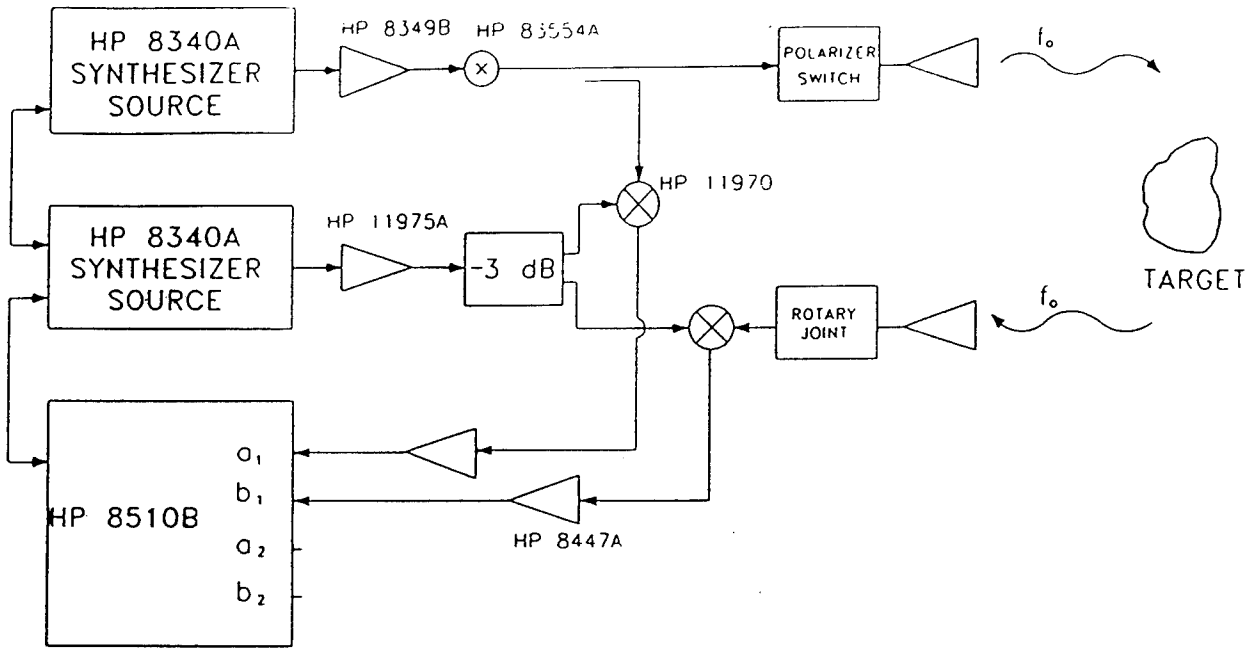

Figure 3.9. Block diagram of MIRSL's polarimetric scatterometer.

automatically. Communication between the network analyzer and the rest of the system is accomplished via an HP–IB cable. Connecting this cable in parallel to a computer any instruction executed by the network analyzer is also programmable. This cable is also used to transfer the processed data to the storage media. A detailed discussion of the system follows below.

3.4.1 Polarization Switch

The Alpha 145A polarization switch [Alpha, 1986], located immediately before the transmitter antenna is a TE_{11} mode device with both the input and output in circular waveguide. This unit is continuously adjustable with a drive current over a ± 90 rotation of the E-field. It also provides a means of rapid or remote controlled polarization change (5-10μ sec). Since this is a Faraday rotation device, it will be frequency sensitive and a different drive current for every single frequency within a bandwidth is needed to keep the rotation constant at all times. The instantaneous bandwidth of these devices is limited to approximately 1% of the center frequency for a fixed current value. In the case of a step frequency polarimetric scatterometer transmitting 51 frequencies over a 2 GHz bandwidth, an input current to the switch that varies along the same RF bandwidth is required to keep the rotation at 90° (or 0°) for all the frequency points. A data sheet (see Appendix A) supplied by the manufacturer shows a table of the current applied to the switch to achieve a 90° rotation versus frequency. In this case the data were supplied every 0.5 GHz over the range of 34 to 36 GHz. A simple circuit using two operational amplifiers was built to supply the right current to the polarization switch at every point. The circuit shown in figure 3.10 has two stages, the first one is a voltage inverter followed by a voltage to current converter which drives the switch [Whitt *et al.*, 1987]. The input voltage of this circuit is generated by the HP 8340B synthesized sweeper (test

signal). The voltage changes 51 times in equal steps from 0 to 10 V corresponding to the 51 frequency points transmitted by the same device.

Adjusting the variable resistors in the circuit, a line intercepting all the current points in the data sheet is created. In this fashion, a rotation of 90° along the whole bandwidth is produced. The GPIO card used along with the HP 9000 series computer drives a 12V DC relay to switch between vertical and horizontal polarizations (i.e. relay open = V, relay closed = H).

Since the maximum RF bandwidth of the polarizer switch is 2 GHz, this is the maximum bandwidth allowed by the system which gives a range resolution of 7.5 cm.

3.4.2 Rotary Joint

Kevlin 1123 rotary joint is a TE_{10} device with both input and output in rectangular waveguide (WR-28). The input is fixed while the output can rotated physically 360°. For the purpose of measuring the scattering matrix, only two positions are of interest, 0° and 90° rotation. These two polarizations are also obtained automatically using a GPIO card. The rotary joint is adapted to be rotated with a step motor to obtain the desired receiver polarization. The GPIO drives a Hurst motor control card that is inside the box containing the RF front end. The motor control card is especially designed to be used with step motors with an error of less than .1 degrees. Diagrams of the control card are attached in Appendix E.

3.4.3 Transmitter Antenna

The Millitech's SFH-28 scalar horn antenna [Millitech, 1986] is symmetrical both physically and electromagnetically, and therefore lend themselves to multiple polarizations operation. The SFH-28 antennas have nearly identical beamwidths and low sidelobes in both the E and H planes. The antenna cross-polarized response is

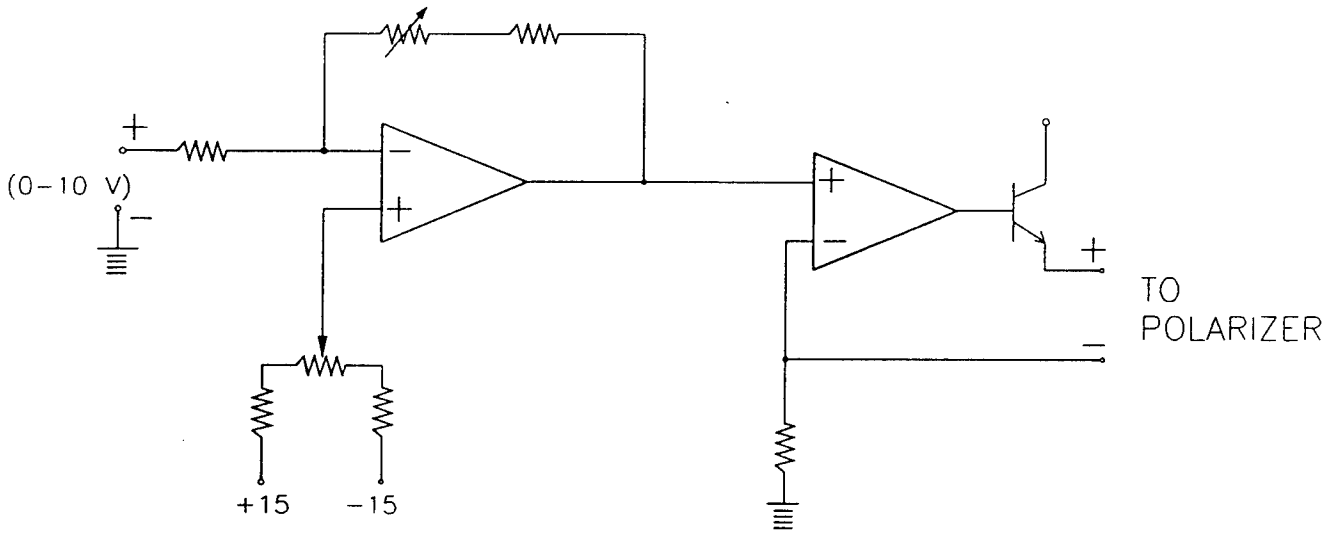

Figure 3.10. Current driver circuit for polarizer

typically around -30 dB. The standard design provides a 25° beamwidth and 17 dB gain. See Appendix B for data sheet supplied by Millitech.

The input to the antenna is a circular waveguide which matches the output of the polarization switch. Any polarization produced with the switch will be propagated to the space through the antenna. The frequency range of interest in this case is 34-36 GHz, for a center frequency of 35 GHz. The far–field of the antenna is given by [Balanis, 1982]:

$$FF = \frac{2D^2}{\lambda} = \frac{2(.0254)^2}{.00857} = .15 \text{ m} \tag{3.3}$$

where D is the diameter of the antenna and $\lambda = c/f$.

3.4.4 Receiver Antenna

The receiver's antenna is a Millitech's Standard Gain Horn (SGH-28) [Millitech, 1986]. They are solidly constructed to withstand rough handling. The antenna has a gain of 25 dB typical at 35 GHz. At this frequency (f) the beamwidth at the H and E planes is calculated from [Stutzman and Thiele, 1981]:

$$\begin{aligned} \beta_H &= 78\lambda/A = 78(.00857)/.049 = 13.6^\circ \\ \beta_V &= 54\lambda/B = 54(.00857)/.037 = 12.5^\circ \end{aligned} \tag{3.4}$$

where A and B are the width of the antenna aperture in the H and E plane, respectively, and $\lambda = c/f$.

The far field is calculated from 3.3 as;

$$FF = \frac{2D^2}{\lambda} = \frac{2(.049)^2}{.00857} = .56 \text{ m} \tag{3.5}$$

where D is the maximum dimension of the antenna, A.

The input of this antenna is rectangular waveguide and is connected to the output of the rotary joint. To obtain a set of orthogonal polarizations (V and H) the antenna is physically rotated with the rotary joint. See Appendix C for specifications.

3.4.5 *Noise Figure*

The process of detection and downconversion of the received signal results in the addition of excess noise due to circuit losses, noise generated within the semiconductor used in the mixers, and noise generated in the IF amplifiers that follows the mixers.

The Noise Figure, F of the receiver is a measure of the efficiency and noise contribution of the receiver components. F is defined as:

$$F = \frac{S_i/N_i}{S_o/N_o} \tag{3.6}$$

where,

S_i = input signal power

S_o = output signal power

N_i = input noise power

N_o = input noise power.

The ratio S/N is known as the signal to noise ratio. If a receiver does not add noise then it will amplify the input signal and input noise by the same amount G or gain of the receiver. If the network does introduce noise, then F is greater than unity.

For the cascade network shown in figure 3.11 consisting of a mixer followed by an IF amplifier, the total noise figure is given by [Skolnik, 1980]:

$$F_T = F_1 + \frac{F_2 - 1}{G_1} \tag{3.7}$$

where,

F_1 = noise figure of the mixer

G_1 = gain of the mixer

F_2 = noise figure of the IF amplifier.

Figure 3.11. Cascaded network for the calculation of total noise figure.

The gain of the mixer is expressed as $1/L_C$ where L_C is the conversion loss and is defined as:

$$L_C = \frac{\text{available RF power}}{\text{available IF power}} \tag{3.8}$$

For a high conversion loss, as is the case for a harmonic mixer, the total noise figure is approximated by [Schaubert, 1988]:

$$F_T \approx L_C\, F_2 \quad or \quad F_T(\text{dB}) = L_C(\text{dB}) + F_2(\text{dB}) \tag{3.9}$$

Substituting values of L_C and F_2 given by the manufacturer, the noise figure of the system is approximately (see Appendix E),

$$F_T(\text{dB}) = 22 \text{ dB} + 7 \text{ dB} = 29 \text{ dB}$$

This is a very high noise figure for any receiver, but the real limiting factor is the thermal level or the minimum detectable signal, which is determined by a product of noise figures and system bandwidth. This is discussed in the next subsection.

3.4.6 Dynamic Range

The minimum signal level which is equal to the noise floor is given in terms of noise figures and system bandwidth by [Schaubert, 1988]:

$$P_{min} = N = kTB_{IF}F_T \tag{3.10}$$

where,

k= Boltzman constant ($1.38\times10^{-}23$ J/K Hz)

T= Ambient temperature (300 K)

B_{IF}= Narrower IF bandwidth in the system (Hz)

F_T= Total noise figure (29 dB).

Because the network analyzer is a coherent device, its bandwidth is very narrow and noise flow is not a limiting factor. For the second IF conversion (100 kHz) a

bandpass filter with a 10 kHz bandwidth (B_{IF}) [Hewlett-Packard, 1987] is employed and 3.10 is reduced to:

$$P_{min} = N = -80.8 \text{ dBm}$$

The maximum detectable signal for the network analyzer is given by HP as -10 dBm. This gives a receiver dynamic range (RDR) of;

$$RDR = P_{max} - P_{min} = 71 \text{ dB} \tag{3.11}$$

With the HP 8510B, an averaging factor up to 128 can be used without significantly slowing down the trace update time. This average is performed at each frequency point and reduces the system noise floor proportional to the square root of the averaging factor. For an average factor of 128 the noise floor is reduced by 10.5 dB, expanding the dynamic range up to 81.5 dB.

3.4.7 Signal to Noise Ratio (SNR)

The signal to noise ratio is calculated experimentally for certain ranges using a trihedral corner reflector. For this scatterometer ranges of interest are between 1 to 3 meters.

Figure 3.12 is the power returned from the corner reflector in dB for four different ranges. The return is displayed using the time domain option of the network analyzer. The values are normalized to unity (0 dB) for a range of 1.38 meters. Figure 3.13a shows the SNR versus range for the corner reflector using the data from figure 3.12. Figure 3.13b is the SNR versus range for fresh snow, obtained for three different ranges.

3.4.8 Unambiguos Range

Another consideration in the RCS measurements using a Network Analyzer based scatterometer is called the alias-free range or unambiguous range. The frequency domain data are taken at discrete frequencies and when changed to the time

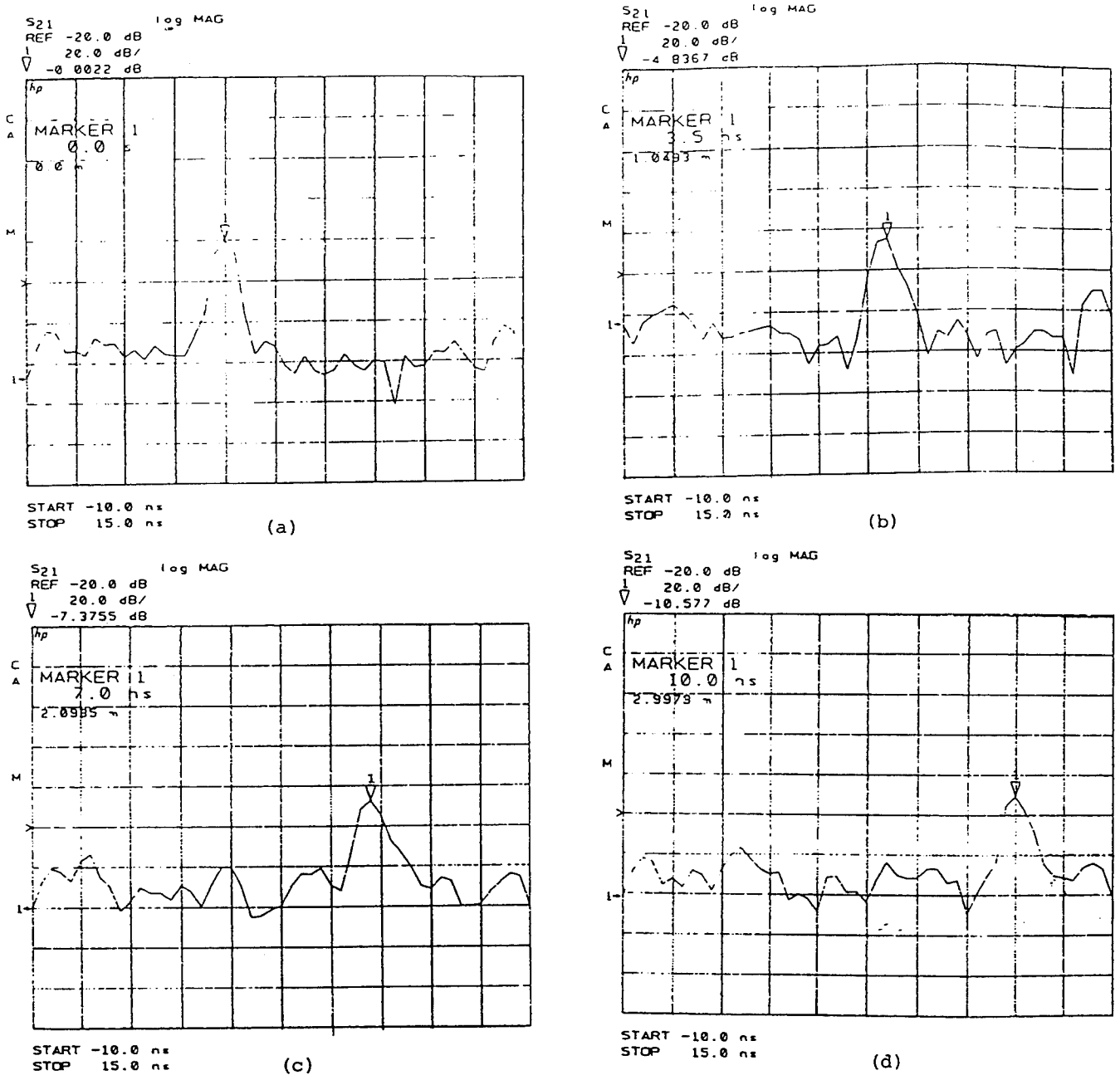

Figure 3.12. Power return for 1.38 m (a), 1.90 m (b), 2.42 m (c), 2.88 m (d).

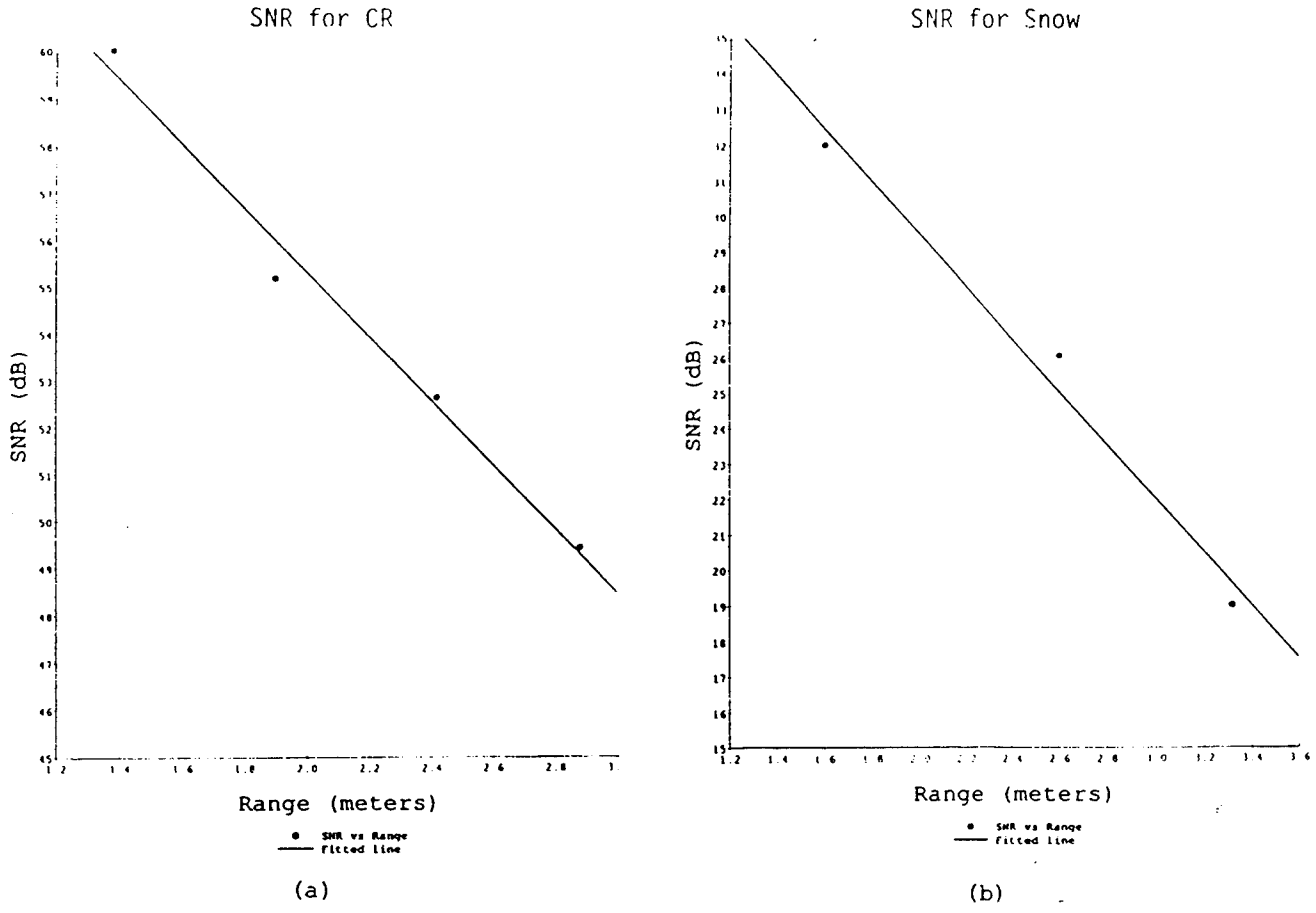

Figure 3.13. SNR for corner reflector (a), fresh snow (b).

domain using the Fourier techniques of the network analyzer, periodic repetitions called aliasing are present [Hewlett–Packard, 1985]. The alias-free range of the system is calculated from equation 2.11.

Figure 3.14 is a graph of frequency points versus unambiguous range for an RF frequency bandwidth of 2 GHz. The number of points (51 to 801) are selectable by the user of the network analyzer. It is good to know that the range resolution of the system is not affected by the spacing between frequencies Δf, but by the RF bandwidth. The system uses a maximum RF bandwidth of 2 GHz due to the limitations of the polarization switch. The range resolution is then calculated from equation 2.12 as 7.5 cm.

3.4.9 System Stability

For an accurate radar cross section measurement, stability of the overall system is necessary. Figure 3.15 shows a plot of received power from a 3" trihedral corner reflector at 1.38 meters from the antennas over a period of two hours. The system has to be turned on for at least half hour previous to start the measurements to achieve temperature stabilization. By looking at the plot it is notice that no frequency or amplitude instabilities are present in the system, this is inferred by comparing the position and the peak power of the returned signal at every sample.

3.4.10 System Performance

To verify the proper operation of the system, the radar range equation (2.19) is solved to calculate the power (P_R) at the terminals of the receive antenna. This calculation is later compared to experimental results. The equation was solved for a σ_{max} = -3.17 dB (3" corner reflector) [Ulaby *et al.*, 1982] placed at a distance of 1.38 meters from the antenna at a center frequency of 35 GHz.

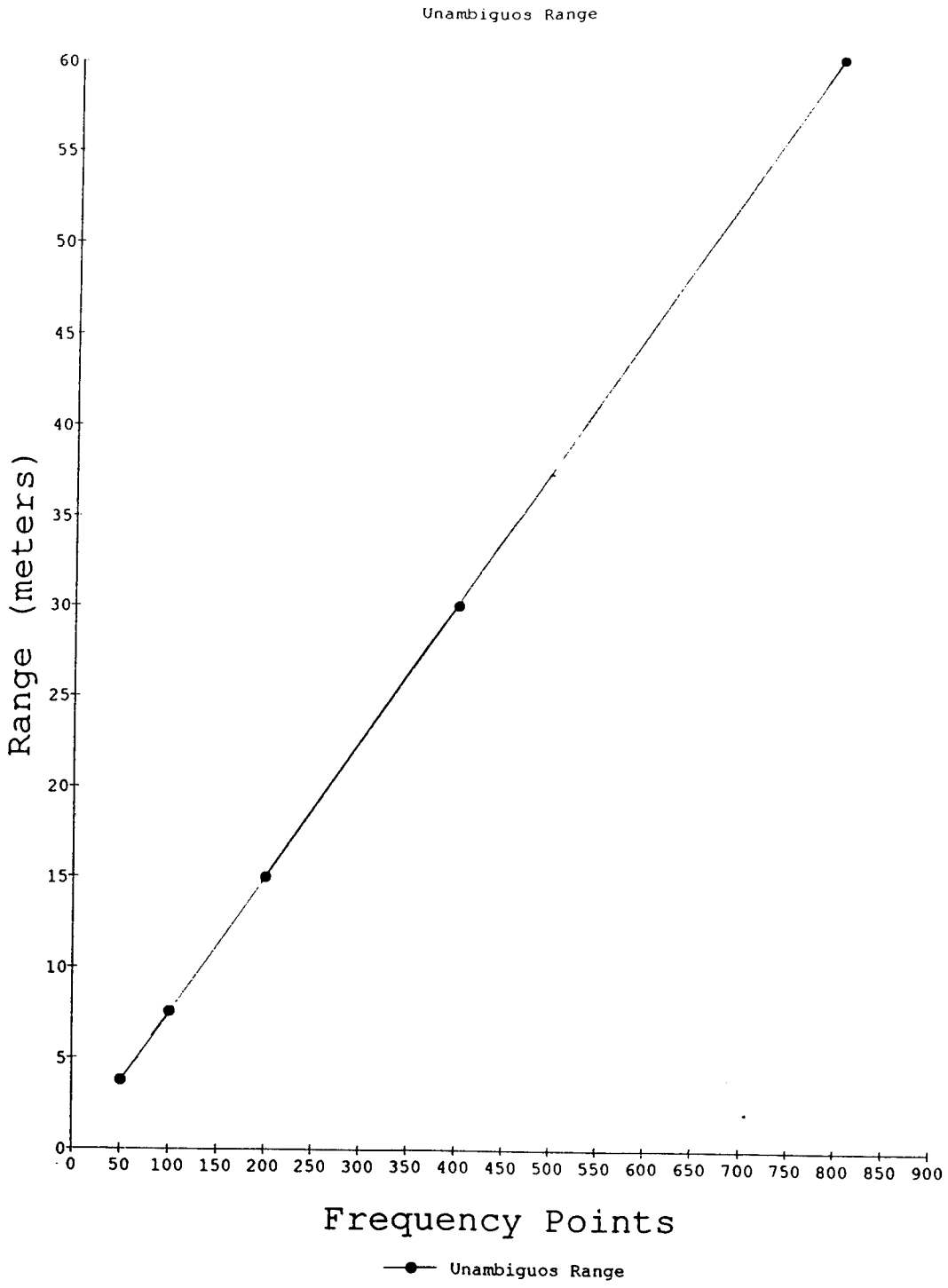

Figure 3.14. Frequency points versus unambiguos range for B = 2 GHz.

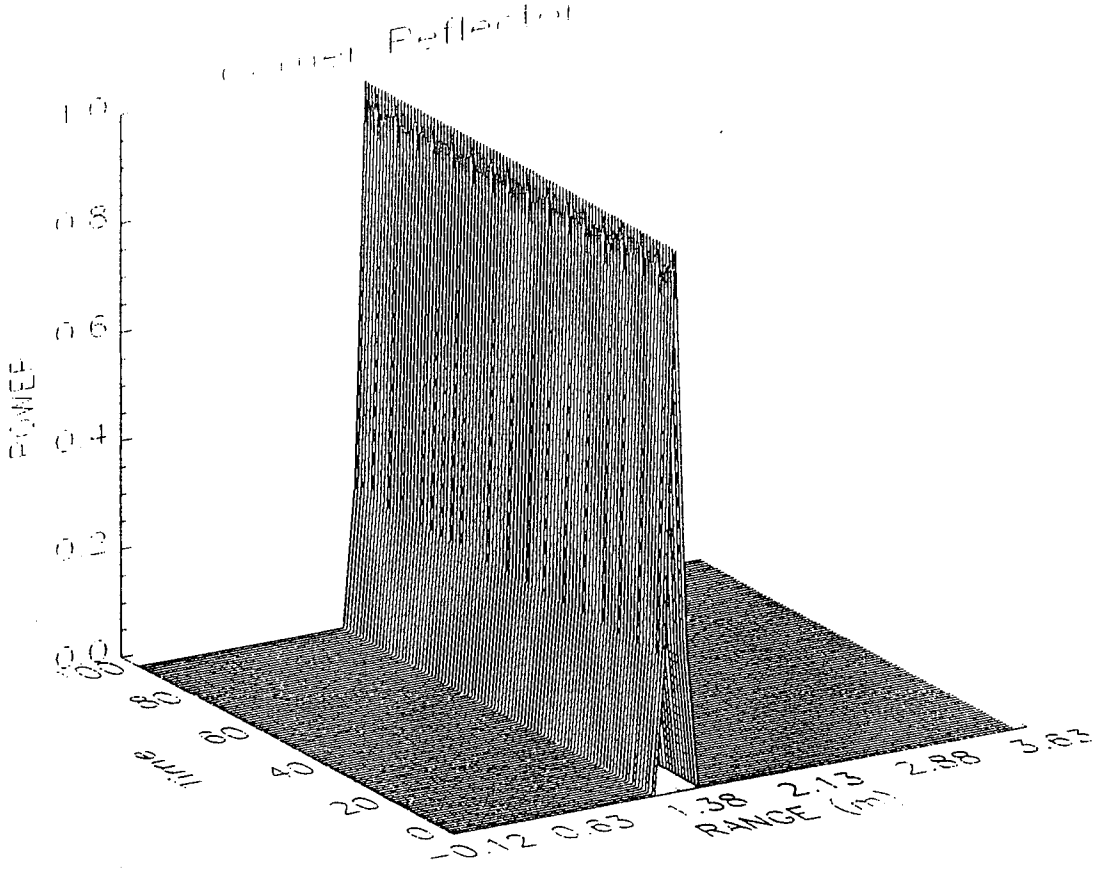

Figure 3.15. A response of a trihedral corner reflector over a two hour period.

The output power from the frequency upconverter (refer to figure 3.9) is 10 dBm, losses from the isolator, directional coupler and polarizer attenuates the transmit power to 8.5 dBm. With all the other parameters known, equation 2.19 yields,

$$P_R = \frac{(7.1 \times 10^{-3})(.00857)^2(316)(50)(.482)}{64\pi^3(1.38)^4} = -32.6 \text{ dBm}$$

This is the received power at the antenna terminals. Before processing the signal, insertion loss from the rotary joint, isolator and the harmonic mixer contributes to the attenuation of the signal, then,

$$P_R(\text{dB}) = -32.6 \text{ dBm} - 2 \text{ dB} - 1 \text{ dB} - 21 \text{ dB} = -56.6 \text{ dBm}$$

The signal is then amplified (+20 dB), detected, processed and displayed. A power of approximately -36.6 dBm should be measured. If the time domain option is selected the power is then increased by the number of points N. For 51 frequency points the received power is measured as,

$$P_R(\text{dB}) = -36.6 \text{ dBm} + 10\,log(51) = -19.6 \text{ dBm}$$

Comparing the calculated received power with the experimental results shown in figure 3.16, it is observed that the measurement agrees very well with the calculations (within .03 dB).

3.4.11 Time Domain Gating

For short range measurements leakage signals due to mismatch within system can be present at the target range. When the signal is displayed in the time domain, time-gating can be used to isolate the return due to targets at a particular range. Figure 3.17 shows the process to isolate the signal of interest and then transformed back to the frequency domain. However, it is important to note that with the use of time-gating the unwanted signals are removed mathematically, these signals are still physically present in the receiver and can limit dynamic range of the system [McCarter, 1989].

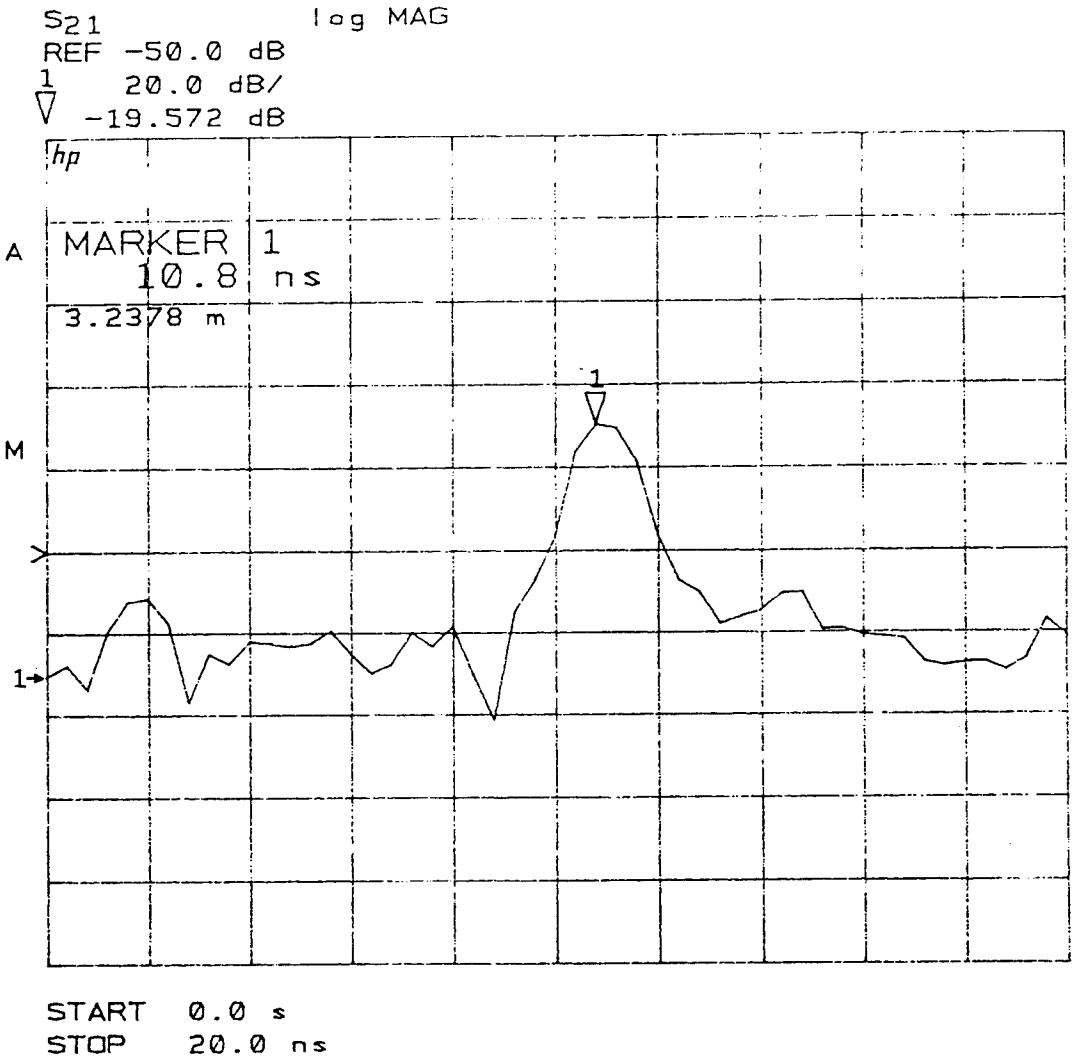

Figure 3.16. P_R for a 3" corner reflector at 1.38 meters.

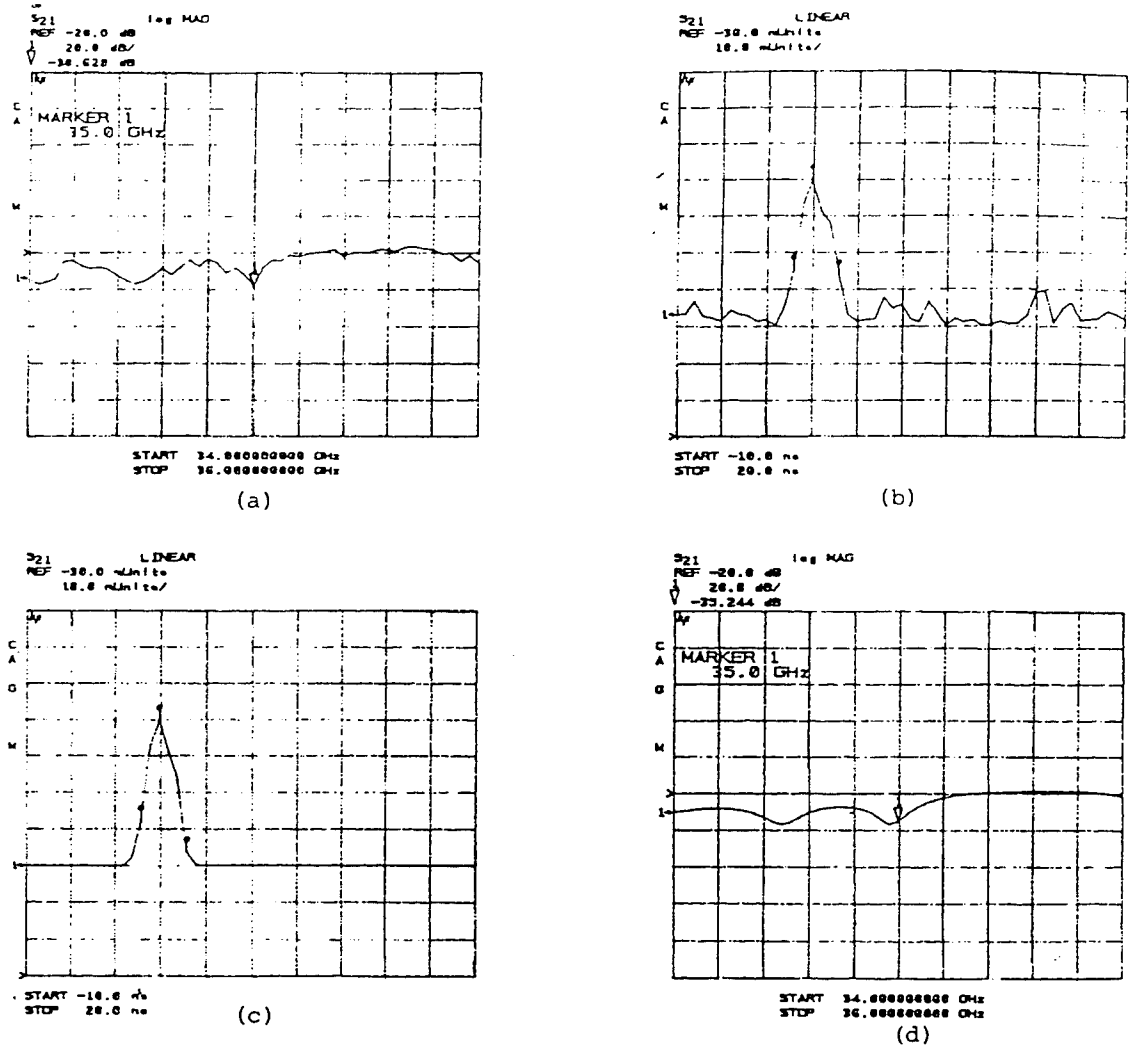

Figure 3.17. Frequency domain (a), Time domain (b), Time gating (c), Frequency response after time gating (d).

3.4.12 *Measurement Speed*

By using the HP 8510B and an HP 8340B synthesizer source in the step frequency mode the data acquisition time becomes 50 ms per point. When the averaging is turned on, it is done on a point by point basis but an average factor up to 128 can be used without slowing down the trace update time. With the use of an HP 8360A synthesizer source the acquisition time might be reduced two to three times [McCarter, 1989]. Figure 3.18 is a plot of time versus frequency points for both the HP 8340B and the HP 8360A.

The step mode is slower but it provides improved frequency stability that results in more accurate measurements and greater dynamic range. With such a slow system, polarimetric measurements only for stationary targets are possible. A full complex scattering matrix is computed in more than one minute taking in account the time that it takes to the step motor to change the polarization of the receiver antenna. The acquisition time may be cut in half when the receiver has a vertical and horizontal channel operating at the same time (OMT at the receiver).

In the case of fluctuating (moving) targets, if the decorrelation time of the received voltage is less than the time it takes the radar to measure the scattering matrix of the target, the matrix will be uncorrelated, leading to erroneous results.

3.4.13 *Independent Samples*

For an accurate estimate of σ^o from a stationary distributed target, the measurement has to be statistically independent [Narayanan, 1988]. This is achieved by averaging a number of independent samples. The samples are obtained by moving the radar by one half the aperture diameter of the antenna.

This is another time-consuming task in the remote-sensing of stationary targets at short range. Scattering measurements of snow were performed at the Cold Regions and Research Engineering Laboratory, Hanover, N.H., during the winter

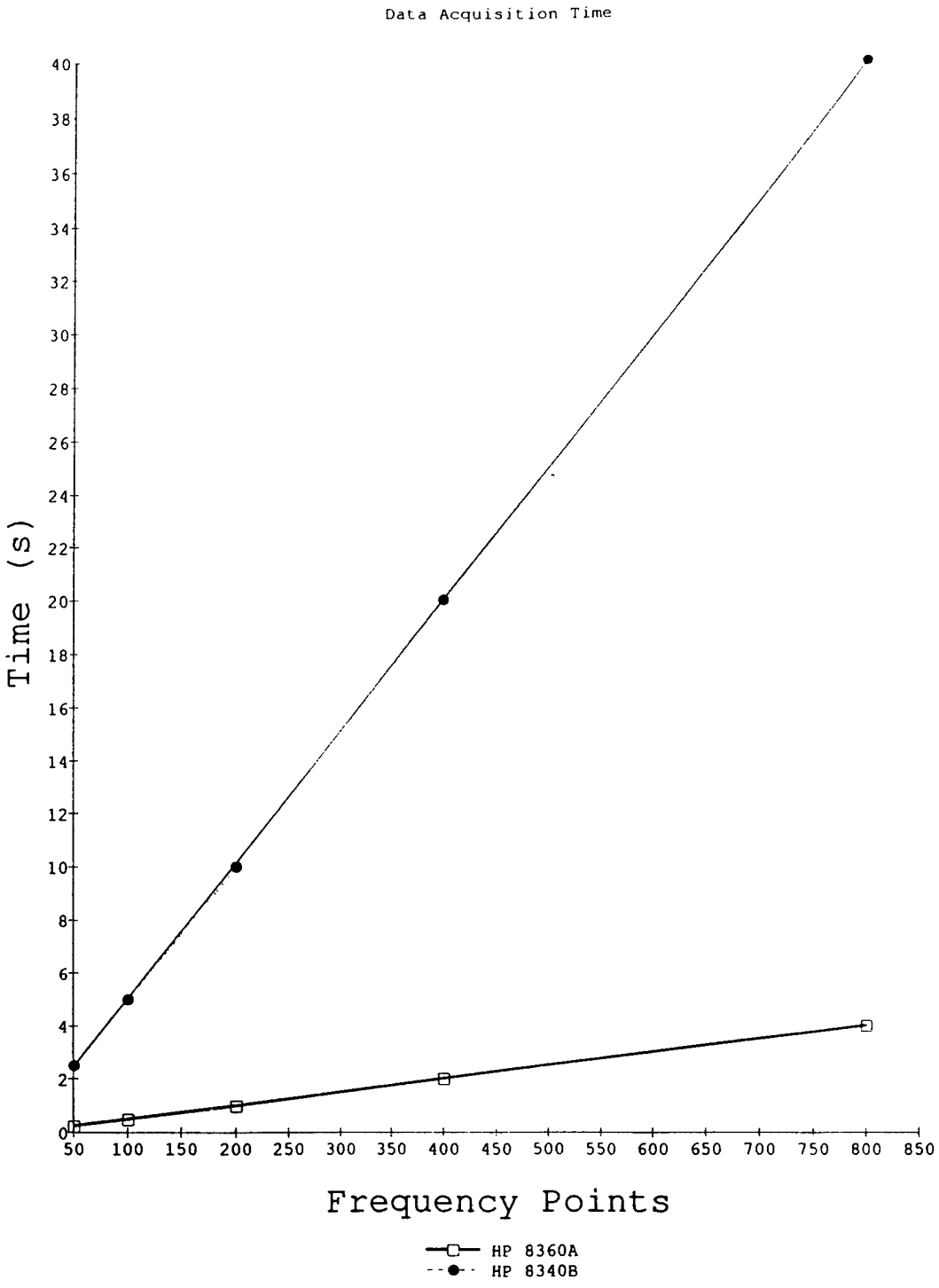

Figure 3.18. Measurement speed, time versus frequency points.

of 1990–91 using the system described in this thesis. The experiment shows that a set of 100 samples and two polarizations (VV,VH) at a specific incidence angle takes over an hour and 15 minutes.

3.5 RCS Measurements

Basically we are interested in two types of targets, the point target (corner reflector) which has a well known RCS and is used for calibration purposes of the radar (this will be further discussed in the next chapter). The second type of target is the distributed target which consists of many scatterers located within the radar resolution cell defined by the antenna beam shape and the pulse length. Since the number of scatterers illuminated by the radar is a function of the radar resolution cell, the reflected energy is also a function of the cell size.

The radar range equation gives the power return from these types of target as:

1. Point Target

$$P_{Rp} = \frac{P_t G_T G_R \lambda^2 \sigma_p}{(4\pi)^3 R_p^4} \tag{3.12}$$

where,

P_{Rp} = received power from point target

R_p = range to point target

σ_p = RCS of point target

P_t = transmitted power

G_T = transmit antenna gain

G_R = receive antenna gain

λ = wavelength

The transmit and receive gain are considered constants if the target is along the boresight of the transmit and receive antenna when they are collocated.

2. Distributed Target

The form of the radar equation to determine the incremental received power from a surface is given by [Narayanan, 1988]:

$$dP_R = \frac{P_t \lambda^2 G_T G_R \tau}{64\pi^3 R^4} f_T(\theta,\phi) f_R(\theta,\phi) \sigma^o dA \tag{3.13}$$

where,

$f_T(\theta,\phi)$ = transmit antenna power pattern

$f_R(\theta,\phi)$ = receive antenna power pattern

σ^o = average backscatter coefficient of the target under consideration ($\sigma^o = \sigma/A_{ill}$, A_{ill} = illuminated Area)

On making appropriate substitutions and integrating we obtain the total received power for two cases, the beam–limited case and the pulse–limited case. This problem was already solved by Narayaran, 1988. Assuming a Gaussian power pattern for the transmit and receive antennas given by:

$$f_T(\theta,\phi) = \exp\left(\frac{-4\ln 2(\theta^2+\phi^2)}{\theta_{BT}^2}\right) f_R(\theta,\phi) = \exp\left(\frac{-4\ln 2(\theta^2+\phi^2)}{\theta_{BR}^2}\right) \tag{3.14}$$

where θ_{BT} and θ_{BR} are the 3 dB beamwidth of the transmit and receive antennas, respectively.

For the beam–limited case the illuminated area on the surface can be computed by considering the geometry of figure 3.19. In this case the illuminated area is delimited by the beam of the antennas. The received power is given by:

$$P_R = \frac{P_t \lambda^2 G_T G_R \sigma^o \theta_{BT}^2 \theta_{BR}^2 \pi}{64\pi^3 4\ln 2 R^2 \cos\theta_i (\theta_{BT}^2 + \theta_{BR}^2)} \tag{3.15}$$

For the system under consideration:

θ_i = incident angle

$\lambda = 0.0086$ m

$\theta_{BT} = 27^o$

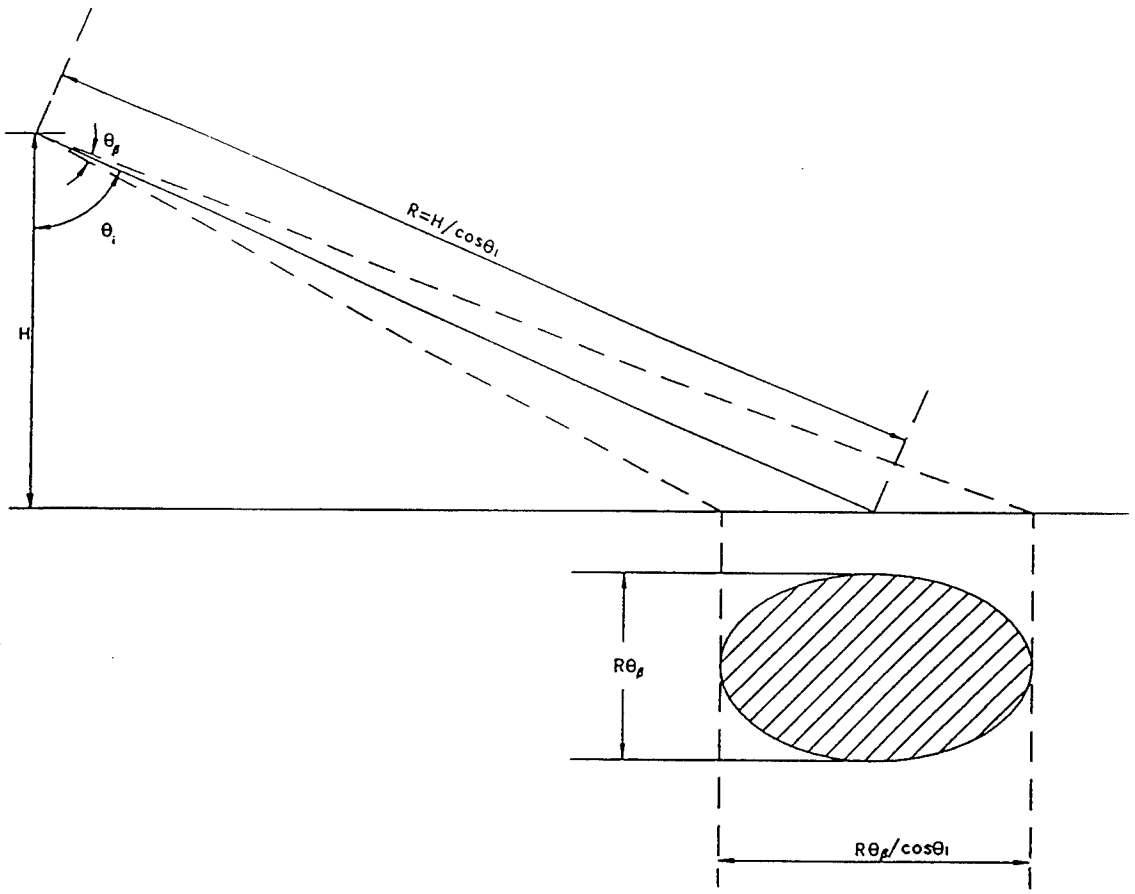

Figure 3.19. Geometry for the beam–limited case.

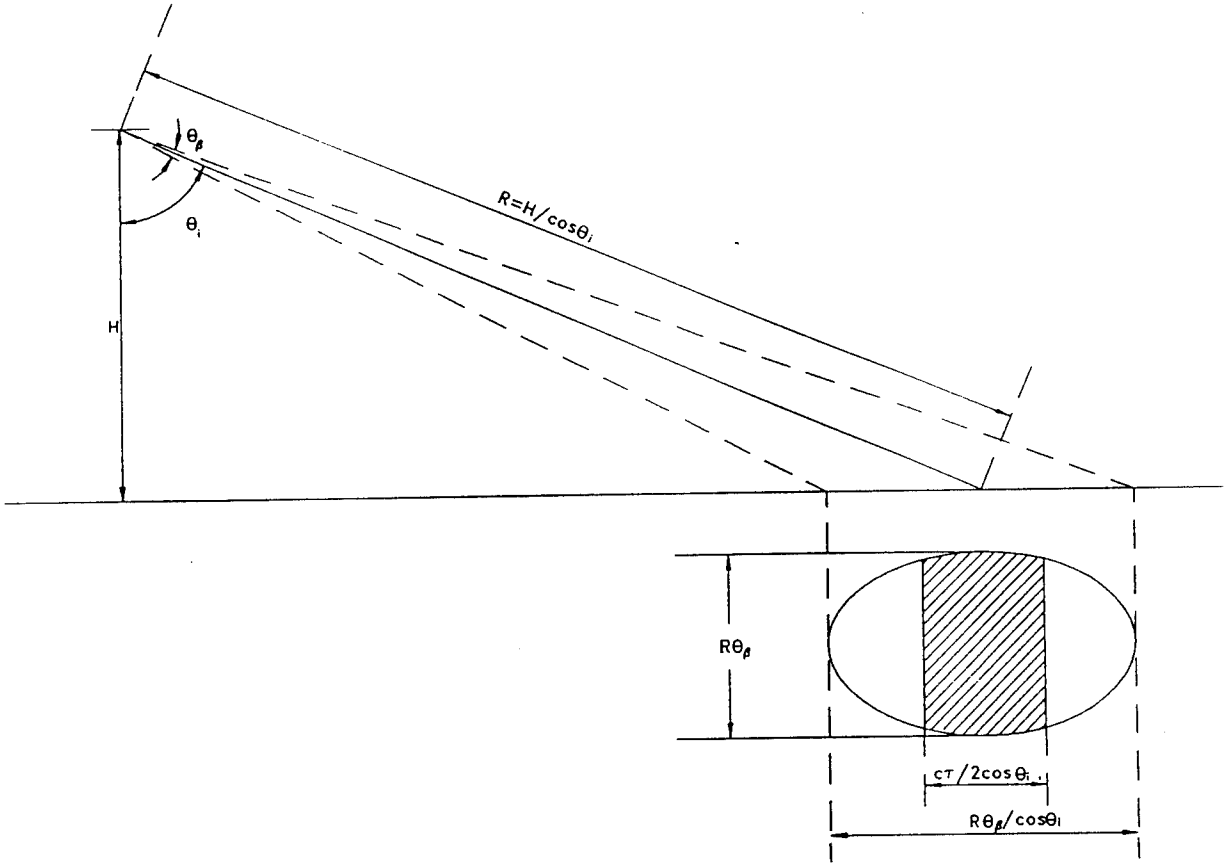

Figure 3.20. Geometry for the pulse–limited case.

$\theta_{BR} = 12^o$

R = range to the target

$P_R = |S_{12}|^2$

Solving for σ^o,

$$\sigma^o = 24(\frac{64\pi^3|S_{12}|^2 R^2 \cos\theta_i}{P_t\lambda^2 G_T G_R}) \tag{3.16}$$

For the pulse limited case the illuminated area is delimited by the pulse width, i.e. the range resolution is smaller than the area illuminated by the antenna beam. The geometry for the pulse–limited case is given in figure 3.20 and the received power is given by:

$$P_R = \frac{P_t\lambda^2 G_T G_R c\tau\sigma^o\theta_{BT}^2\theta_{BR}^2}{128\pi^3 R^3 \sin\theta_i\sqrt{\theta_{BT}^2 + \theta_{BR}^2)}}\sqrt{\frac{\pi}{4\ln 2}} \tag{3.17}$$

where,

τ = pulse duration ($1/B$) = .5 ns

$c = 3\times\ 10^8$ m/s

and all other parameters were specified above.

Solving for σ^o,

$$\sigma^o = 65.8(\frac{64\pi^3|S_{12}|^2 R^3 \sin\theta_i}{P_t\lambda^2 G_T G_R}) \tag{3.18}$$

This two results are used to compute σ^o of a distributed target. The decision of which one to use (pulse or beam limited case) is discussed in the next chapter.

3.6 Volume Scattering

An analogous parameter to σ^o exists also for volume scattering. The parameter is called σ_v and is given by [Eaves and Reedy, 1987]:

$$\sigma_v = \sigma/V_{ill} \tag{3.19}$$

where V_{ill} is the illuminated volume. An easy way to consider volume scattering is considering the illuminated-volume as an elliptical cylinder. For the geometry shown in figure 3.21 the illuminated volume is given by [Eaves and Reedy, 1987]:

$$V_{ill} = \frac{\pi R^2 \theta_{eff}^2 c\tau}{8\alpha^2} \tag{3.20}$$

where α = beam shape factor for a Gaussian power pattern and

$\theta_{eff} = \frac{\sqrt{2}\theta_{BT}\theta_{BR}}{\sqrt{\theta_{BT}^2+\theta_{BR}^2}}$ is the effective beamwidth.

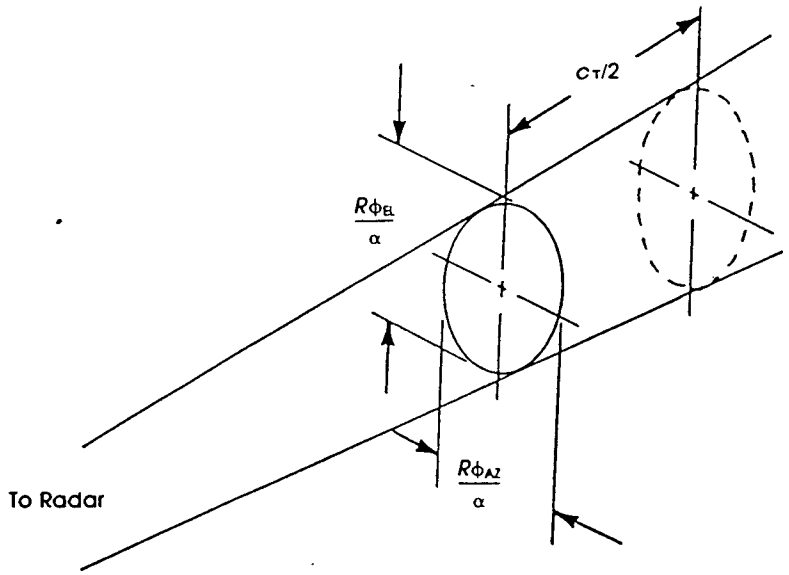

Figure 3.21. Geometry for illuminated volume.

CHAPTER 4

CALIBRATION

Calibration of a system permits correct measurements to be taken. A good relative calibration is accomplished if the measurements are repeatable, in this case the readings are considered precise. To consider the measurements accurate then a good absolute calibration has to be performed. The calibration is accomplished by referencing the received power of an unknown target to that of a target with known radar cross section (e.g. corner reflectors, conducting spheres, plates, etc.).

Three calibration procedures are discussed in this chapter. The internal calibration, which takes advantage of the internal error correction capabilities of the HP 8510B network analyzer. The external calibration which takes into account amplitude drifts in the system and permits absolute normalized radar cross section for a specific target to be calculated. Finally a calibration for coherent radars is applied to correct for polarimetric errors. Sources for this type of errors are from non-ideal antenna polarization characteristics, magnitude gain and phase imbalance between the transmitter and receiver and errors in the processing of phase and magnitude detection.

4.1 Internal Calibration

When corrected S-parameters measurements of a device under test are desired using an HP 8510B Network Analyzer, the system has to be first calibrated with a known calibration standard. Consider that a transmission measurement of

a device under test is desired ($S_{21} = b_2/a_1$). If no calibration is performed, unwanted signals are introduced in the measurement, leading to erroneous results of S_{21}.

For transmission measurements, choosing the "response" internal calibration option from the network analyzer removes systematic errors due to the frequency dependance of cables, connectors, amplifiers, and harmonic mixers. This is done using vector normalization of the the measured value to the response of a single known transmission calibration standard. The error model for the "Response" calibration consists (see figure 4.1) of a single error term E_τ. The measured value, S_{21M} (b_2/a_1) is equal to the actual response S_{21A} times E_τ.

The calibration standard for transmission measurement is a zero-length zero loss transmission line. This standard is called a "through" and is obtained by connecting the test set port #1 to the test set port #2. The frequency response of the "through" is known to be $1\angle 0°$. The vector difference between the measured value and the theoretical $(1\angle 0°)$ is the frequency response of the error term E_τ. The time domain response is given as an unit impulse at time equals zero.

When the test device is measured, the equation for the actual value is solved for each frequency point using the measured value and the appropriate error coefficient.

An error model for RCS measurements was developed [Hewlett-Packard, 1985] based on the frequency response model for S_{21} as discussed above. Figure 4.2 shows a flowgraph of the error model, in this case the measured value is given by:

$$S_{21M} = \frac{V_{receive}}{V_{transmit}} = b_2/a_1$$

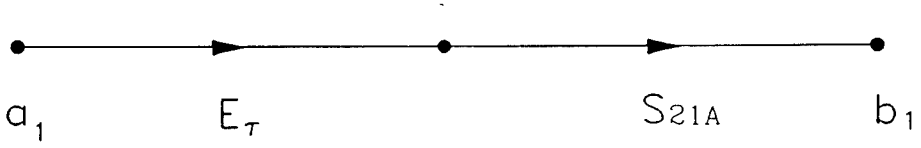

Figure 4.1. Single error term model.

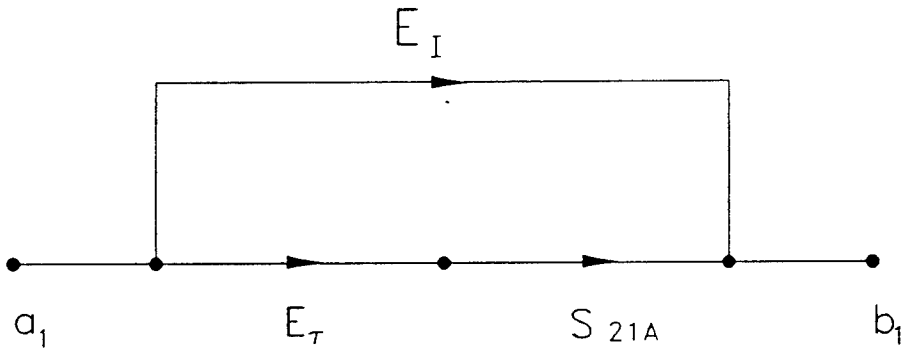

Figure 4.2. Error model for RCS measurements.

Another error term, E_I has been introduced to take into account error signals arriving in parallel with the main signal reflected from a target (for example, leakage between antennas and multiple reflections). A different equation will be solved to measure the actual S_{21A}.

Figure 4.3 shows the setup used for an internal calibration. Now the calibration standard is a corner reflector which ideally reflects all the power incident upon it with no losses. An imaginary zero-length zero loss transmission line is assumed up to the corner reflector completing a "through" connection between the receive and transmit antennas.

The corner reflector is placed in the far–field of the antenna ($\sim$ 1 m) and the error term E_τ, is calculated in the same manner (i.e. $S_{21M} = S_{21A} \times E_\tau$). All the measurements are now relative to the corner reflector response at the calibration distance. The error term E_I is calculated by pointing the radar to the sky, so that the reflections within the system and leakage between antennas are later subtracted from the returned signal. The actual power return (S_{21A}) from the target will be calculated for every frequency point by solving,

$$S_{21A} = \frac{S_{21M} - E_I}{E_\tau} \tag{4.1}$$

To illustrate this, an example is shown in figure 4.4. The returned power from a corner reflector is measured as -19.57 dB. After the internal calibration is performed, the returned signal is normalized to unity (0 dB) and is placed at zero seconds (Range = 0 meters). The range to the corner reflector is stored because the distance to the target measured by the radar is relative to this value. As an example figure 4.5 shows the same corner reflector that was moved to a distance of 2.4 meters from the radar. The real distance to the target under consideration will be, the range measured by the radar displayed in the time domain option plus the distance to the corner reflector at the moment

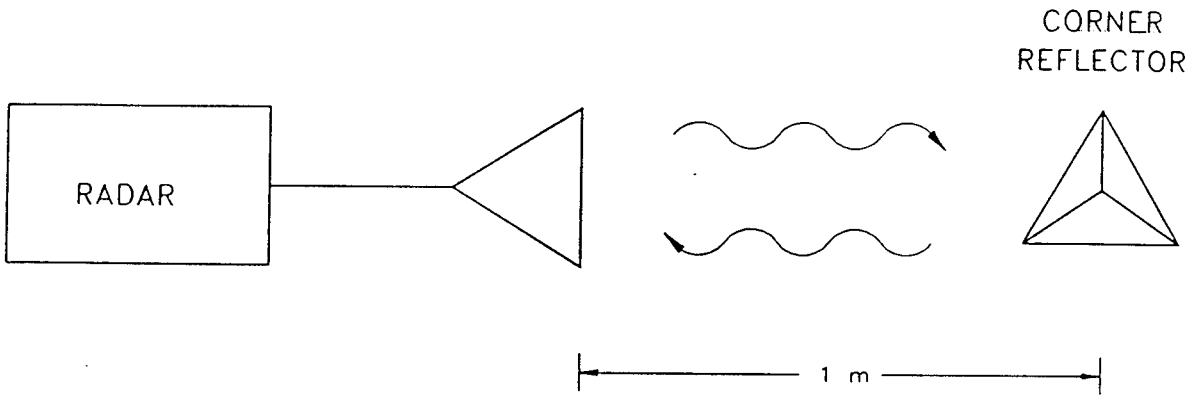

Figure 4.3. Internal calibration setup.

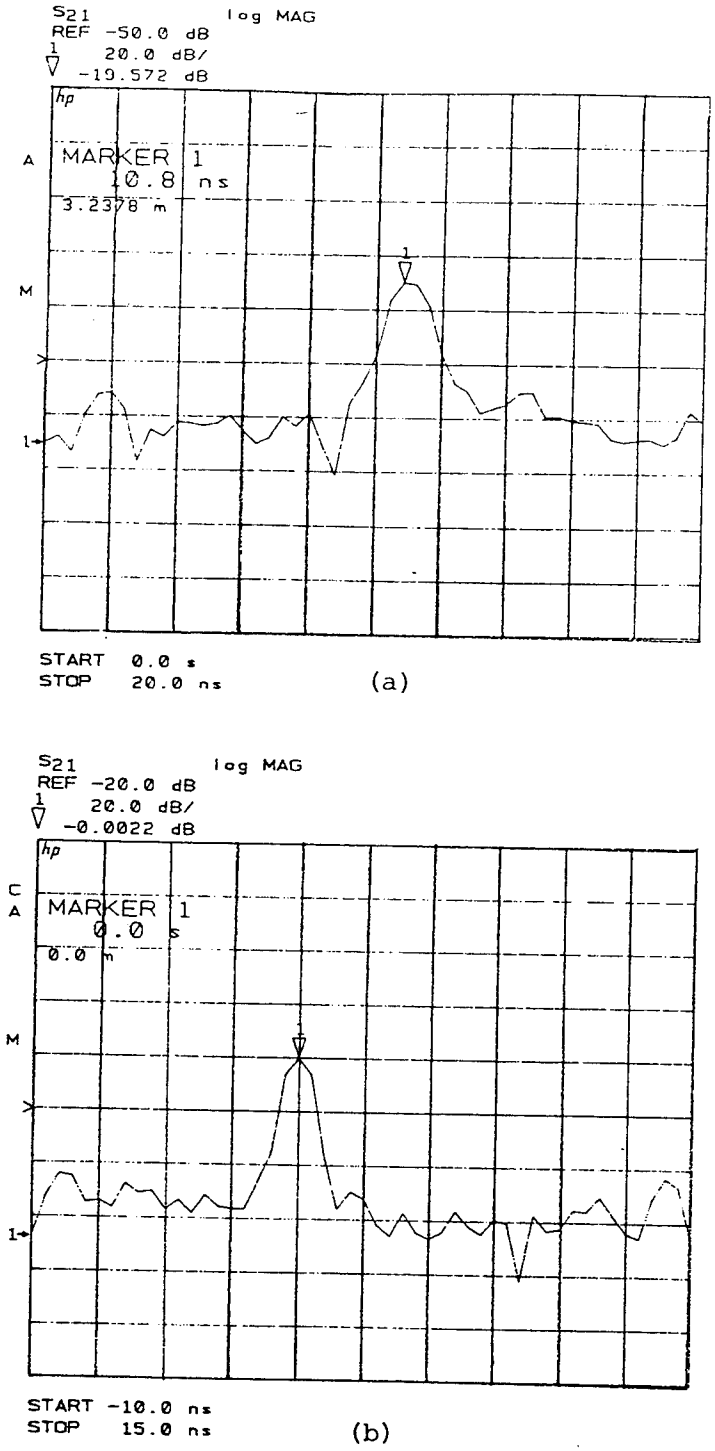

Figure 4.4. Corner reflector before (a), and after internal calibration (b).

of calibration. The calibration was performed at 1.38 meters and the marker value is 1.045 m (half of 2.0985 m) which yields a range of 2.425 meters, the difference of 2.5 cm is within the range resolution and is acceptable.

4.2 External Calibration

It is desirable to calibrate a scatterometer by measuring the returned power from a target of known radar cross section. In order to compute absolute radar cross section of a target systematic errors have to be removed through internal calibration. This errors are variables since the antenna gain and transmitter power may change with temperature, cable position or other variables. System errors will then change with time even though most of this variations are removed with the internal calibration. But differences between the signal path from the received and reference signal when a target is measured at different distances are not removed. To account for all this errors an external calibration with a point target of known radar cross section (corner reflector) is performed regularly during the collection of data.

Using equation 3.14, the received power from the corner reflector is calculated by,

$$P_{CR} = \frac{P_t \lambda^2 G_T G_R \sigma_{CR}}{64\pi^3 L_s R_{CR}^4}$$

the parameter L_s has been added to account for system losses, and the subscript CR refers to corner reflector. From this a calibration constant dependant upon system parameters is defined as,

$$K_{cal} = \frac{P_t \lambda^2 G_T G_R}{64\pi^3 L_s}$$

or combining with the equation above,

$$K_{cal} = \frac{P_{CR} R_{CR}^4}{\sigma_{CR}}$$

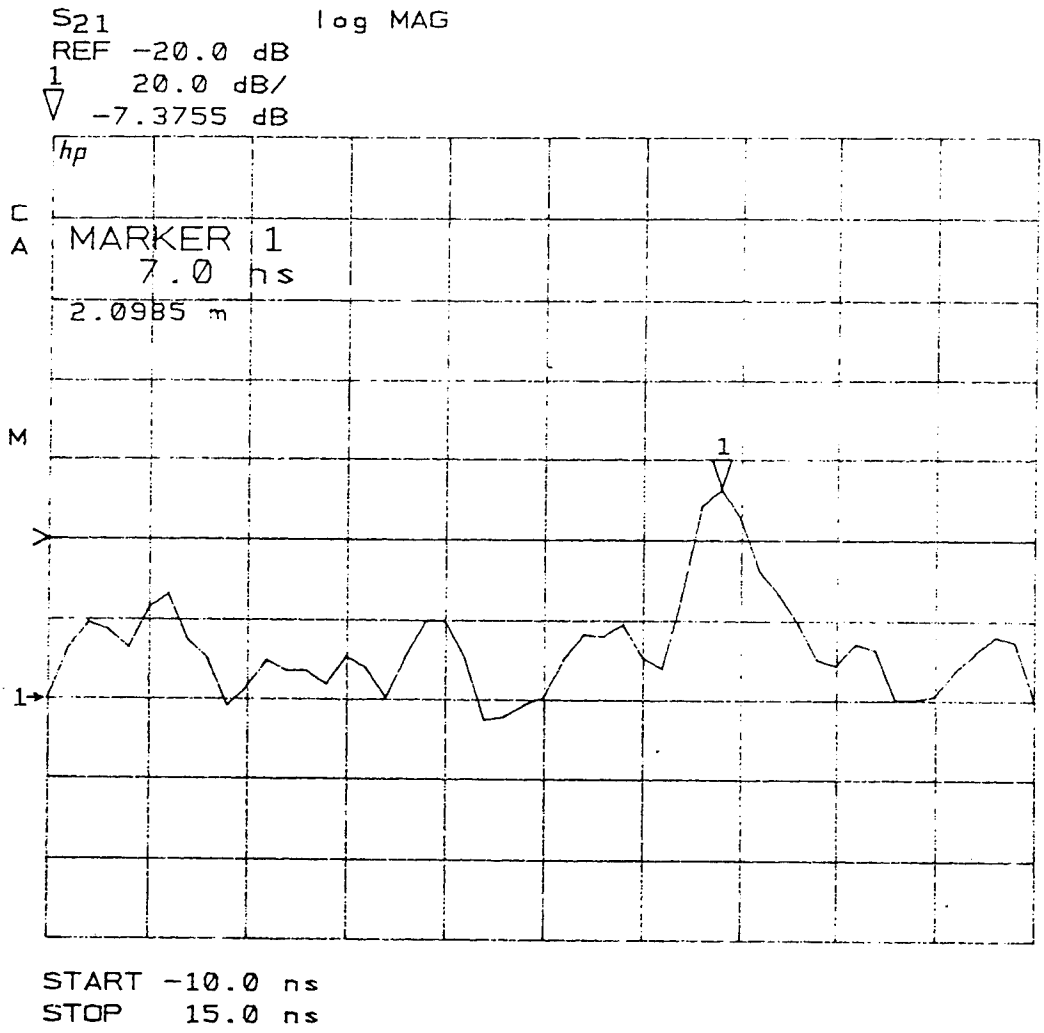

Figure 4.5. Corner reflector at 2.4 meters from the radar.

where,

$$P_{CR} = |S_{21}|^2 \text{ (measured)}$$

$$\sigma_{CR} = .482 \text{ (theoretical)}$$

$$R_{CR} = \text{Range to corner reflector (measured)}$$

The calibration constant K_{cal} is calculated by illuminating a corner reflector. This value is later used to calculate the unknown normalized radar cross section (σ^0) of the target under consideration.

Using K_{cal}, equation 3.15 is then reduced for the beam-limited case to,

$$\sigma^o = \frac{24|S21|^2 R^2 cos\theta_i}{K_{cal}}$$

where K_{cal} and R are measured, and σ^o can be computed.

In the same fashion equation 3.18 for the pulse-limited case is reduced to,

$$\sigma^o = \frac{65.78|S21|^2 R^3 sin\theta_i}{K_{cal}}$$

In the next section a discussion of correction for polarimetric errors is discussed. This calibration is based on correction matrices constructed for the receiver and transmitter.

4.3 Polarimetric Calibration

The polarimetric calibration is achieved by measuring the receiver signal of a target with well known scattering and polarimetric properties (such as a corner reflector), and appropriately orienting thin wire gratings in front of the receiver antenna. The major sources of polarimetric errors are due to non-ideal antenna polarization characteristics, magnitude and phase imbalance between the transmitter and receiver channels, and errors in the signal processing used to determine the magnitude and phase of the received signals.

The voltage measured by the radar receiver can be expressed in matrix notation using an orthogonal basis (i.e. horizontal–vertical) by [Wood, 1986]:

$$\begin{bmatrix} V_{vv} & V_{vh} \\ V_{hv} & V_{hh} \end{bmatrix} = \begin{bmatrix} 1 & A \\ B & C \end{bmatrix} \begin{bmatrix} S_{vv} & S_{vh} \\ S_{hv} & S_{hh} \end{bmatrix} \begin{bmatrix} 1 & G \\ H & J \end{bmatrix} \tag{4.2}$$

or, in a simpler form,

$$[\mathbf{V}] = [\mathbf{R}][\mathbf{S}][\mathbf{T}] \tag{4.3}$$

where [S] is the scattering matrix of the target and [V] is the measured or corrected scattering matrix, and [R] and [T] are known as distortion matrices for the receiver and transmitter respectively.

For an ideal radar no errors are introduced in the system and [V]=[S], then [R] and [T] are identity matrices. When errors are introduced, the terms A, B, C, G, H and J have to be calculated.

The corrected scattering matrix [S] will be given by,

$$[\mathbf{S}] = [\mathbf{R}]^{-1}[\mathbf{V}][\mathbf{T}]^{-1} \tag{4.4}$$

For calibration the receiver distortion matrix [R] is first calculated by illuminating a target with known scattering and polarimetric characteristics. In this case a 3" trihedral corner reflector was illuminated with an incident wave employing horizontal and vertical transmit antenna polarizations. The returned signal was measured for a vertical and horizontal receive antenna polarization with a wire grid in front of the receiver antenna. The received signal was stored for three different wire grid positions (vertical, horizontal and $-45°$ linear).

The elements of [R] are then calculated from by [Wood, 1986]:

$$A = \frac{\Gamma_h - \Gamma_{45}}{\Gamma_v - \Gamma_{45}} \tag{4.5}$$

$$B = \Gamma_h - \Gamma_{45}(1 - A) \tag{4.6}$$

$$C = \Gamma_h \tag{4.7}$$

where,

$$\Gamma_i = (\frac{V}{H})_i \qquad i = h, v, 45 \tag{4.8}$$

is the complex ratio of the vertical and horizontal components measured at the receiver for the i^{th} wire grid position.

With knowledge of the receiver distortion matrix [R] the distortion matrix for the transmitter is easily calculated by,

$$[\mathbf{T}] = [\mathbf{R}]^{-1}[\mathbf{S}]^{-1}[\mathbf{V}] = [\mathbf{R}]^{-1}[\mathbf{V}] \tag{4.9}$$

where [R] was calculated, [V] is the measured signal at the receiver from the 3" trihedral corner reflector, and [S] is the theoretical (corrected) scattering matrix of the corner reflector given by:

$$[\mathbf{S}] = \begin{bmatrix} 1 & 0 \\ 0 & 1 \end{bmatrix} \tag{4.10}$$

Now, with the knowledge of both distortion matrices, the corrected scattering matrix, [S], is calculated for any target with an uncorrected scattering matrix [V].

CHAPTER 5

RESULTS AND CONCLUSIONS

During the last three years, data from different natural targets such as snow, urea ice and saline ice have been collected in the Cold Regions and Research Laboratory (CRREL), New Hampshire. The data were collected under controlled environmental conditions with the idea of understanding more the response of the target to electromagnetic radiation for given physical characteristics (such as roughness, salinity, ice temperature, thickness, etc.). Calculations of NRCS for the ice and snow are presented for different incidence angle and antenna polarization. Polarimetric signatures from saline ice are also presented for different incidence angles.

5.1 Normalized Radar Cross Section

From equation 3.14 and 3.15, it can be seen that σ^o can be calculated for either the beam or the pulse limited case. The decision of which equation to use is made by equating the width of the illuminated area for figures 3.19 and 3.20. The ratio of the width for the two cases yields,

$$\frac{c\tau}{2\sin\theta_i} = \frac{R\theta_B}{\cos\theta_i} \tag{5.1}$$

$$\tan\theta_i = \frac{c\tau_p}{2\theta_B R} \tag{5.2}$$

This is assuming the case when both width are the same (i.e. pulse length is the same as the length given by the beam-limited case). But if,

$$\tan\theta_i > \frac{c\tau_p}{2\theta_B R} \tag{5.3}$$

the geometry for the pulse–limited case predominates and equation 3.18 is used to calculate σ^o. On the other hand if,

$$\tan\theta_i < \frac{c\tau_p}{2\theta_B R} \tag{5.4}$$

the geometry for the beam–limited case predominates and equation 3.15 is employed to compute σ^o.

For a short range system the beam–limited case is always predominant up to incidence angles of 60°. In the analysis of the data we found that only for one type of measurements (snow), an angle of 60° was reached and the pulse limited case was predominant.

For a perfectly smooth surface a monostatic radar [Ulaby *et al.*, 1982] would theoretically receive no return power except for normal incidence (0°). An angular radiation pattern of the reflected wave will be a delta function at 0°. For a slightly rough surface, the angular radiation pattern consists of a reflected component and a scattered component. Part of the scattered component will be detected by the radar receiver. The magnitude of the power for the scattered component will decay with the incidence angle. As the surface becomes rougher the reflected component becomes negligible and the radiation pattern consists of only diffuse scattering.

Preliminary measurements of wet sand in the laboratory were performed to verify the operation of the system. These measurements were made in a 4' × 4' × 7" box where the sand was kept smooth at all times. Figure 5.1 shows that the plot of σ^o versus incidence angle decays as expected and that VV and HH should be approximately the same. The difference between both NRCS might be due to the small amount of independent samples obtained (15) for each angle. The measurements assures us that the radar is working properly

and that a large amount of independent samples should be considered in future measurements.

Figure 5.2 shows the NRCS of smooth urea ice at different incidence angles. Urea ice is structurally the same as sea ice, but with lower conductivity and presumably less attenuation than natural sea ice. The prime purpose here was to obtain baseline radar backscatter from a smooth surface with negligible volume scattering. The figure shows an exponential decay of the NRCS. This is so because the surface is "smoother" and at higher incidence angles, the signal bounces off from the surface and less energy is received producing this kind of response. The result will follow the antenna pattern of the radar. For this experiment 25 independent samples were averaged.

The second part of the experiment compared the backscatter of the smooth ice to that of very rough ice, since it is known that roughness is a primary effect in the backscatter process. The rough ice was simulated by spacing pieces of new ice over the sheet of smooth ice. The pieces were in the order of 1 to 2 square inches. Due to the high attenuation of the new ice, volume scattering contribution from the received signal is negligible and only surface backscatter is compared between the two kinds of ice. Figure 5.3 shows the NRCS of rough ice versus incidence angle. Note here that σ° is higher than that of the smooth ice, especially at large incidence angles. This is expected since more energy is scattered in all directions from a rough surface, or in other words the reflected component becomes negligible as explained before. received signal

A second experiment was conducted to determine temperature effects on surface scattering. A smooth sheet of urea ice was grown indoors until it was 12 inches thick. The surface was smooth enough so that volume scattering is negligible. The temperature of the room was slowly raised over a period of 48 hours to

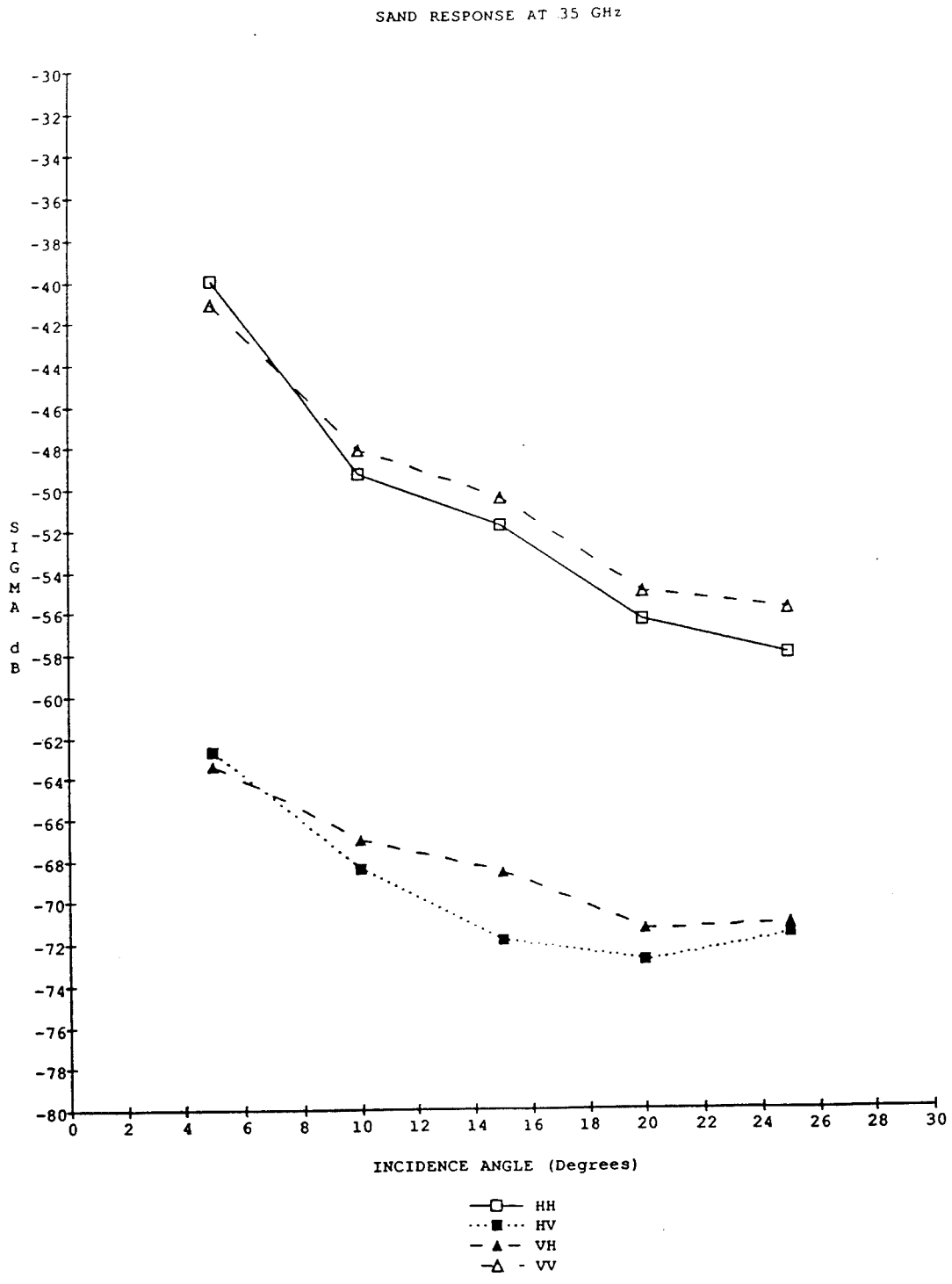

Figure 5.1. NRCS of sand at 35 GHz.

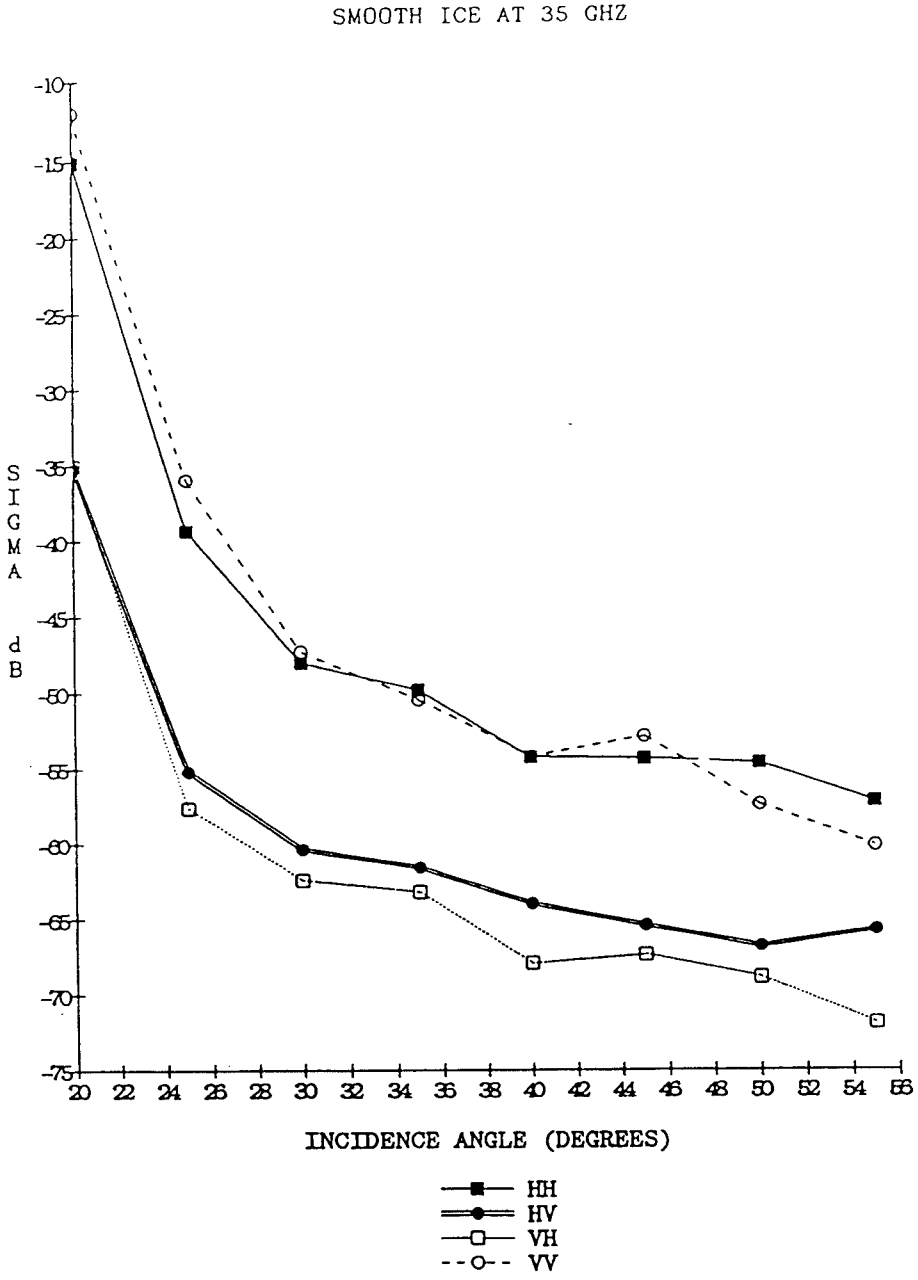

Figure 5.2. NRCS of smooth ice at 35 GHz.

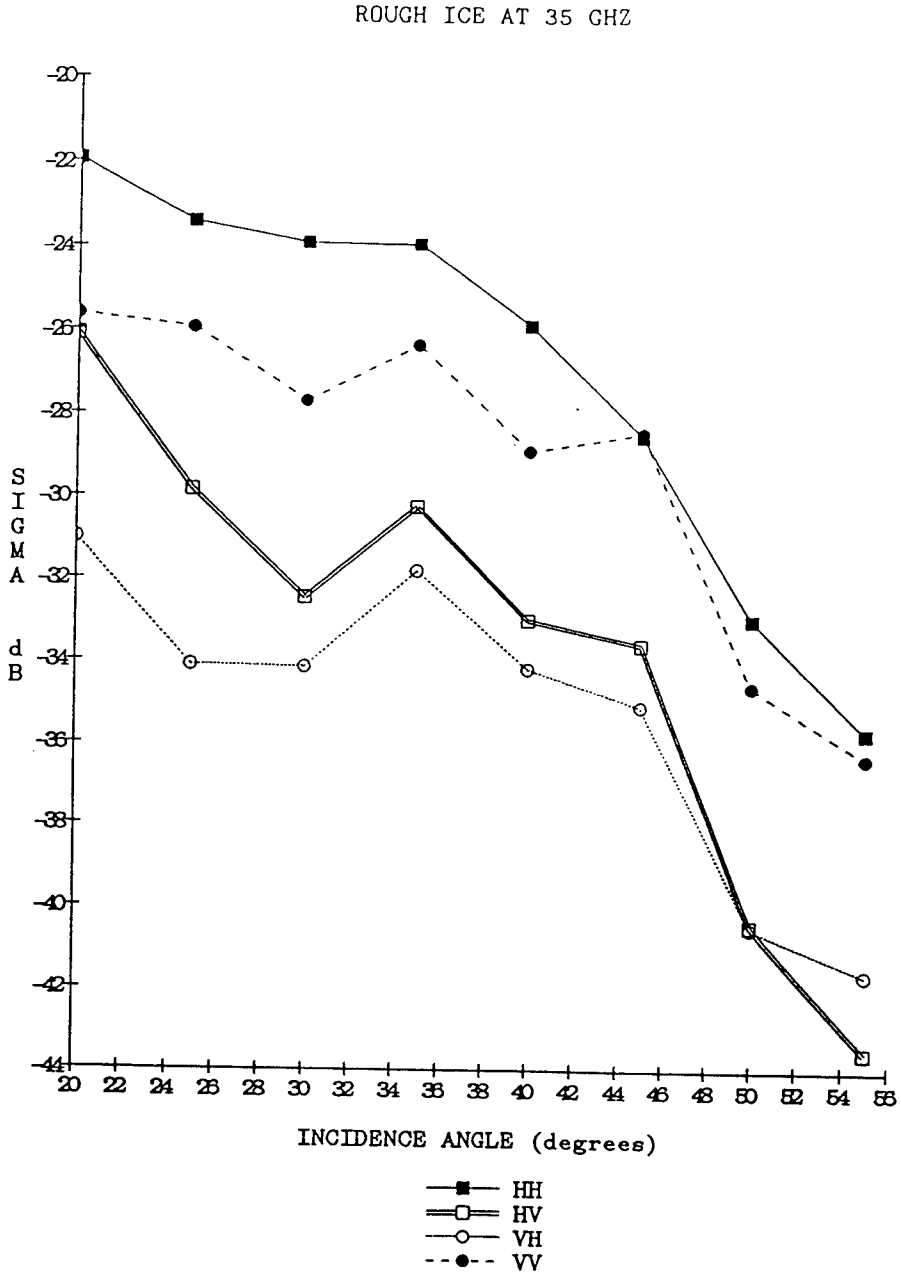

Figure 5.3. NRCS of rough ice at 35 GHz.

observe any change in the resultant backscatter.

Figures 5.4 and 5.5 show the results of this experiment at 35 and 45 degrees of incidence where σ^o was plotted versus the ice temperature. Note that the trend for the two figures are consistent for the four polarizations. A comparison of the co-polarized response at 35° and 45° is shown in figure 5.6. Note also that σ^o is lower for larger incidence angles as expected. Both figures show a lower σ^o for the smooth ice at temperatures of around $-9°C$ and $-8°C$. The NRCS increases slowly until it reaches a maximum around $-1°C$ and then drops off.

The effect of higher temperature is to raise the dielectric constant of the sea ice [Kim *et al.*, 1984]. An approximation to calculate the dielectric constant in terms of ice temperature was used to later compute the Fresnel reflection coefficient for an incidence angle of 35° [Vant *et al.*, 1974]. Figure 5.7 is a plot of the magnitude of this coefficient versus ice temperature. Note that the magnitude increases when increasing the temperature and then more backscattered power is expected at higher temperatures (figures 5.4 and 5.5). Between $-1°C$ and $0°C$ the ice surface becomes wet and the high loss masks the scattering from the surface. During the duration of the experiment, air bubbles in the order of 2-5 mm were observed near the surface for a temperature range of $-2°C$ to $0°C$. The skin depth for the sea ice at this frequency is in the vicinity of 1 cm [Onstott, 1980], it is assumed then that some volume scattering within this depth might contribute in the resultant backscattered energy. In conclusion, the change in NRCS with ice temperature is primarily due to the variation in the dielectric constant which affects the backscattered power by changes in the Fresnel reflection coefficient.

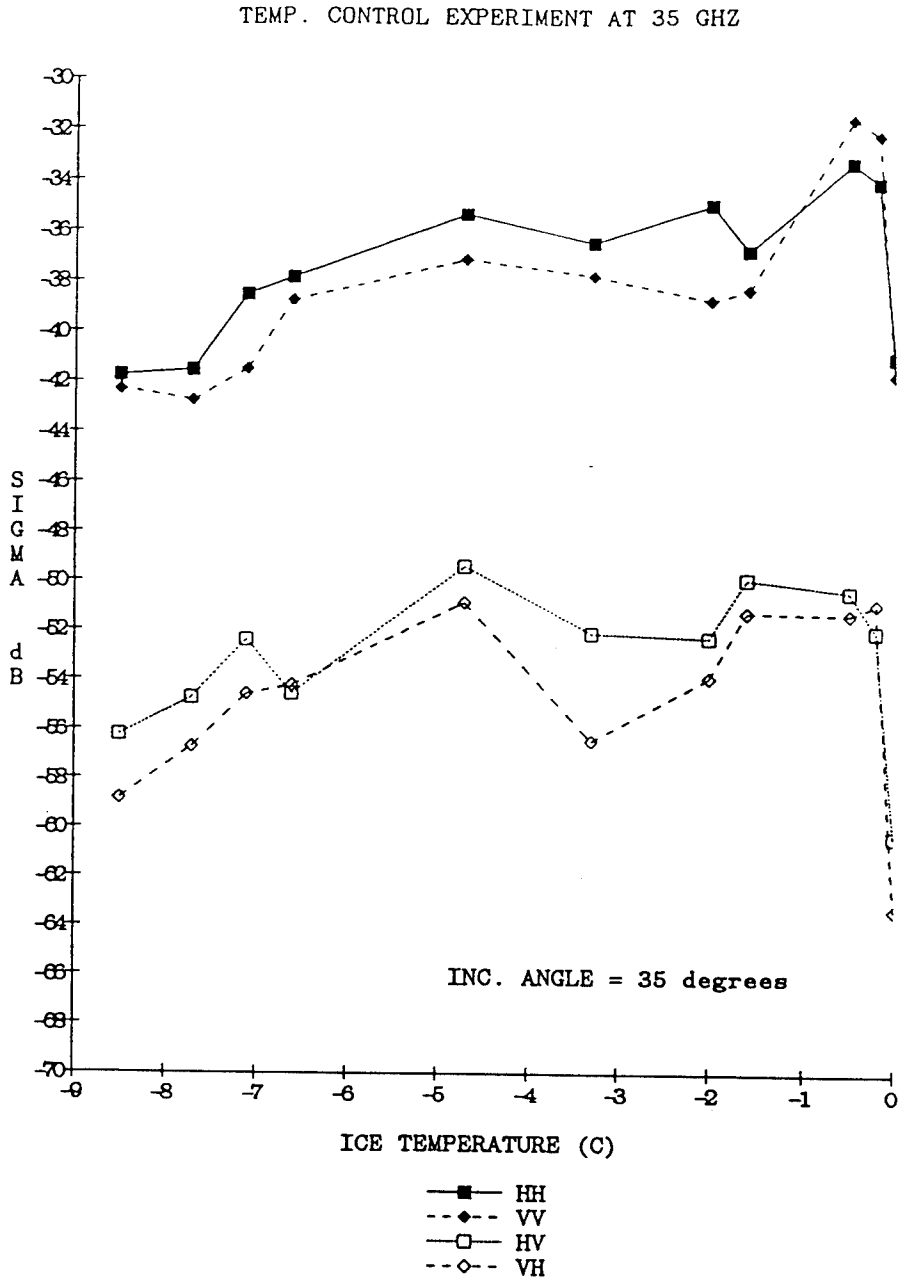

Figure 5.4. NRCS versus ice temperature at 35°.

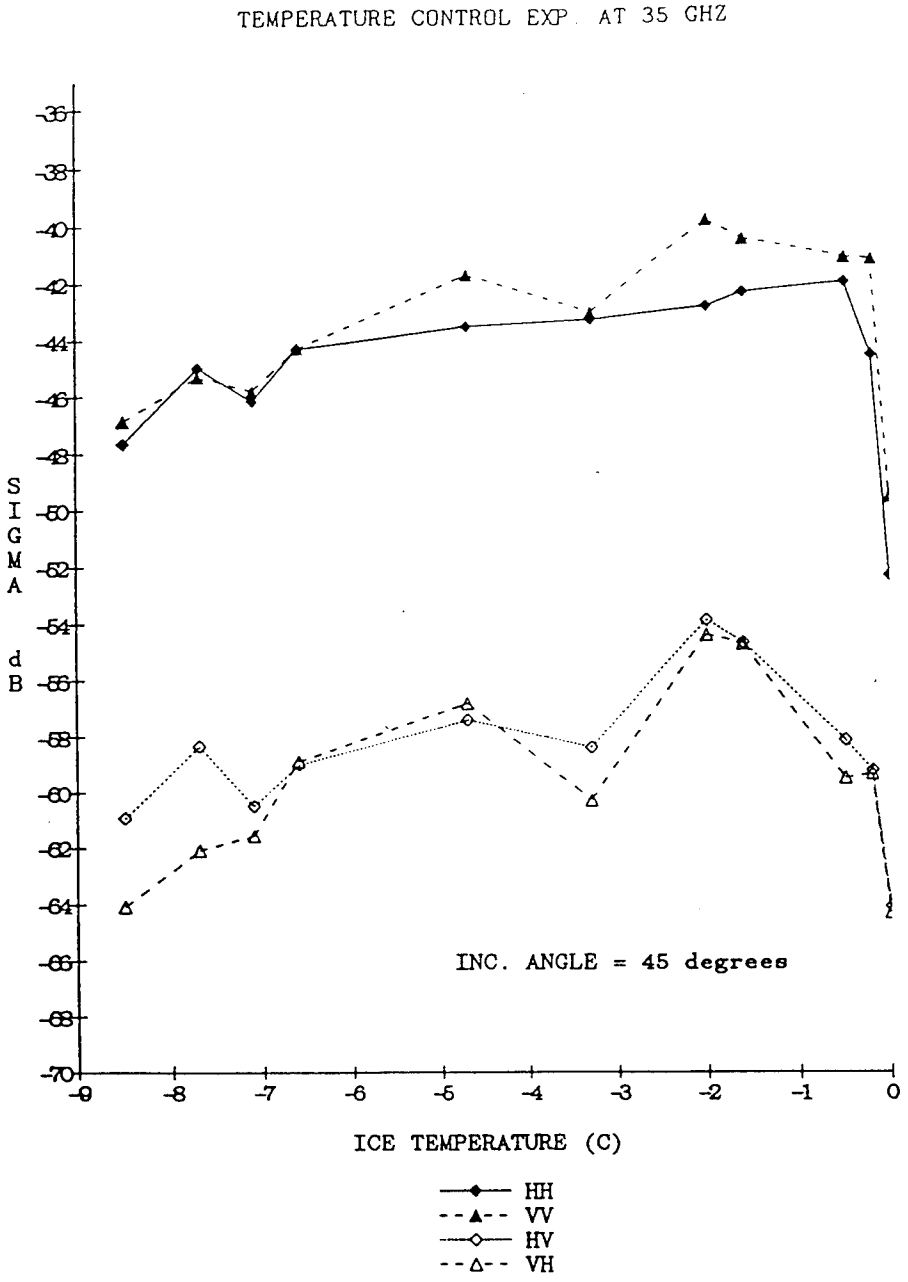

Figure 5.5. NRCS versus ice temperature at 45°.

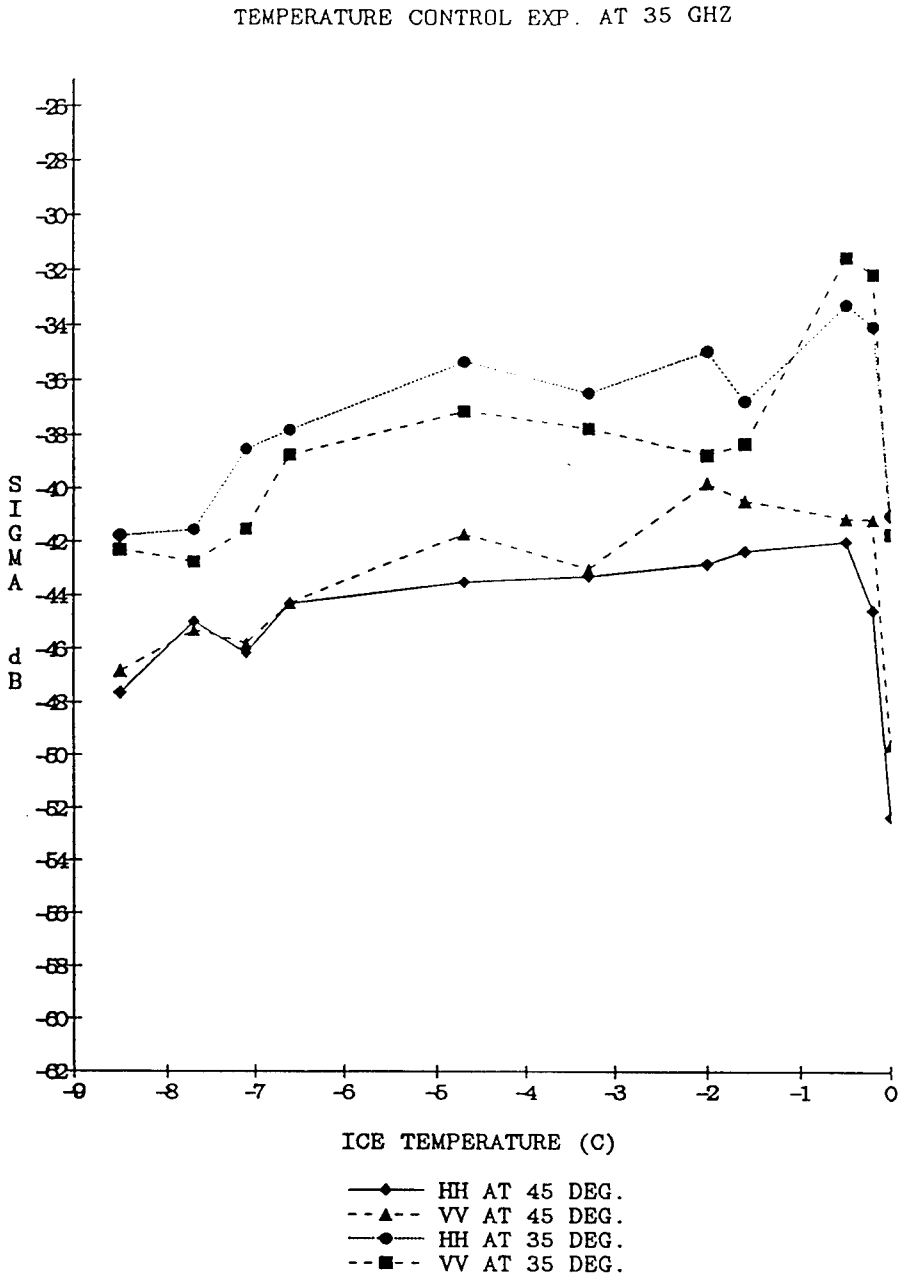

Figure 5.6. NRCS versus ice temperature at 35° and 45°.

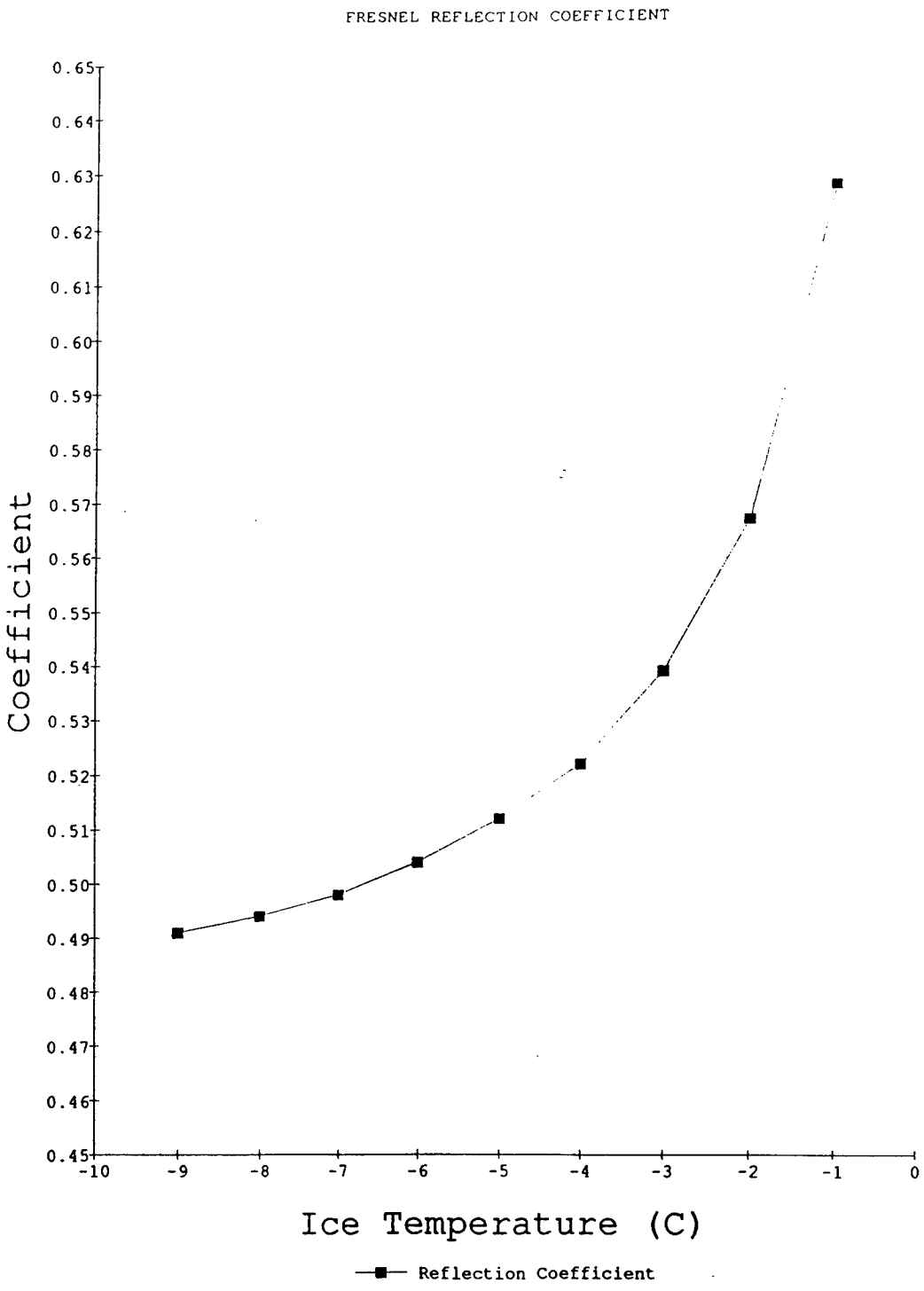

Figure 5.7. Fresnel reflection coefficient versus ice temperature.

5.2 Polarimetric Measurements

Polarization signatures for smooth saline ice were computed for 5,10,15,20,25 and 30 degrees of incidence angle. The first step was to calculate the NRCS versus incidence angle using the regular technique explained in section 5.1. Figure 5.8 shows the response of the four polarizations. Note that σ^o decays exponentially with the incidence angle as expected for a smooth surface. The difference in the cross polarized response may be due to the small amount of independent samples (23). Since a polarimetric calibration to correct for magnitude and phase errors was introduced in this experiment, polarimetric signatures for the ice were calculated using equation 2.37. By using equation 4.4 , we can also calculate the corrected scattering matrix [S] and recalculate σ^o with the new values. Figure 5.9 shows the result of σ^o using the corrected scattering matrix [S], for the co-polarized values. The change is minimum, for the cross-polarized values the change is more significant, but there are still some differences by the order of a few dB. This might be explained again by the fact that a small amount of independent samples was averaged.

The polarization signatures for the co-polarized and cross-polarized response for 5,10,15,20, and 30 degrees are shown in figures 5.10 to 5.14. Note that for the co-polarized response of 5 and 10 degrees, VV (τ=0, ϕ=0) is smaller than HH (τ=0, ϕ= $\pm$90). This agrees with figure 5.9 for 5° and 10°. For the co-polarized response of 15, 20 and 30 degrees, VV is higher than HH, which also agrees, being the signature for 15° the maximum difference between both HH and VV ($\sim$ 2 dB) as figure 5.9 shows. Note also that at lower incidence angles (5 and 10°) the response is similar to that of a corner reflector, the only difference being an offset or pedestal at the base of the signature. This is also expected for smooth surfaces at low incidence angles since there is more energy

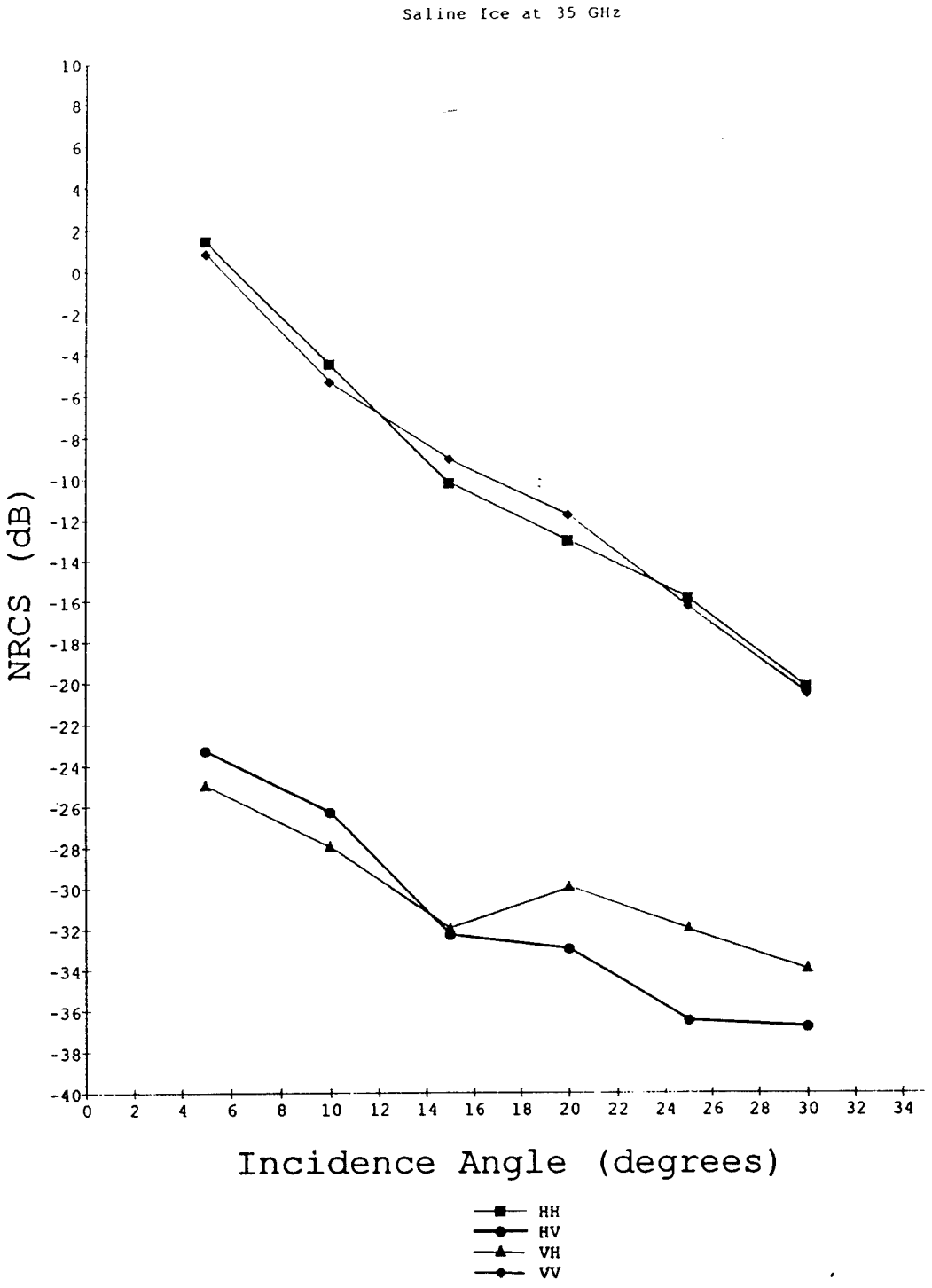

Figure 5.8. NRCS of saline ice before polarimetric calibration.

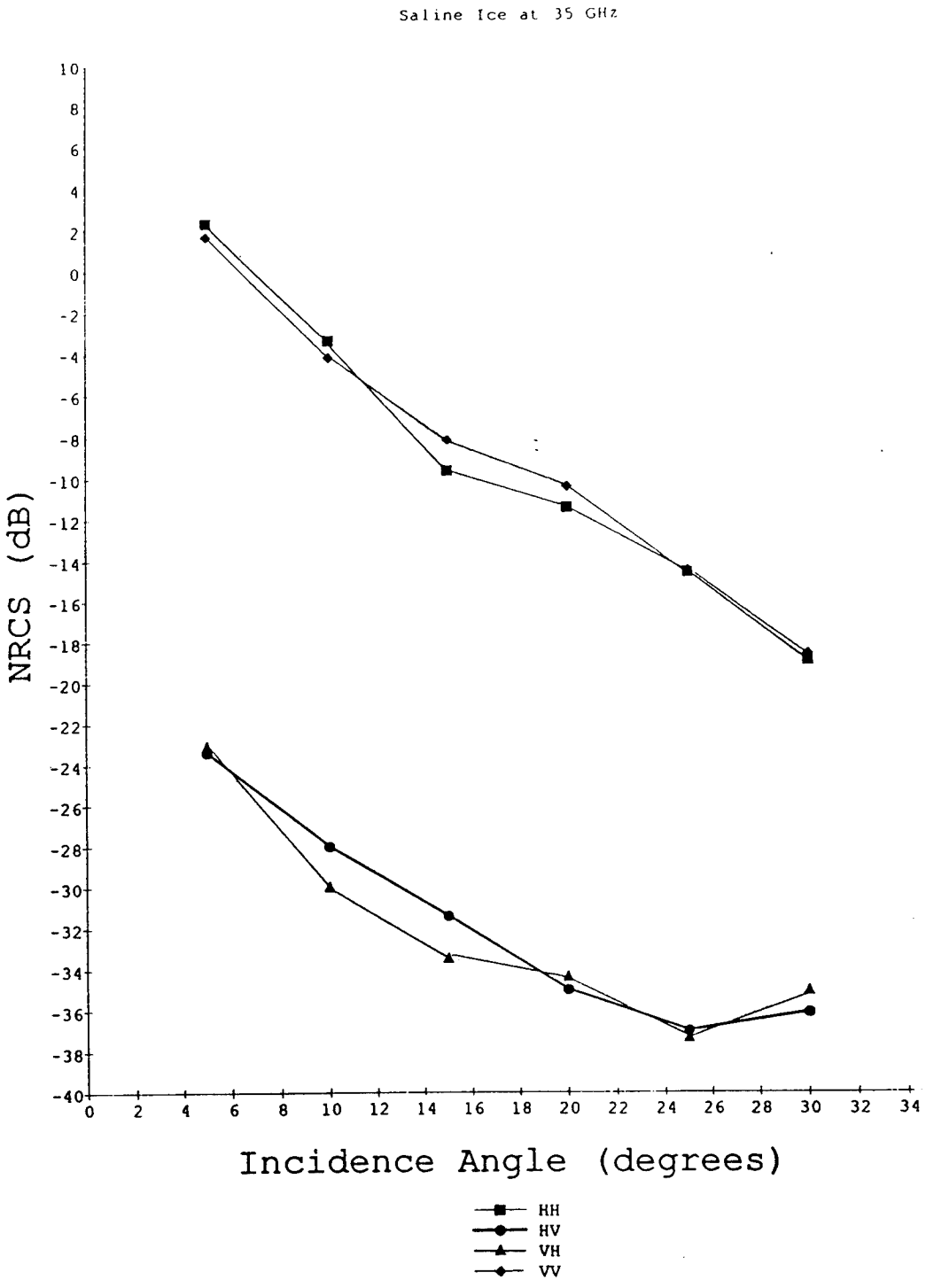

Figure 5.9. NRCS of saline ice after polarimetric calibration.

reflected. The pedestal also gives information about the polarization response of the target. It is a sign of how depolarized is the target. For example, a corner reflector is completely polarized, it does not presents any pedestal. In the case of the ice, it can be seen that the pedestal increases with incidence angle, which is an indication of depolarization of the target or, in other words, indicates randomly polarized signals coming back from the target.

5.3 Snow Measurements

Snow measurements during the winter of 1990-91 were performed at CRREL over two types of terrain, rough and medium rough. The measurements were made in different days, and the conditions of the snow were also different. This time at least 100 independent samples were averaged for 20, 40 and 60 degrees of incidence at two different polarizations; VV and HV.

Figures 5.15, 5.16 and 5.17 present the power return of snow for the 100 independent samples versus range for each of the incidence angles at VV.

Figures 5.18, 5.19 and 5.20 present the averaged power of all the samples. Note that at 20° the averaged power is higher and narrower and it will spread out for 40° and 60° due to the size of the illuminated area. Also note that the range to the target increases with incidence angle as expected.

Figure 5.21 shows the co-polarized measurements (VV) for four different snow conditions. The snow from January 15 and January 23 are both around 15 cm of dry snow. The difference in σ^o might be due to the fact that the snow from January 15 was fresh snow and a smooth surface was observed. On the other hand, the snow from the 23^{th} had some degree of roughness.

The snow from December 20, was very rough. Light snow was covering the ground and roughness of the same degree of the terrain was observed. This

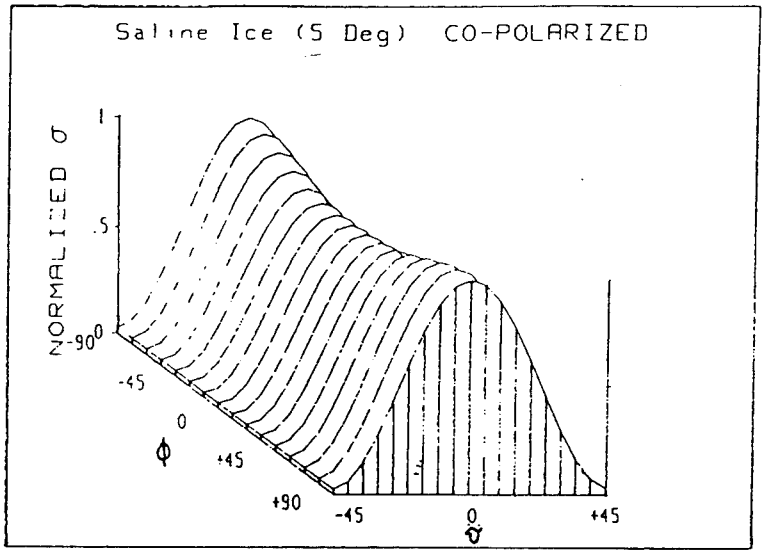

(a)

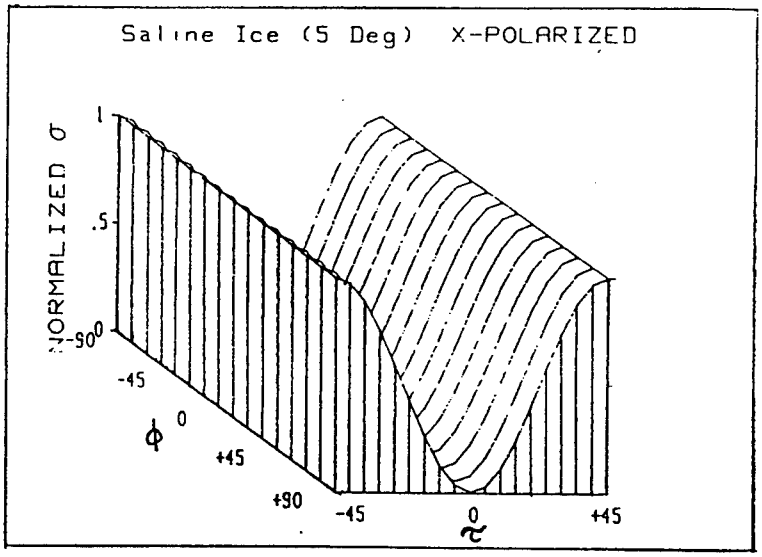

(b)

Figure 5.10. Co-polarized (a) and cross-polarized (b) response of saline ice at 5°.

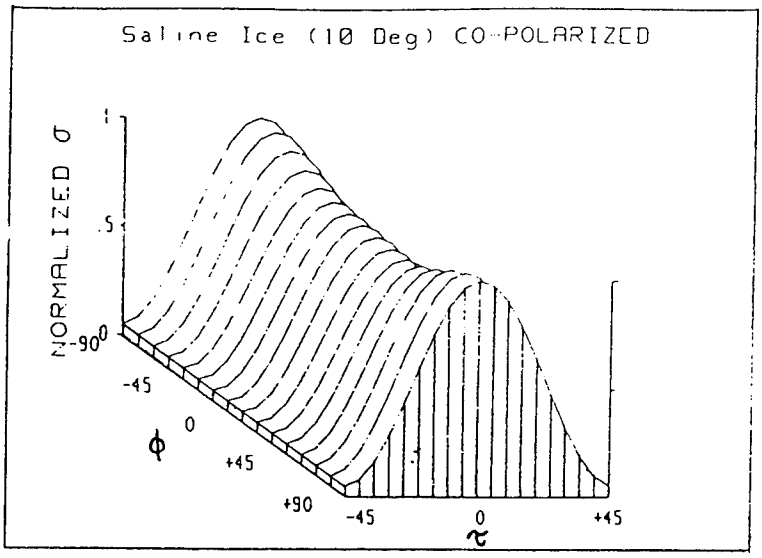

(a)

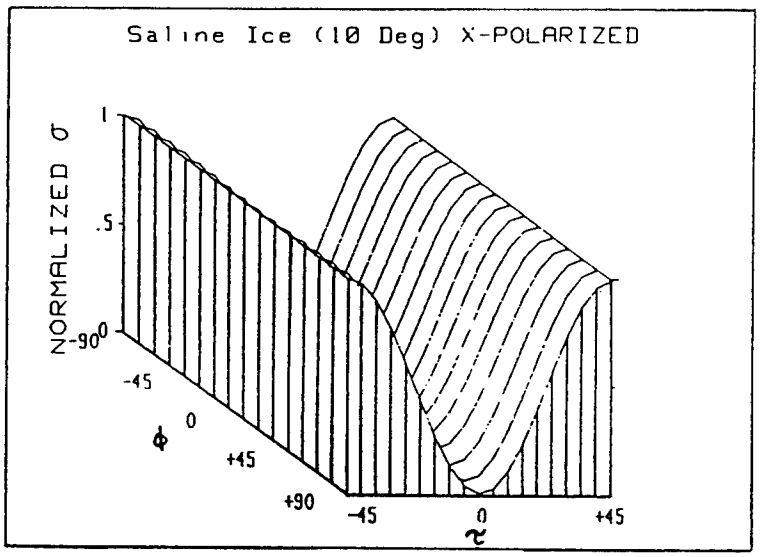

(b)

Figure 5.11. Co-polarized (a) and cross-polarized (b) response of saline ice at 10°.

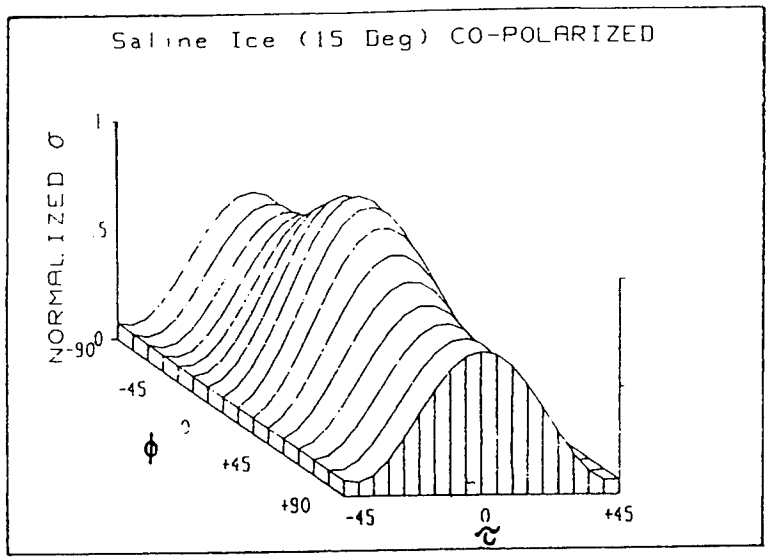

(a)

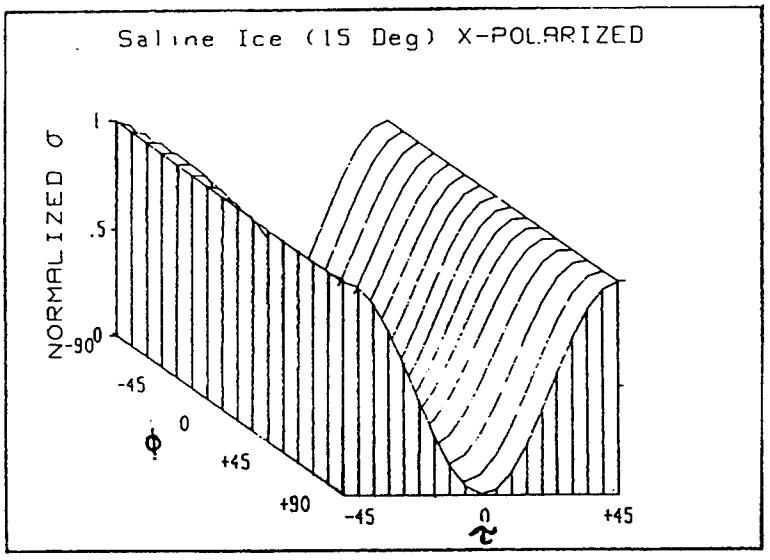

(b)

Figure 5.12. Co-polarized (a) and cross-polarized (b) response of saline ice at 15°.

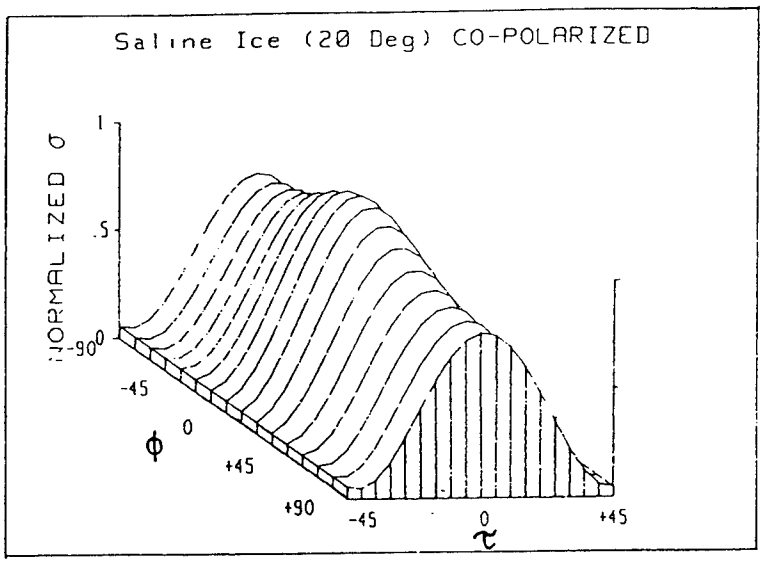

(a)

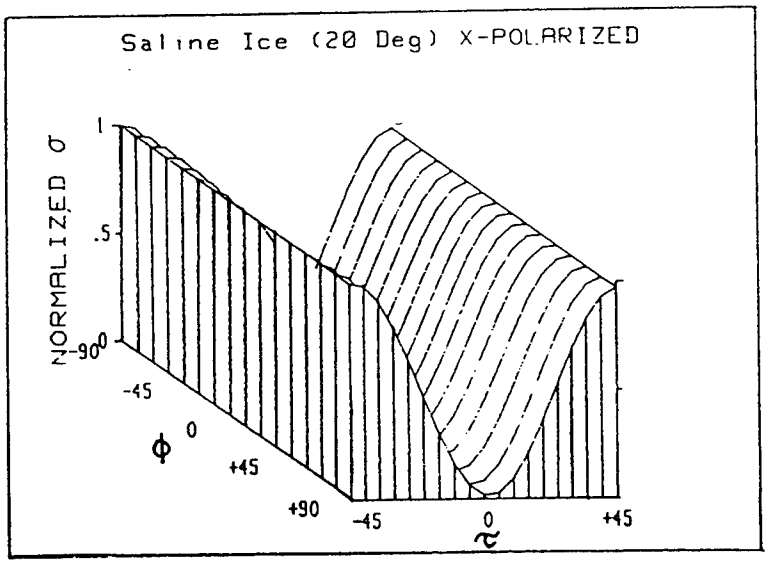

(b)

Figure 5.13. Co-polarized (a) and cross-polarized (b) response of saline ice at 20°.

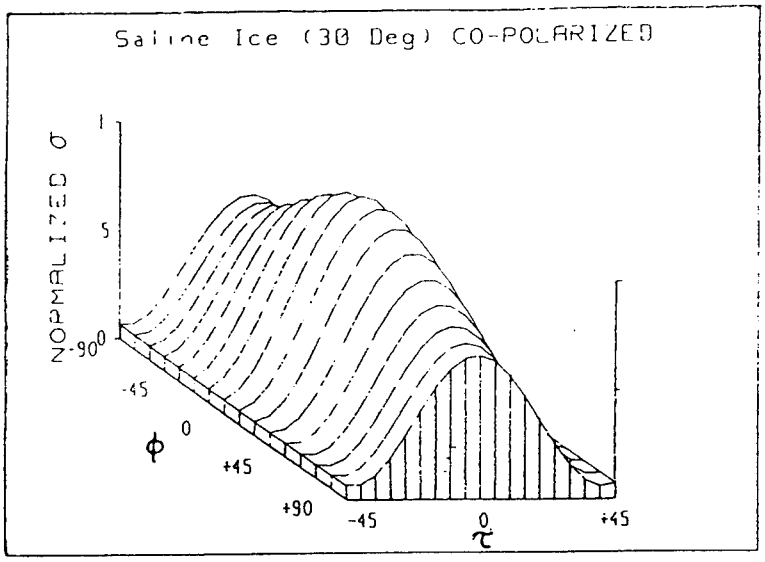

(a)

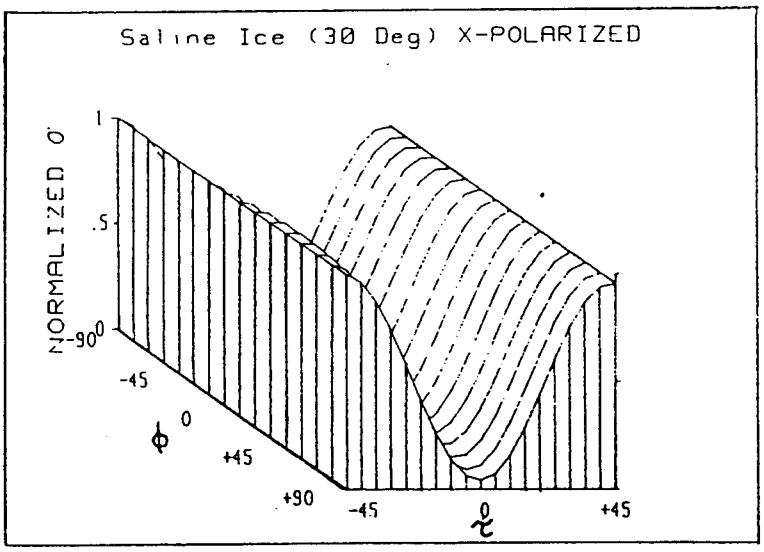

(b)

Figure 5.14. Co-polarized (a) and cross-polarized (b) response of saline ice at 30°.

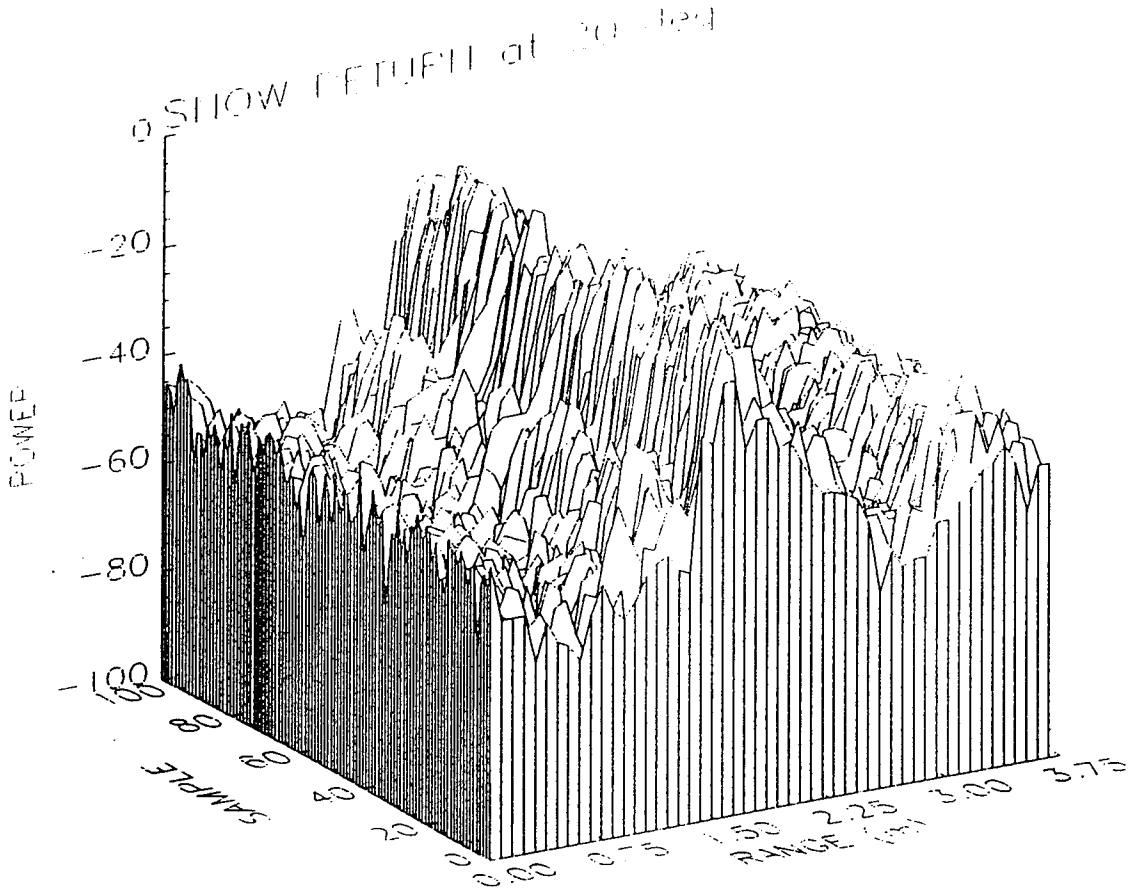

Figure 5.15. Power returned of 100 samples at 20°.

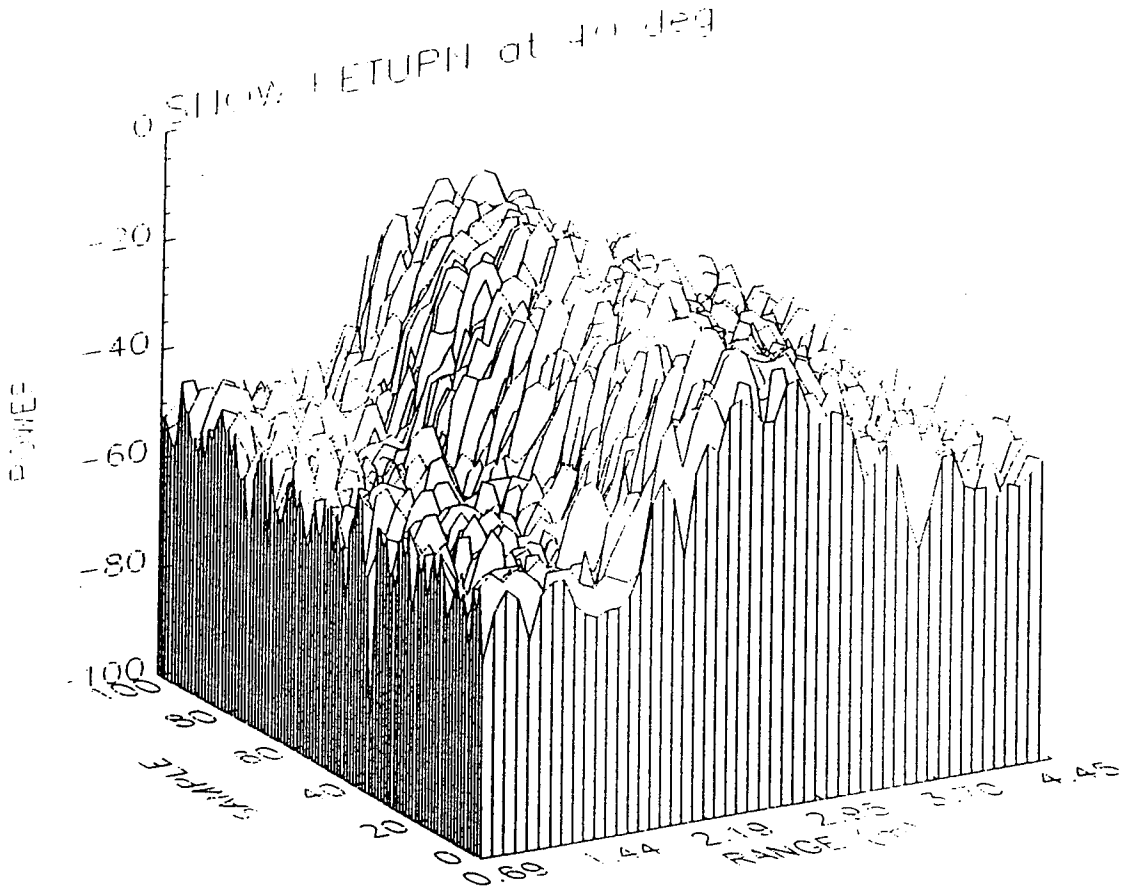

Figure 5.16. Power returned of 100 samples at 40°.

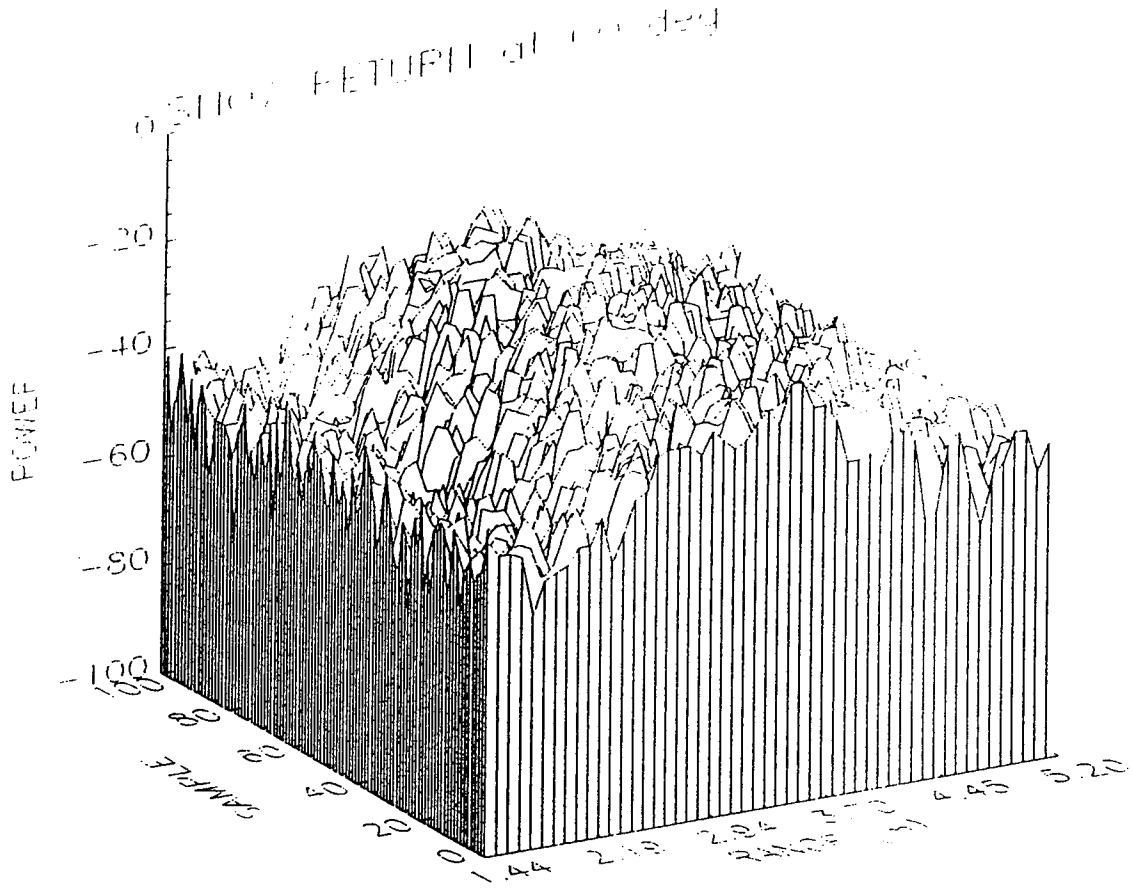

Figure 5.17. Power returned of 100 samples at 60°.

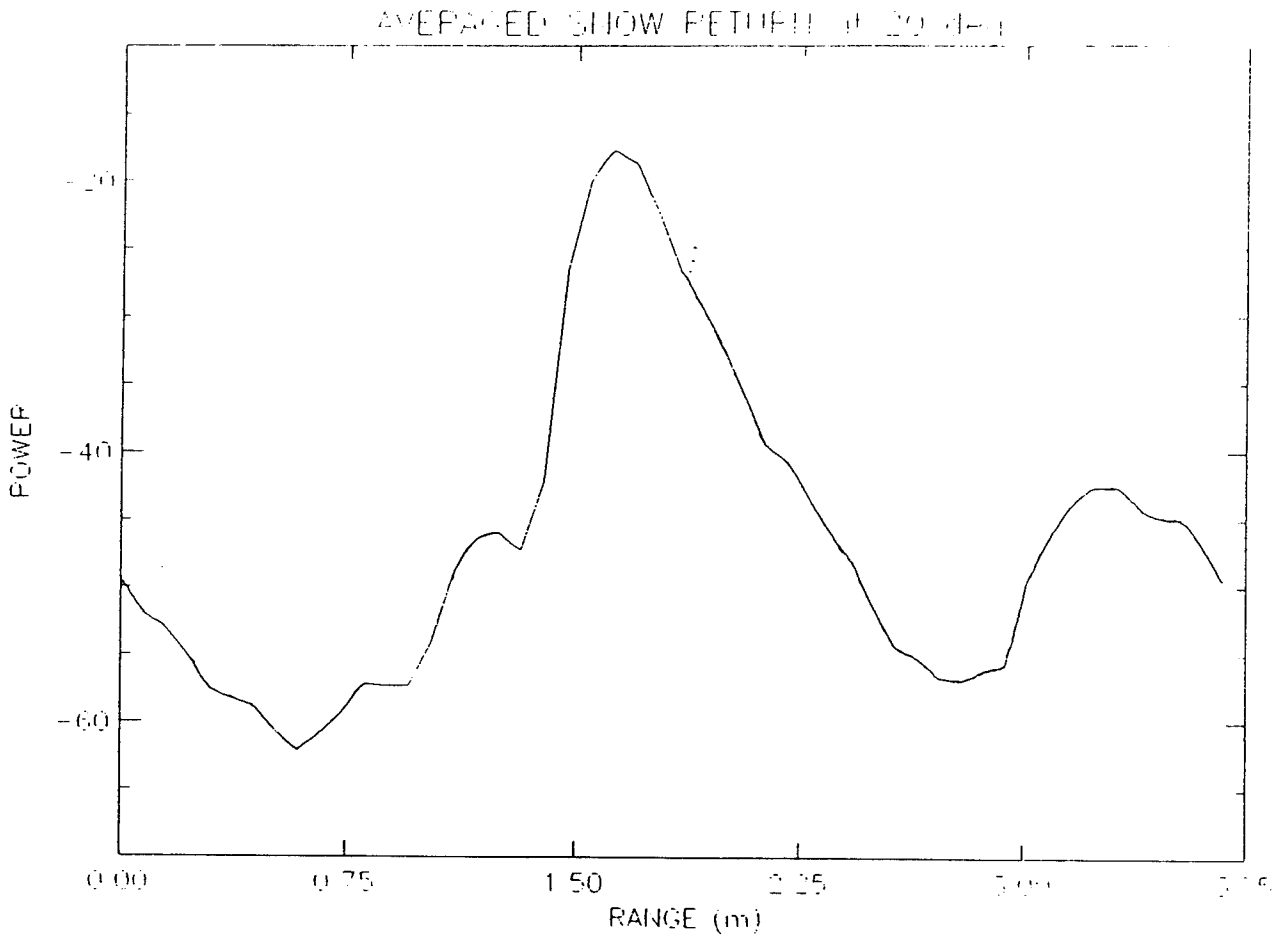

Figure 5.18. Power averaged at 20°.

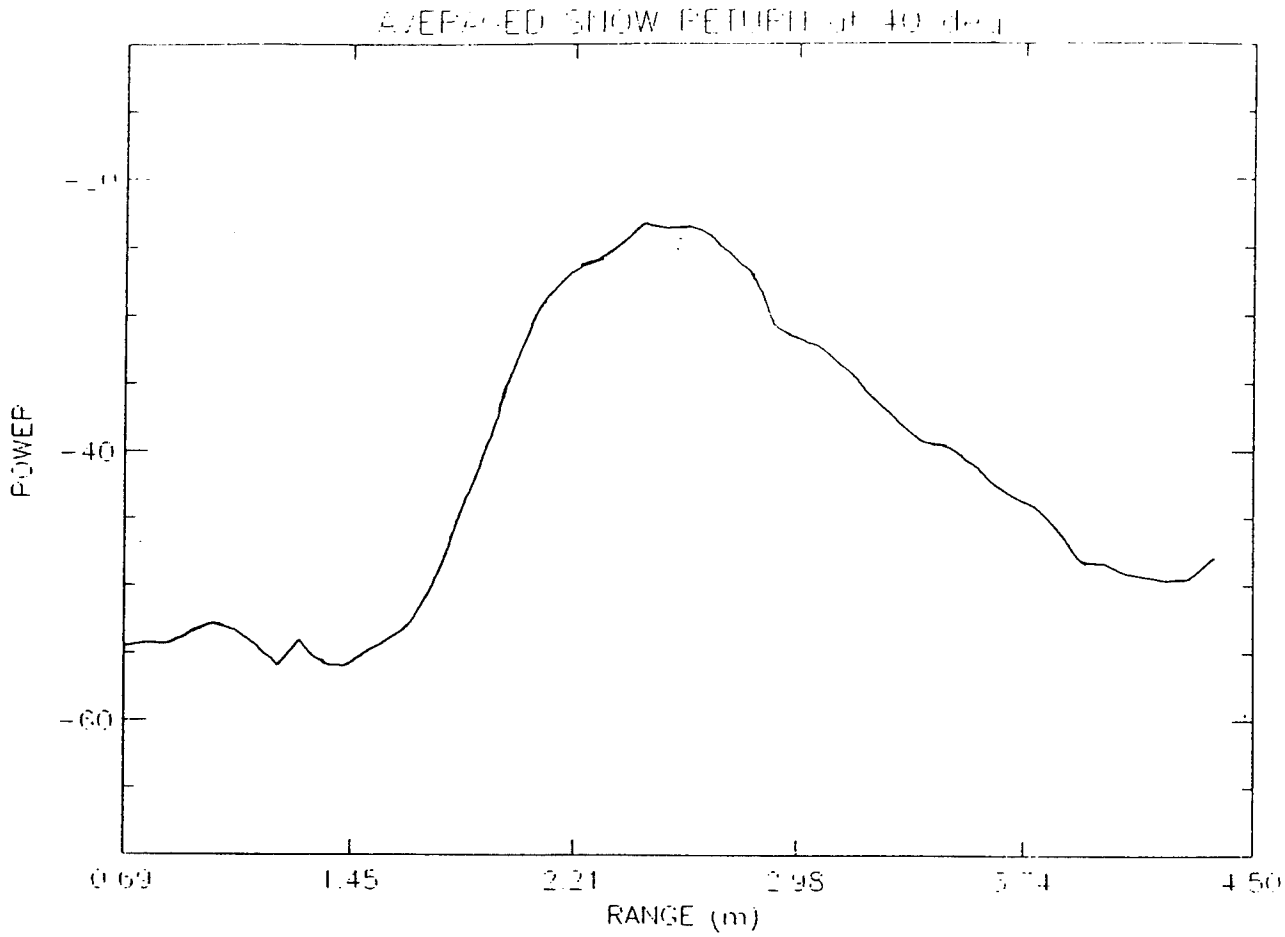

Figure 5.19. Power averaged at 40°.

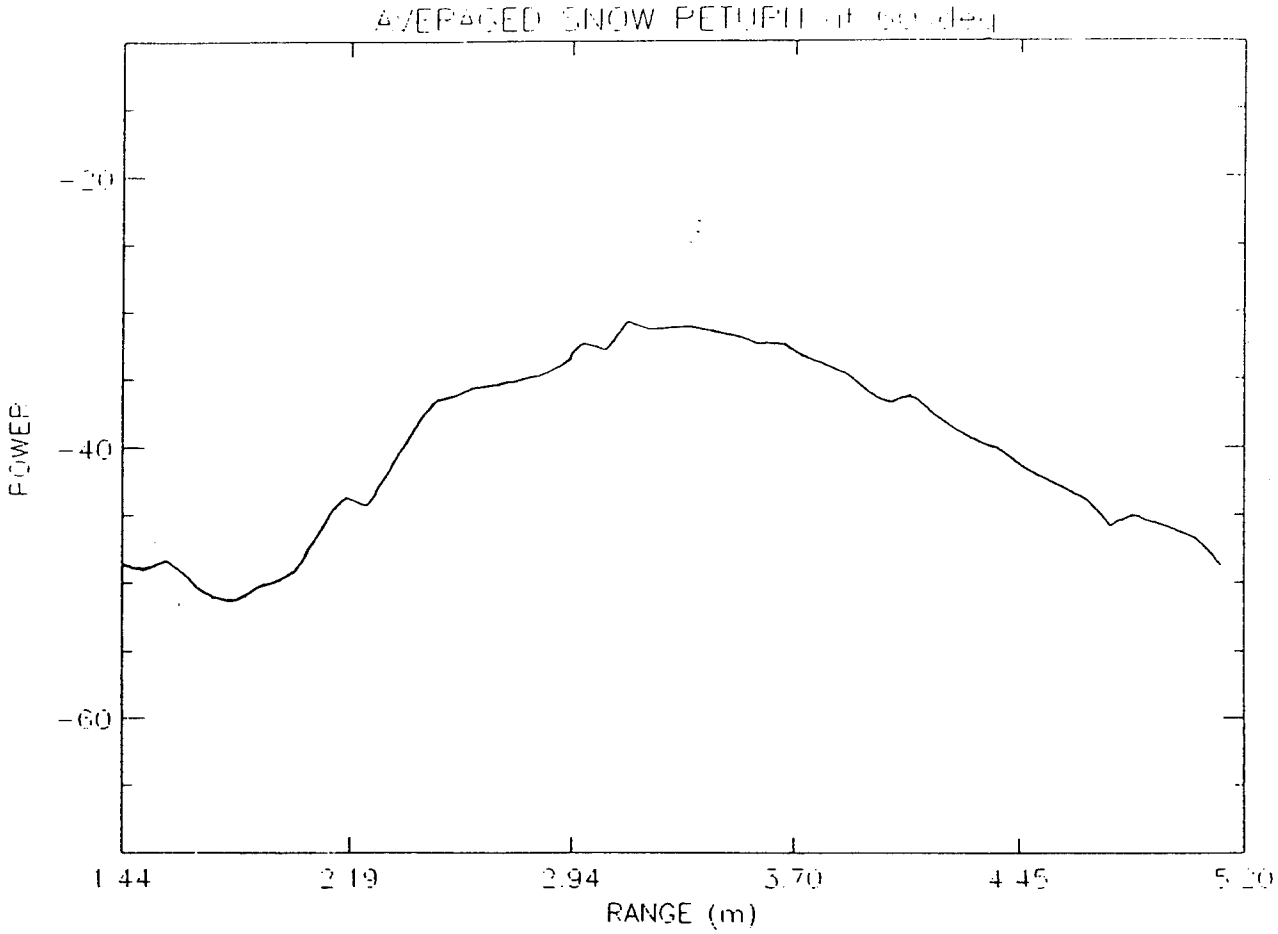

Figure 5.20. Power averaged at 60°.

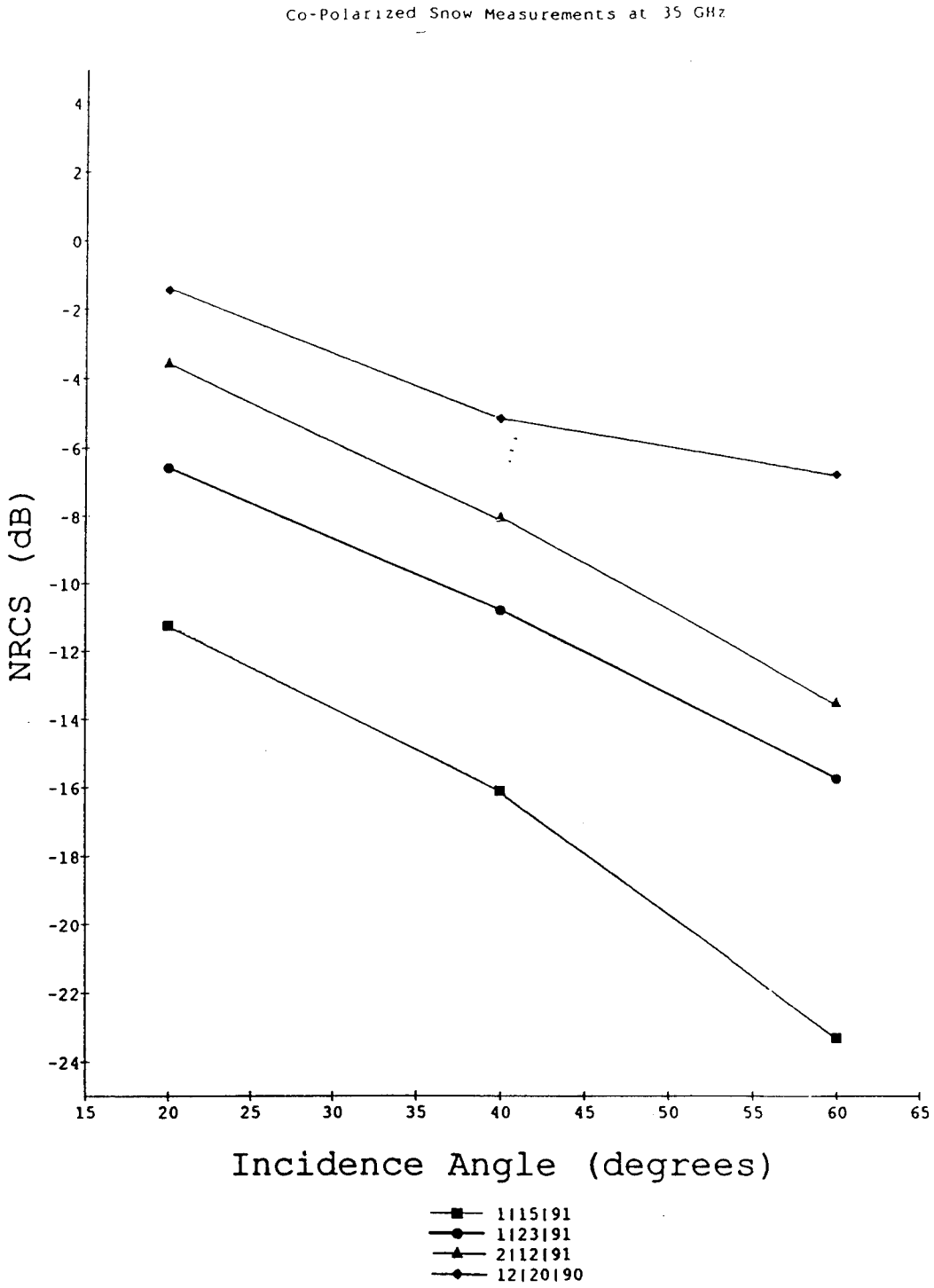

Figure 5.21. Co-polarized snow measurements at 35 GHz.

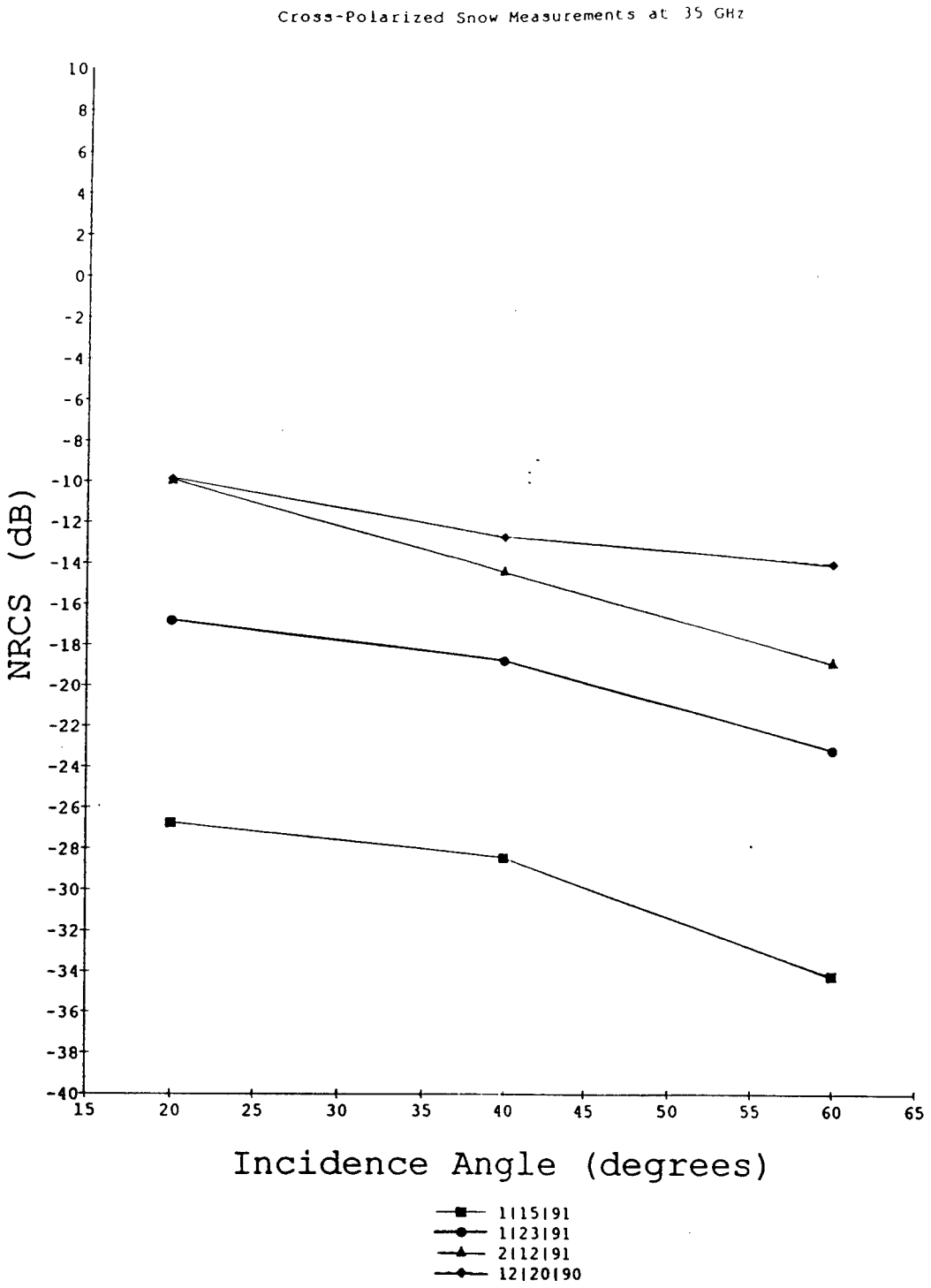

Figure 5.22. Cross-polarized snow measurements at 35 GHz.

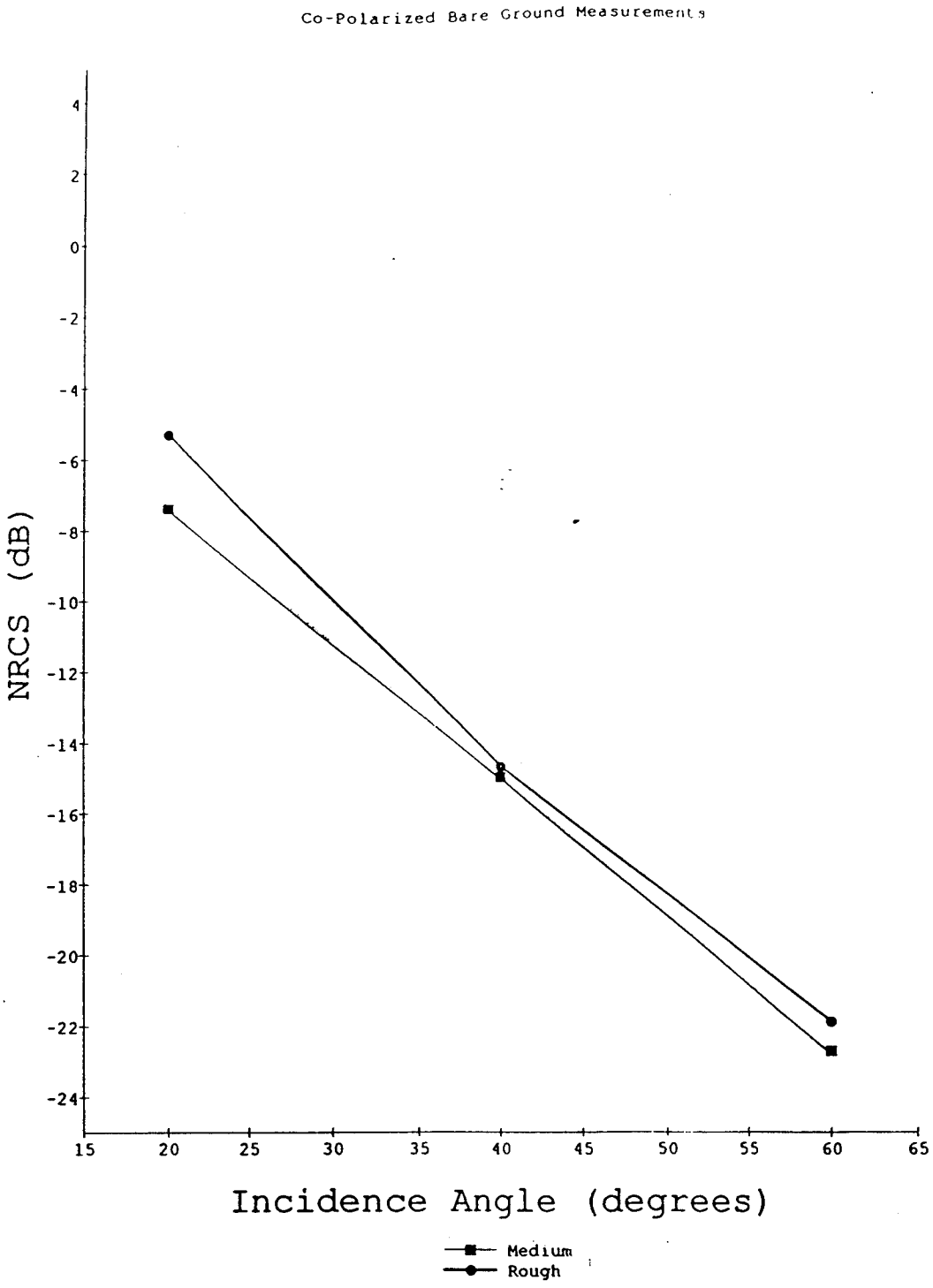

Figure 5.23. Co-polarized terrain measurements at 35 GHz.

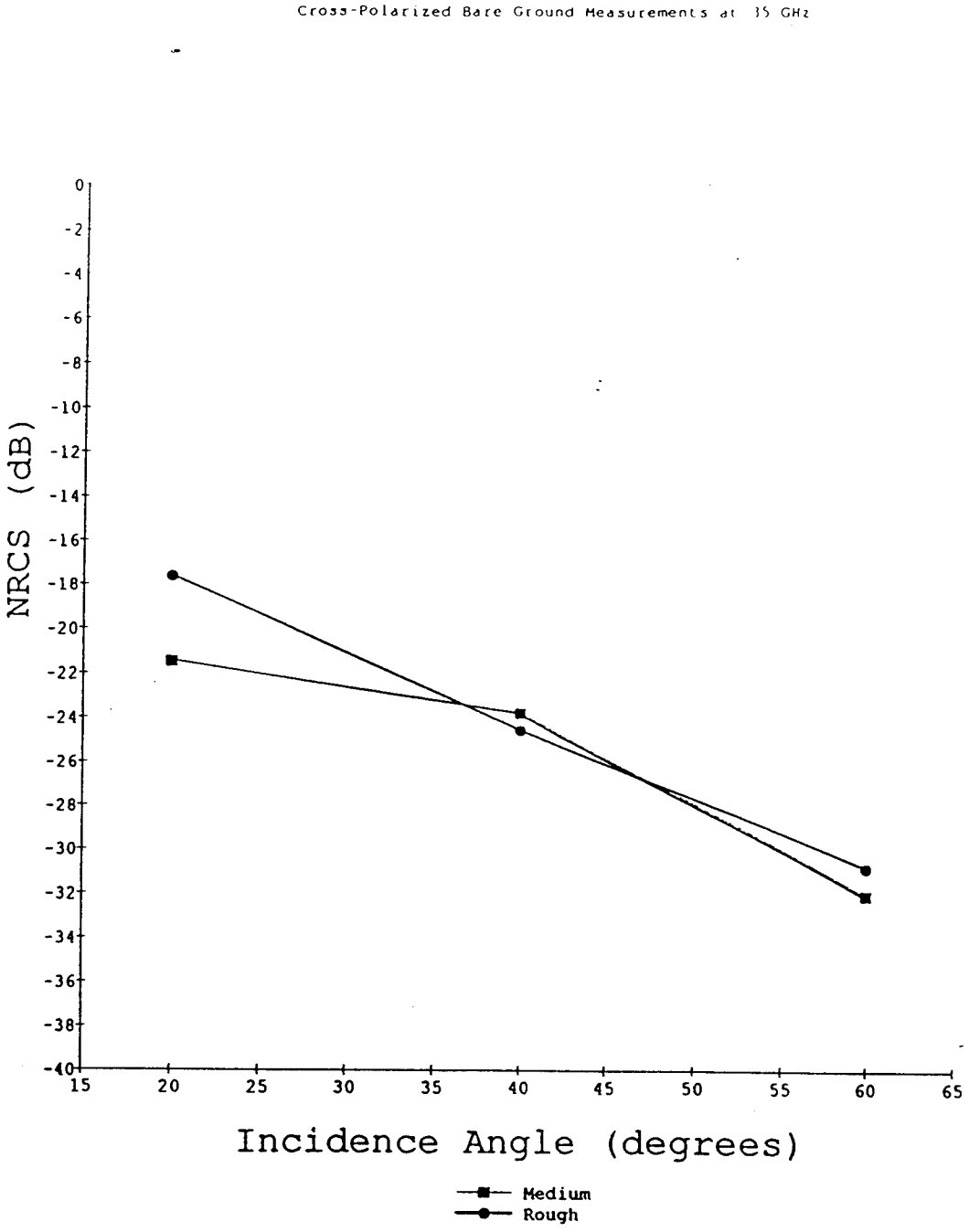

Figure 5.24. Cross-polarized terrain measurements at 35 GHz.

explains why σ^o is higher in this case. On February 12 we had frozen snow which presents a higher σ^o than the measurements of dry snow. Figure 5.22 shows the results for the cross polarized term HV. Figure 5.23 presents the co-polarized response for the bare ground after the snow measurements were done. The higher curve corresponds for the rough area and the lower one for the medium rough area. The cross-polarized σ^o for both areas is compare in figure 5.24.

5.4 Conclusions

A network analyzer able to operate in the millimeter-wave range can be configured in a matter of hours into a scatterometer. The availability of both phase and magnitude detection makes the design also particularly attractive for a polarimetric scatterometer design. The same unit can be used as a signal processor to operate a polarimetric scatterometer up to 110 GHz.

Data collected shows that this kind of scatterometer has an excellent range resolution. It also agrees with expected results of smooth and rough surface and the characterization of surface and volume scattering. Polarimetric data were also collected and it was shown that polarimetric measurements were done successfully for saline ice, or any kind of stationary target. This method allows us to subtract more information about the polarization response of the target under consideration.

The main problem with this system is the amount of time required to make a single measurement. Since a large amount of independent samples is desired, the collection of data takes several hours for different polarizations and angle of incidence. If the environmental conditions are not stable, this amount of

time is enough to produce any change in the structure of the target under consideration leading to erroneous results.

5.5 Future Recommendations

The HP 8510B network analyzer can be operated in a radar mode for frequencies up to 100 GHz. One of the frequency band of interests in remote sensing is around the window of 94 GHz.

Figure 5.25 is a block diagram of a possible 94 GHz polarimetric scatterometer design. Additional millimeter-wave hardware to obtain two orthogonal polarizations at the receiver and transmitter was quoted to a total cost of $ 10,000. Note that a OMT is used at the receiver channel allowing simultaneous measurements of a vertical and horizontal polarization, reducing by a factor of two the acquisition time. Also a polarizer is used in the transmitter section. Both antennas are scalar feedhorns with a circular waveguide to hold different kind of polarization. Systems like this have been done successfully up to frequencies of 140 GHz.

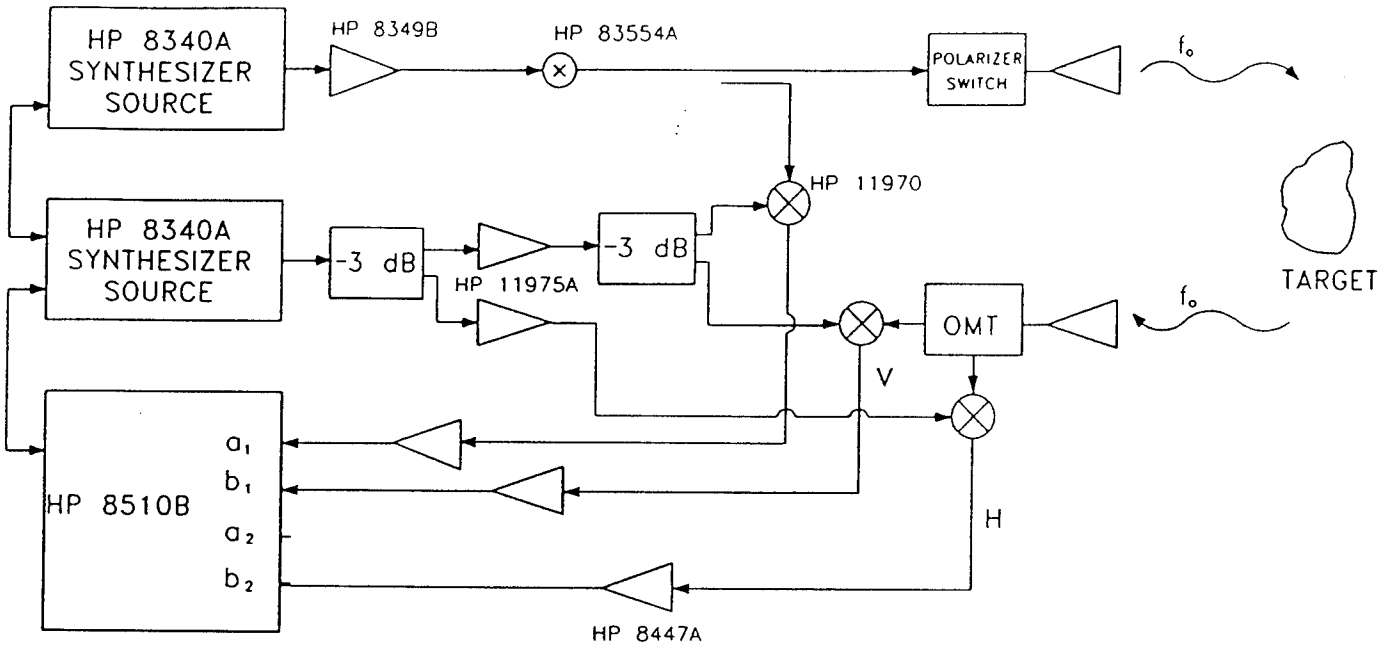

Figure 5.25. Block diagram for a 94 GHz polarimetric scatterometer

APPENDIX A

POLARIZER SWITCH SPECIFICATIONS

ALPHA INDUSTRIES, INC. TRG

TRG MODEL 145 - 250 SERIAL NO. 124

POLARIZATION SWITCH

FREQUENCY (GHz)	LOSS (dB)	CROSS POLARIZATION (ISOLATION) dB	*DRIVE CURRENT (mA) FOR ROTATION			
			0°	45°	90°	135°
34.0	0.3	>25	0	38	84	180
34.5	0.3	>25	0	35	76	147
35.0	0.3	>25	0	33	64	122
35.5	0.3	>25	0	31	60	100
36.0	0.3	>25	0	29	54	90

*NOTE: OBSERVE POLARITY ON TERMINALS. R+

TESTED BY P. Peltola

DATE 9/18/89

APPENDIX B

TRANSMITTER ANTENNA SPECIFICATIONS

TEST INFORMATION

MODEL NO.: SFH-28-.252.25 REF. NO: A17ic

SERIAL NO.: 082 CUSTOMER P.O. NO: 144559

SPECIFICATIONS AND REQUIREMENTS:

(1)	(2)	(3)
FREQ: 35GHz	FREQ:	FREQ:
FWHM: 25°	FWHM:	FWHM:
GAIN: 16dBi	GAIN:	GAIN:
SIDELOBES: >25dB	SIDELOBES:	SIDELOBES:
VSWR: —	VSWR:	VSWR:
POL. ISOLATION: —	POL. ISOLATION:	POL. ISOLATION:
AXIAL RATIO: —	AXIAL RATIO:	AXIAL RATIO:
INSERTION LOSS: —	INSERTION LOSS:	INSERTION LOSS:

TEST DATA

FREQ (GHz)	PLANE	PORT	FWHM (deg)	GAIN (dBi)	SIDELOBES (dB)	VSWR	POLARIZATION ISOLATION (dB)	AXIAL RATIO (dB)	INSERTION LOSS (dB)
35	E	—	27.7	17	>25	—	—	—	—
	H	—	27.0	17	>25	—	—	—	—

NOTES:

FROM TEST DATA RECORDED IN: Antenna Log II . PAGE: 198

TEST ENGINEER: [signature] . DATE: 7/12/89

Millitech Corporation, South Deerfield Research Park, Post Office Box 109, South Deerfield, Massachusetts 01373, U.S.A.
(413) 665-8551 Telex: 3719662 MILTH UB FAX: (413) 665-7536

APPENDIX C

RECEIVER ANTENNA SPECIFICATIONS

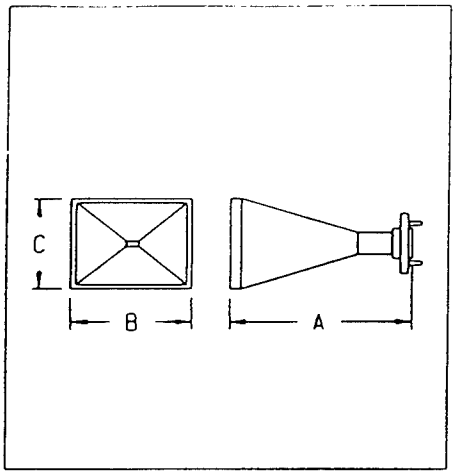

Electrical Specifications

MODEL	RF BAND		MAXIMUM VSWR
	FREQUENCY GHz	EIA WAVEGUIDE	
SGH-42F	18-26.5	WR-42	1.20
SGH-28F	26.5-40	WR-28	1.20
SGH-22F	33-50	WR-22	1.20
SGH-19F	40-60	WR-19	1.20
SGH-15F	50-75	WR-15	1.20
SGH-12F	60-90	WR-12	1.20
SGH-10F	75-110	WR-10	1.20
SGH-08F	90-140	WR-8	1.20

Mechanical Specifications

MODEL	A in.(mm)	B in.(mm)	C in.(mm)	WEIGHT oz(g)	WAVEGUIDE FLANGE
SGH-42F	3.3(85)	2.4(60)	2(50)	4.6(130)	UG-595/U
SGH-28F	2.6(65)	1.9(49)	1.5(37)	2.8(80)	UG-599/U
SGH-22F	2.4(60)	1.6(42)	1.2(31)	2.5(70)	UG-383/U
SGH-19F	2.2(55)	1.5(38)	1.15(29)	2.4(67)	UG-383/U-M
SGH-15F	2(50)	1.4(35)	1.1(27)	2.3(65)	UG-385/U
SGH-12F	1.5(38)	1.1(29)	0.9(22)	2.1(60)	UG-387/U
SGH-10F	1.1(28)	1.1(21)	0.7(18)	1.8(50)	UG-387/U-M
SGH-08F	1.1(28)	0.8(20)	0.6(15)	1.6(45)	UG-387/U-M

Typical Performance

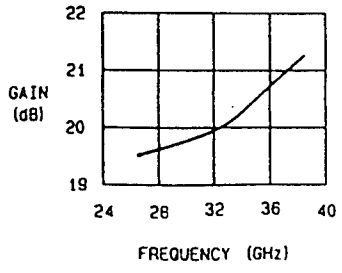

APPENDIX D

HARMONIC MIXER SPECIFICATIONS

NOTE

Unless otherwise stated, all specifications apply for an IF of 321.4 MHz and for RF input amplitudes of less than – 20 dBm.

GENERAL

LO Amplitude Range:
+ 14 to + 18 dBm[1]

Calibration Accuracy:
11970K/A/Q/U:
± 2.0 dB with LO amplitude range of 14.5 to 16 dBm
11970V/W:
± 2.2 dB with LO amplitude range of 14.5 to 16 dBm
11970K/A/Q/U:
± 3.0 dB with LO amplitude range of 16 to 18 dBm
11970V/W:
± 3.2 dB with LO amplitude range of 16 to 18 dBm

Bias Requirements:
None

Maximum CW RF Input Level:
+ 20 dBm (100 mW)

Maximum Peak Pulse Power:
+ 24 dBm with <1 μsec pulse (avg. power: + 20 dBm)

Environmental:
Meets MIL-T-28800C, Type III, Class 3, Style C

IF/LO Connectors:
SMA female (replaceable)

MODEL 11970K

RF Frequency Range:
18 – 26.5 GHz

LO Harmonic Number: 6

LO Input Frequency Range:
2.95 – 4.36 GHz

Maximum Conversion Loss: 24 dB

HP 8566B Noise Level at 1 kHz Bandwidth, and + 14.5 to + 16 dBm LO Input Power:
– 110 dBm

Frequency Response at + 14.5 to + 16 dBm LO Input Power:
± 1.9 dB

Frequency Response at + 14 to + 18 dBm LO Input Power:
± 2.8 dB

MODEL 11970A

RF Frequency Range:
26.5 – 40 GHz

LO Harmonic Number: 8

LO Input Frequency Range:
3.27 – 4.96 GHz

Maximum Conversion Loss: 26 dB

HP 8566B Noise Level at 1 kHz Bandwidth, and + 14.5 to + 16 dBm LO Input Power:
– 108 dBm

Frequency Response at + 14.5 to + 16 dBm LO Input Power:
± 1.9 dB

Frequency Response at + 14 to + 18 dBm LO Input Power:
± 2.8 dB

[1]The HP 11975A Amplifier, or a similar amplifier, must be used to provide sufficient LO power (14 to 18 dBm) to the mixers. Leveled power capability of + 16 dBm, as is available with the HP 11975A, is necessary to achieve the maximum amplitude accuracy with the mixers.

APPENDIX E

CONTROL CARD DIAGRAM

HURST ELECTRONIC STEPPING MOTOR CONTROLS

DRIVER CIRCUITRY:

MOTOR CONNECTIONS (terminal strip connectors 1-6)
The phase drivers are n-channel MOSFET devices with a drain to source rating of 100 volts. They will drive motors with currents up to 2 amps per phase. Motor phases are connected to terminals 1 through 4 (or terminals 1 through 3 in the case of 3 phase motors). Phase commons are connected to terminal 5, 6, or 7 for both types of motors. The sequences generated at terminals 1 through 4 are shown in figure 2. The lead wire color code for 4 phase Hurst motors is shown in figure 1.

POWER SUPPLY:

EXTERNAL SUPPLY CONNECTIONS (terminal strip connectors 7 and 8)
Power supply requirements for the controller alone are 6-30 VDC, 20 ma maximum. Motor current requirements must be added to the latter value. The positive side of the external DC supply is connected to terminal 5, 6, or 7, and the negative side to terminal 8 (COMMON).

5V REGULATOR OUTPUT (edge terminals 1 and 22)
The +5V output of the on-board regulator is available at edge terminal 1 and the power supply COMMON at edge terminal 22. The regulator can supply up to 100 ma to external circuitry with power supply voltages from 6 to 24 volts. With supplies above 24 volts the maximum current is approximately 80 ma.

TYPICAL APPLICATION WITH HURST STEPPING MOTORS

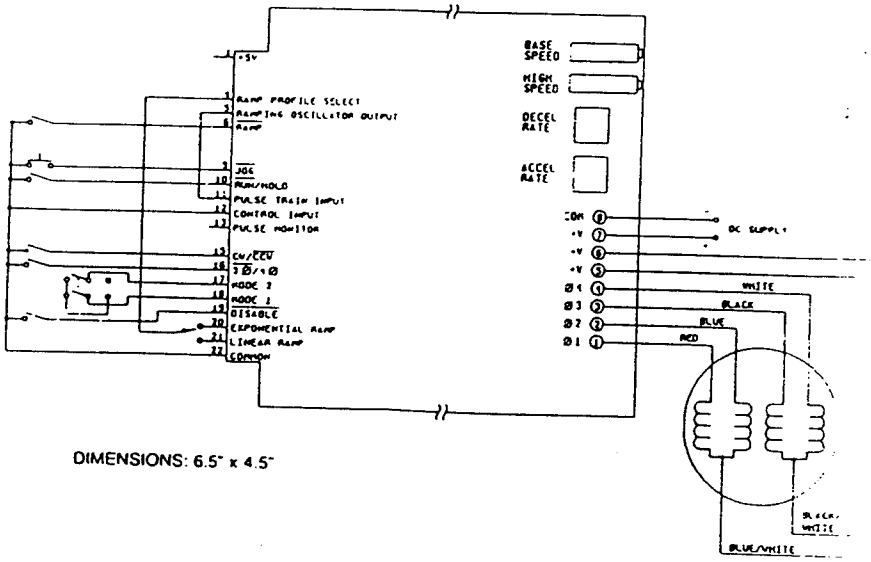

DIMENSIONS: 6.5" x 4.5"

APPENDIX F

QUOTATION FOR 94 GHZ SCATTEROMETER

millitech®

Millimeter and Submillimeter Components, Instruments and Subsystems

MEMORANDUM

TO: Jose Columb, University of Massachusetts

FROM: Diane Greenman for Dean Dixon, Millitech

DATE: May 24, 1991

SUBJECT: Q.4783

Millitech is pleased to provide the following quotation:

Item	Quantity	Description	Unit Price	Total Price U.S.$
01	2	SFH-10-094-15 Scalar Horn Antenna Circular Waveguide Diameter: .094" Bandwidth: 15° Ship Date: 60 DARO	$2,900	$5,800
02	1	OMT-10-094 Circular Waveguide Diameter: .094" Ship Date: 90 DARO	$3,000	$3,000
		Total:		$8,800

Terms: Net 30 days - FOB South Deerfield, Massachusetts. Prices do not include shipping, taxes, or insurance. Shipping and insurance charges will be added to the invoice.

This quotation is valid for 60 days from date of quotation.

Millitech Corporation, South Deerfield Research Park, Post Office Box 109, South Deerfield, Massachusetts 01373, USA
(413) 665-8551 Telex: 4720682 MILTECH FAX (413) 665-8651

References

[Alpha, 1986] Alpha. *TRG Millimeter Wave Products Catalog.* Alpha Industries, 1986.

[Balanis, 1982] C. A. Balanis. *Antenna Theory Analysis and Design.* Harper and Row, 1982.

[Born and Wolf, 1965] M. Born and E. Wolf. *Principle of Optics.* Pergamon Press, 1965.

[Currie and Brown, 1987] N. C. Currie and C. E. Brown. *Principles and Applications of Millimeter-wave Radar.* Artech House, 1987.

[Eaves and Reedy, 1987] J. L. Eaves and E. K. Reedy. *Principles of Modern Radar.* Van Nostrand Reinhold, 1987.

[Hewlett-Packard, 1985] Hewlett-Packard. *Radar Cross Section Measurements with the HP 8510 Network Analyzer.* Product Note 8510-2, 1985.

[Hewlett-Packard, 1987] Hewlett-Packard. *HP 8510B Network Analyzer Operating Manual.* 1987.

[Jones, 1941] R. C. Jones. A new calculus for the treatment of optical systems. *Journal Optical Society of America*, 31(7):488–493, 1941.

[Kennaugh, 1951] E. M. Kennaugh. *Effects of the Type of Polarization on Echo Characteristics.* Report 389-9, Ohio State University, 1951.

[Kim *et al.*, 1984] Y. S. Kim, R. K. Moore, and R. G. Onstott. *Theoretical and Experimental Study of Radar Backscatter from Sea Ice.* Report 331-37, University of Kansas, 1984.

[McCarter, 1989] G. McCarter. Software or hardware gating; what's best for RCS measurements? *Microwave Systems News*, 19(11):60–63, 1989.

[Millitech, 1986] Millitech. *Millimeter and Submillimeter Components, Instruments, Subsystems.* Millitech Corporation, 1986.

[Narayanan, 1988] R. M. Narayanan. *Measurement and Analysis of Electromagnetic Scattering from Vegetation and Fallen Snow at 215 GHz.* PhD thesis, University of Massachusetts, 1988.

[Onstott, 1980] R. G. Onstott. *Radar Backscatter Study of Sea Ice.* PhD thesis, University of Kansas, 1980.

[Schaubert, 1988] D. Schaubert. *Introduction to Radar Systems.* ECE course, University of Massachusetts, 1988.

[Skolnik, 1980] M. E. Skolnik. *Introduction to Radar Systems.* McGraw Hill Inc., 1980.

[Stutzman and Thiele, 1981] W. L. Stutzman and G. A. Thiele. *Antenna Theory and Design.* John Wiley & Sons, 1981.

[Ulaby and Elachi, 1990] F. T. Ulaby and C. Elachi. *Radar Polarimetry for Geoscience Applications.* Artech House, 1990.

[Ulaby *et al.*, 1982] F. T. Ulaby, R. Moore, and A. Fung. *Microwave Remote Sensing; Active and Passive vol. 2.* Artech House, 1982.

[Ulaby *et al.*, 1990] F. T. Ulaby, M. W. Whitt, and K. Sarabandi. AVNA - based polarimetric scatterometer. *IEEE Antennas and Propagation Magazine*, 32(5):6–17, 1990.

[Vant *et al.*, 1974] M. R. Vant, R. G. Gray, R. O. Ramseier, and V. Makios. Dielectric properties of fresh and sea ice at 10 and 35 ghz. *Journal Applied Physics*, 45(11):4712–4717, 1974.

[Whitt *et al.*, 1987] M. W. Whitt, F. T. Ulaby, and T. F. Haddock. *The Development of a Millimeter-wave Network Analyzer Based Scatterometer.* Report 022872-1-T, University of Michigan, 1987.

[Wood, 1986] M. A. Wood. *Theoretical Study of Calibration Procedures for Coherent and Non-coherent Polarimetric Radars.* Report 86011, Royal Signals and Radar Establishment, 1986.